PolyPublie
Polytechnique Montréal

POLYTECHNIQUE MONTRÉAL
UNIVERSITÉ D'INGÉNIERIE

Titre: Title:	Design of Precast and Prestressed Steel Fibre Reinforced Concrete T-Girders
Auteur: Author:	Nicola Cordoni
Date:	2015
Type:	Mémoire ou thèse / Dissertation or Thesis
Référence: Citation:	Cordoni, N. (2015). Design of Precast and Prestressed Steel Fibre Reinforced Concrete T-Girders [Mémoire de maîtrise, École Polytechnique de Montréal]. PolyPublie. https://publications.polymtl.ca/1675/

Document en libre accès dans PolyPublie
Open Access document in PolyPublie

URL de PolyPublie: PolyPublie URL:	https://publications.polymtl.ca/1675/
Directeurs de recherche: Advisors:	Bruno Massicotte, & David Conciatori
Programme: Program:	Génie civil

Ce fichier a été téléchargé à partir de PolyPublie, le dépôt institutionnel de Polytechnique Montréal
This file has been downloaded from PolyPublie, the institutional repository of Polytechnique Montréal

https://publications.polymtl.ca

UNIVERSITÉ DE MONTRÉAL

DESIGN OF PRECAST AND PRESTRESSED STEEL FIBRE REINFORCED CONCRETE T-GIRDERS

NICOLA CORDONI

DÉPARTEMENT DES GÉNIES CIVIL, GÉOLOGIQUE ET DES MINES

ÉCOLE POLYTECHNIQUE DE MONTRÉAL

MÉMOIRE PRÉSENTÉ EN VUE DE L'OBTENTION

DU DIPLÔME DE MAÎTRISE ÈS SCIENCES APPLIQUÉES

(GÉNIE CIVIL)

FÉVRIER 2015

© Nicola Cordoni, 2015.

UNIVERSITÉ DE MONTRÉAL

ÉCOLE POLYTECHNIQUE DE MONTRÉAL

Ce mémoire est intitulé:

DESIGN OF PRECAST AND PRESTRESSED STEEL FIBRE REINFORCED CONCRETE T-GIRDERS

présenté par : CORDONI Nicola

en vue de l'obtention du diplôme de : Maîtrise ès sciences appliquées

a été dûment accepté par le jury d'examen constitué de :

M. LÉGER Pierre, Ph. D., président

M. MASSICOTTE Bruno, Ph. D., membre et directeur de recherche

M. CONCIATORI David, Ph. D., membre et codirecteur de recherche

M. DE MONTAIGNAC Renaud, Ph. D., membre

DEDICATION

To my family

ACKNOWLEDGEMENTS

Foremost I would like to express my sincere gratitude to my thesis advisor professor Bruno Massicotte for his patience, motivation and professionalism. His experience and huge knowledge in the domain of concrete structures guided me throughout the whole research work. I also would like to thank him for the financial support during this two-year experience. His working attitude, availability, experience and competences inspired me and made me grow up with a view to my future career.

Beside my advisor, my sincere thanks go to professor David Conciatori – co-advisor of this research project. From the beginning of my project he has always been available and kind helping me in solving any problems and difficulties. His computer skills associated with a huge competence in the concrete structure domain enabled me to learn and handle all the different software used for the project.

Special thanks do to Professor Ferrara, who gave me the possibility to present this thesis at the Politecnico of Milan to obtain the Italian degree. Even if for a short lapse of time, I thank him for his patience, his time and his helpful advise.

I thank my parents and my whole family, who always supported me financially and morally. Their constant presence – even if far away – has been important and necessary, especially during the first few months of my experience.

I have also to thank all friends I met in this six-year experience of studies. A special thank goes to Pippo, Ahm, Berga, Frenk and Giampy, with whom I had the pleasure to share 4 fantastic years of my life. Some of the friends I met in Montréal, who made my experience unforgettable: Federico, Jacopo, Arthur, Erik, Thomas, Emilie, Thomas, Heloïse, Luca, Nicolò, Lidia, Carolina, Filippo, Simone and Christelle. Last but not the least my colleagues of the Structures department who shared with me some great moments even outside the working environment: Nathan, Léa, Amadou, Alex, Maxime M., Michel-Ange, Jalila, Maxime H., Véronique and Maxime G.

I also thank Cédric for his help and professionalism during the short period I did some experimental works in the structure laboratory.

RÉSUMÉ

Les écarts de température significatifs, l'utilisation massive de sels de déglaçage et le volume de trafic croissant mettent à l'épreuve durement les structures en béton, amenant des coûts importants pour l'entretien, les réparations ou le remplacement prématuré de celles-ci. L'utilisation des seules barres d'armature ne peut pas empêcher complètement la fissuration des dalles de pont en service, ce qui conduira éventuellement à la détérioration de la structure. Les travaux de recherche menés à l'École Polytechnique de Montréal depuis près de 20 ans impliquant l'utilisation de fibres d'acier dans le béton permet à la fois d'améliorer la durabilité des ponts et d'en simplifier la conception. Ce mémoire présente le développement d'un nouveau type de tablier de pont entièrement préfabriqué.

Le type de tablier choisi consiste en des poutres en T ou en double T en béton renforcé de fibres (BRF), précontraintes longitudinalement, et jointent entre elles par des joints longitudinaux en béton fibré à ultra-haute performance (BFUP). Ce type de poutres vise des ouvrages couvrant une plage de portées comprises entre 15 m et 30 m. L'utilisation de fibres d'acier permet de réduire l'espacement et la largeur des fissures, tant pour la dalle que pour la partie en traction de la poutre aux états limites de service. De plus les fibres participent à la résistance en cisaillement et augmentent la ductilité en flexion à l'état limite ultime – comme démontré par les analyses numériques et expérimentales réalisées pour ce projet de recherche. Le profil optimisé de la section transversale permet d'utiliser un seul lit de barres d'armature pour la dalle. En outre, la solution étudiée conduira à un meilleur contrôle des caractéristiques mécaniques des matériaux, réduira les coûts d'entretien de la structure et permettra une mise en place plus rapide de la structure.

L'absence d'une norme reconnue qui couvre la conception des structures en BRF limite l'utilisation des fibres métalliques au niveau structural. La conception de ces structures doit être effectuée avec la combinaison d'essais en laboratoire et d'outils numériques capables de prédire la réponse structurale de façon fiable. Ce mémoire porte sur la partie numérique alors que la partie expérimentale a été réalisée dans un projet précédent.

Pour la flexion, des outils de calculs sont disponibles et les hypothèses assez similaires sont proposées par plusieurs regroupement scientifiques ou normes. Toutefois, les méthodes de calcul diffèrent considérablement pour le calcul à l'effort tranchant. Enfin, très peu de recherches ont

porté sur l'étude des poutres précontraintes en BRF en flexion, encore moins pour l'effort tranchant. Ce mémoire porte spécifiquement sur des poutres précontraintes en BRF et comporte trois parties principales propres à cette application : la validation du logiciel EPM3D utilisé avec ABAQUS/Explicit, la conception en flexion des nouveaux types de poutres avec des méthodes de calcul usuelles et la validation cette conception avec EPM3D. Une amorce d'étude du comportement à l'effort tranchant de poutres en BRF est présentée. Finalement la conception des trois sections types pour des portées de 15 m, 20 m et 25 m est fournie.

ABSTRACT

Major thermal variations, the massive use of de-icing salt and the increasing traffic volume strongly strain concrete structures causing high costs for maintenance, repair and eventually their premature replacement. Conventional reinforcement in concrete bridge decks cannot completely prevent cracking at serviceability state which will eventually lead to the structure deterioration. A solution involving the use of steel fibres has been investigated at Polytechnique Montréal for almost 20 years. Steel fibres can both improve the durability and simplify the design of concrete structures. This master thesis presents the pre-design of a new type of bridge deck entirely precast.

The deck consists of T or double-T beams made of Steel Fibre Reinforced Concrete (SFRC). Longitudinally prestressed, the beams are transversally connected by ultra-high performance steel fibre reinforced concrete (UHPFRC) joints to span lengths up to 30 m. The addition of steel fibres reduces the extent of cracking and crack widths in service conditions, both for the concrete slab and the beams. As shown in this master thesis, at the ultimate limit state fibres contribute to enhancing the ductility and the shear capacity of concrete structures. The optimized profile of the transverse cross section and the UHPFRC joints connecting the different precast beams permit to use a single layer of reinforcing bars in the slab. The retained solution would lead to a better control of the casting process, lower costs for the structure maintenance and reduced construction time.

The absence of design codes or standards limits the use of SFRC at structural level. The design of such structures must be carried with the aid of numerical tools able to predict a reliable structural response for each limit state investigated. This master project focuses on the numerical study of this new type of bridge super-structure following an experimental investigation carried out in a previous project.

For bending, several calculation methods based on similar hypothesis are presented in many scientific articles and standards. For shear, there is not yet a worldwide-recognized approach that can be used for SFRC structures. More experimental campaigns have to be carried out in order to completely investigate both bending and shear behaviours of prestressed beams.

This master thesis focuses the attention on the numerical study of prestressed SFRC beams, and it can be divided into three different sections: the validation of EPM3D concrete model used in the

software ABAQUS/Explicit, the design in flexure of the new type of beams with conventional design calculations, and the numerical study with EPM3D of the beams designed in the previous step. A study of the shear behaviour is also presented. The design of the beams for three different spans – 15 m, 20 m and 25 m – is provided.

TABLE OF CONTENTS

LIST OF TABLES

LIST OF FIGURES

LIST OF SYMBOLS AND ABBREVIATIONS

ACI	American Concrete Institute
AIS	Analyse Inélastique des Sections (French)
ASTM	American Society for Testing and Materials International
CalInv	Calcul Inverse (French)
CEN	European Committee for Standardization
CL-625	Canadian Bridge Code truck load
CMOD	Crack Mouth Opening Displacement
EN	European standards
EPM3D	Tridimensional multiaxial progressive damage
FE	Finite element
FEM	Finite element method
FLS	Fatigue limit state
LVDT	Linear Variable Differential Transducer
MTQ	Ministère des Transports du Québec
SFRC	Steel fibre reinforced concrete
SLS	Service limit state
ULS	Ultimate limit state
UHPFRC	Ultra-high performance fibre reinforced concrete
UTT	Uniaxial tension test
P-Δ	Load-displacement relation
σ-w	Stress crack-width relation

LIST OF APPENDICES

CHAPTER 1 INTRODUCTION

1.1 Context

The road network in Québec comprises more than 10,000 bridges of which more than half are under the jurisdiction of the Quebec Ministry of Transportation (MTQ). More than seventy percent of these structures have been built before 1980 and consequently the expected service life of several bridges will be reached soon which will require large investments and lead to intensive construction works in the next decades. Just in 2012-2013, the Quebec Ministry of Transportation spent 4 billion dollars to monitor, repair and/or maintain such a large road network and the forecast expenditure is much higher in the years to come (MTQ, 2011).

To add to these numbers, Quebec bridges are exposed to extreme load conditions due to severe weather and the large volume of road transportation that characterises such a large geographic area. Moreover, as the weight and dimension of the trucks, along with the overall volume of traffic, increases, road bridges must be designed differently.

Thus there is the necessity and the urgency to develop new construction solutions that allow replacing old bridges or building with a significant gain in safety, money, time and durability. Moreover the durability shall become an important design factor to consider because the maintenance costs during the life of the structure could become considerable.

A research project has been initiated at École Polytechnique of Montreal for developing entirely precast bridges made of fibre reinforced concrete (FRC) (Massicotte et al. 2010). The retained option for short span girders from 15 m to 30 m was inspired by the NEXT beam concept largely adopted in the USA. The first part of the project focused on selecting the concept for the girders. It was determined that design requirements could be best met by using T or double-T prestressed beams made of Steel Fibre Reinforced Concrete (SFRC). The proposed concept innovates by combining three components for bridges: the structural use of steel fibres in prestressed members, the prefabrication process of girders with integrated deck, and the use of longitudinal UHPFRC joints.

The use prestressing remains the most efficient solution for the design of large span bridge girders. The addition of steel fibres to the concrete mix has an especially important influence for

serviceability requirements: steel fibres provide an exceptional post-cracking strength to the concrete matrix leading to narrower and thinner cracks in the structure. Fibres improve the mechanical resistance, the efficiency and the durability of the structure, allowing a reduction of the transverse section, the elimination of the secondary reinforcement, a simpler positioning of stirrups and the concentration of the prestressed strands only in the lower part of the beam.

Compared to conducting the construction work entirely on-site, prefabrication enables better quality control of material properties, casting techniques and preparation of the beams. Moreover, the fabrication in a factory of girders with integrated decks reduces the construction time by avoiding the installation of formworks and the curing of concrete. .

This innovative idea requires using Ultra-High Performance Fibre-Reinforced Concrete (UHPFRC) longitudinal joints to connect the beams. This joint is cast on the construction site and represent a critical phase of the proposed solution. It requires high quality materials, well trained workers, and precise execution. Such technology has been used for many years in North-America (FHWA, 2014).

Polytechnique Montréal Group for Research in Structural Engineering (GRS) demonstrated in the last 20 years to be at the forefront of research in the fibre reinforced material and several experimental campaigns have been already carried out to investigate the fibre reinforced concrete behaviour. Overall, the combined use of prestressing, SFRC, prefabrication, and UHPFRC joints allows developing more economical and durable bridges.

This thesis is an integral part of the entire project and the diagram in Figure 1–1 presents the chronological succession of phases that will eventually lead to the definitive design of the precast bridge and finally the commercialisation of the innovative solution.

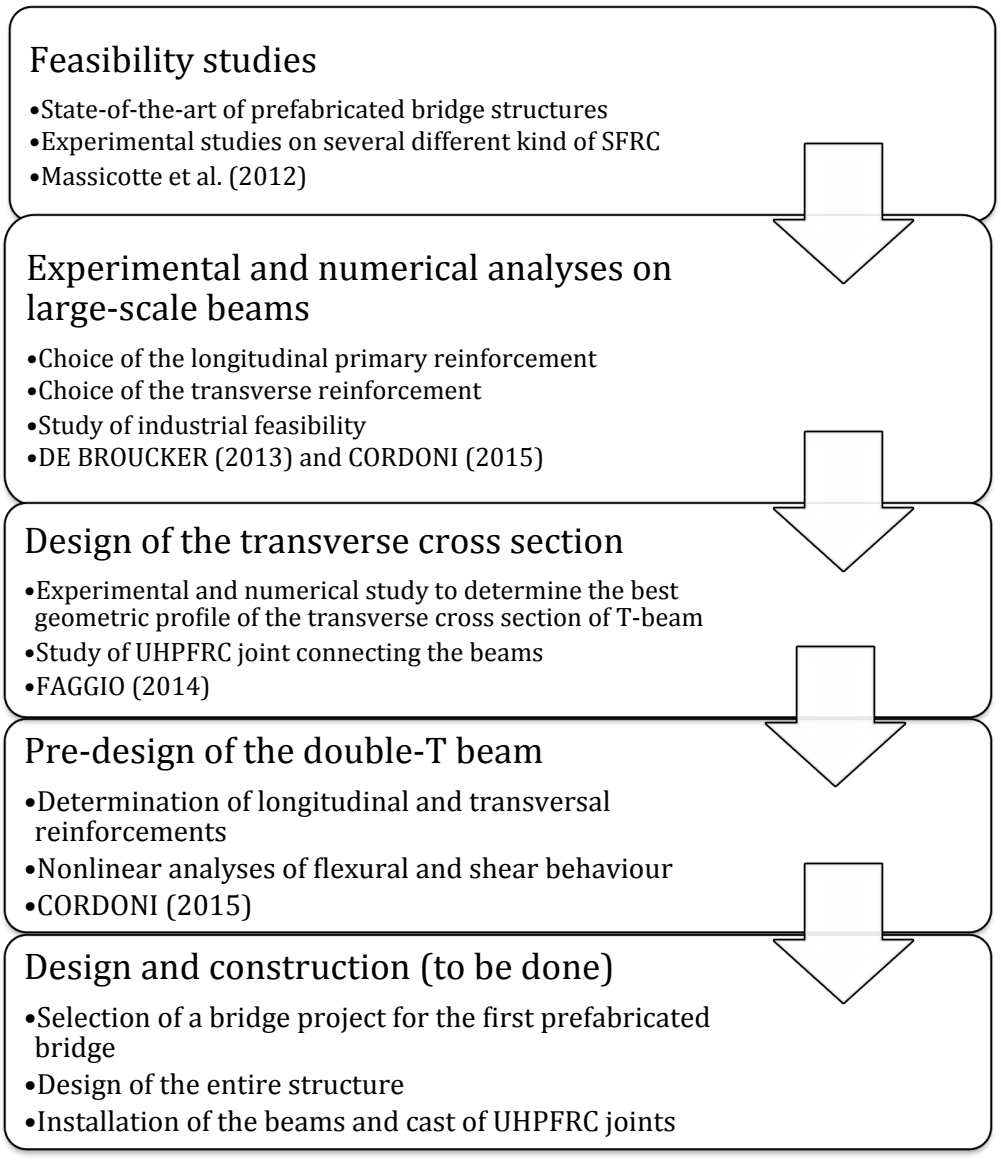

Figure 1–1: Activities related to the development of prestressed SFRC T-girders for bridges

1.2 Objectives and scope of thesis project

As summarised in Figure 1–1 diagram, this thesis project mainly addresses the numerical study of the beams tested by De Broucker (2013). Once the reliability of the finite element constitutive model implemented verified, the design of the double-T beam will be presented through different calculation levels: manual calculations, linear study and nonlinear Finite-Element Analyses (NLFEA). The objectives of the thesis aim at:

- validating EPM3D (Three-dimensional Multi-axial Progressive Damage) concrete constitutive model for fibre reinforced concrete to reproduce with accuracy the results obtained from the experimental campaign on large-scale beams carried out by De Broucker (2013);
- determining the loads and the geometry of the prefabricated T-beams respecting the Canadian Highway Bridge Design Code (CAN/CSA-S6-06), particularly for the longitudinal and shear reinforcement chosen to respect all the design criteria associated with the limit states to be considered – serviceability, fatigue and ultimate limit states;
- predesigning SFRC T-beams for different span lengths using NLFEA for providing important information concerning the crack pattern, the flexural and shear bearing capacities, the failure modes, ductility and displacements;
- establishing the mechanical properties of three different SFRC mixes using a new kind of steel fibres: the DRAMIX 5D.

1.3 Methodology and organization

This thesis is structured as follows. The first chapter aims to introduce the research project context, the subject and the explanation of the main objectives of the entire work.

The second chapter aims to explain in details the main concepts necessary for a clear understanding of the entire thesis. The main aspects considered will be the fundamentals of the combination between steel fibres and concrete, few concepts about prestressed structures and the basis of the FEM technique.

The third chapter is about the validation of the concrete constitutive model EPM3D for such applications. The numerical analyses aim to reproduce the results obtained experimentally on 8 rectangular beams made of SFRC. The experimental program conducted by De Broucker (2013) is briefly presented to aid the comprehension of the numerical analyses done subsequently. The subroutine EPM3D integrated in the Finite Element software ABAQUS is used to model the SFRC used to fabricate the different beams.

The fourth chapter describes the predesign of the beam sections. A brief reminder of the Bridge Code requirements presents how loads are calculated and what are the few geometrical limitations to be respected. The predesign steps are then presented: the determination of the loads

for different beam spans following the code simplified method and 2D framing system, the longitudinal and shear reinforcement, the materials and the design criteria. In this phase only spread sheets, the CAN/CSA-S6-06 code and engineering considerations are used.

The fifth chapter deals with the final design of the T-beam for three different span lengths – 15 m, 20 m and 25 m. Using the geometrical profile of the integrated slab determined in Faggio (2014), this phase aims to compute the quantity of longitudinal and shear reinforcements for each beam. Nonlinear analyses carried out with EPM3D investigate the flexural and shear behaviours for each precast beams. Crack patterns are also examined, exploiting the potentiality of the constitutive model.

The sixth chapter presents the conclusions of the research project. Few recommendations are also presented for possible future developments of the research work.

Appendix A presents the results of tests carried out on a SFRC mix made with a new type of steel fibres. The experimental results so obtained are compared to other different kinds of steel fibres previously tested in De Broucker (2013) and Tordjman (2012). Appendix B summarises the calculation of live load effects with the simplified method of the Canadian Bridge Code. Appendix C presents additional results of EPM3D validation.

CHAPTER 2 LITERATURE REVIEW

2.1 Generality

The principal objective of adding fibres in the concrete mix is to improve the tensile behaviour of the concrete. Moreover, the mechanical properties in bending, shear and compression are also modified by the presence of fibres in the concrete. The ductility is improved by the action of the fibres dispersed in the matrix that are able to transfer tensile stresses through the cracks. The fibres – used to "stitch" the cracks – start acting only after cracking (Rossi, 1998). Fibres reduce both crack- opening and spacing. In doing so, the crack pattern at serviceability state is effectively controlled and the durability of the structure is improved. Different types of fibres can be used for specific applications according to their geometry, volume content and bonding properties. Rossi et al. (1987) detailed the action of the fibres both at the material and the structure levels. This chapter presents details of SFRC technology and the numerical modelling of their behaviour with finite element.

2.2 History of fibre reinforced concrete

The concept of adding fibres to improve the behaviour of building materials is old and intuitive. 3500 years ago straw fibres were used to reinforce sun-baked bricks of the 57 m high hill of Aqar Ouf near Baghdad (Newman et al, 2003). Horsehair was also used to reinforce mortar or plaster (ACI Committee 544.1R, 1996) and asbestos fibres were added to reinforce cement-based material used in the construction of roofing sheets. Fibres were already known to be an effective means to prevent and reduce the crack pattern caused by changes of temperature and humidity. The first pioneer of steel fibre reinforcement was A. Berard who suggested to use the granular waste iron in concrete mix in 1874. Only a few number of fibre patents were granted in the next 80 years addressing different aspects such as: the fibre (Weakly, 1912), the fibre reinforced concrete mix (Costantinesco, 1943), the production process (Etheridge, 1933) or fibre applications (Kleinlogel, 1920).

The modern concept of fibre reinforced concrete was elaborated during 1960s when Romualdi, Batson and Mandel (Romualdi et al, 1963) brought FRC to the attention of academic and industry researchers around the world. Since then, a substantial amount of research development,

experimentation and industrial application of steel fibre reinforced concrete has occurred. At the beginning the benefits of steel fibres were not so clear and easy to be pointed out especially facing to the early disillusionment to obtain a revolutionary heterogeneous material able to provide comparable compression and traction resistances. Problems linked to workability and costs of the fibres initially slowed down the use of steel fibre with dosages larger than 30 kg/m^3. This fibre content was found to be an indicative upper limit to not exceed the cost that the use of conventional reinforcement bars would have provided in the same structure for a similar mechanical strength. At the beginning the development of SFRC focused on applications such as slabs, tunnel linings and roof sheets. For these kinds of applications the use of a little amount of steel fibres could be sufficient to replace completely the conventional reinforcement commonly used. Primarily the elevated costs and the bad workability of the SFRC mixes prevented an early development and research about the addition of steel fibres up to the 1980s.

The use of super-plasticisers to improve the workability and the improvement of new mix design techniques allowed the use of larger dosage of fibres. Research activities started investigating the addition of steel fibres to improve performances of load-bearing structures. Since then numerous papers have been written and conferences have been organized, disseminating the advantages of using SFRC. Several internationally recognized/accepted design code have come out only in the very last few years Chinese Guidelines (Leung, 2014), Draft Australian bridge Code (Forster, 2014), FIB Model Code 2010 (di Prisco, 2014) and the French recommendations (AFGC, 2013), whereas so far guidelines and recommendations were only available.

2.3 The composite material

2.3.1 Steel fibres

There are many types of fibres on the market with extremely different geometrical and mechanical properties. Steel fibres remain the most used (50% of the total tonnage used), followed by polypropylene, glass or other natural materials (Figure 2–1). In this chapter only the steel fibres will be presented according to the project developed in the next few chapters.

The common shapes used for structural or non-structural purposes are indicated in the Figure 2–1. According to their geometry fibres act differently: straight fibres develop bonding stresses along their length preventing the crack opening; corrugated and hooked-end fibres can be less

long fibres because they develop stresses by the anchorage made by the curved geometry. For standard compressive strength concrete, the hooked-end fibres can be considered the most appropriate due to their strain capacity under tensile stresses. Steel fibres can also have coatings like zinc (for improving corrosion resistance) or brass (for improving bond characteristics).

(a) Different types of fibre materials

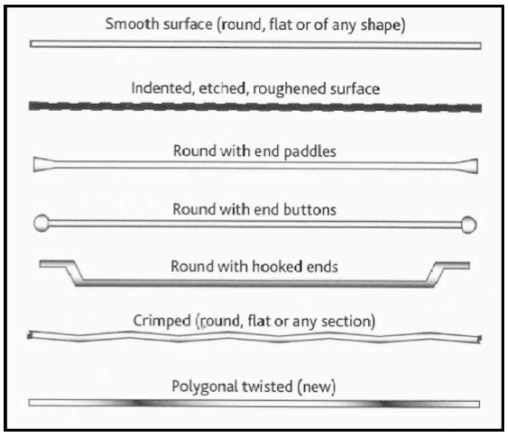

(b) Different steel fibre shapes

Figure 2–1: Different types of fibres (di Prisco, 2007)

There are different ways to classify the different types of steel fibres and three of them are presented herein. In the European standard EN 14889 (CEN, 2006), steel fibres are divided into five general groups and are defined in accordance with the basic material used for the production of the fibres according to:

- Group I, cold-drawn wire;
- Group II, cut sheet;
- Group III, melt extracted;
- Group IV, shaved cold drawn wire;
- Group V, milled from blocks.

The Japanese Society of Civil Engineers (JSCE) has classified steel fibres according to the shape of their cross-section:

- Type 1: Square section;
- Type 2: Circular section;
- Type 3: Crescent section.

ASTM A820 provides a classification for four general types of steel fibres based upon the product used in their manufacture:

- Type I—Cold-drawn wire;
- Type II—Cut sheet;
- Type III—Melt-extracted;
- Type IV—Other fibres.

The length range of this kind of steel fibres is in the order of 30 mm to 60 mm and the typical diameter between 0.5 mm and 1 mm. The common volume content used for structural application ranges from 0.5% to 1.5%, which is equal to a mass content between 40 kg/m^3 and 120 kg/m^3. Long fibres are mainly used to bridge discrete macro-cracks at higher loads. Moreover, Rossi (1998) stated that the introduction of long fibres might cause a little reduction of the compressive strength of the concrete with respect to the same mix without steel fibres.

Micro-fibres have a typical length between 5 and 20 mm and a diameter range of around 0.1 – 0.2 mm. The use of this kind of fibres is common to increase both the tensile and the compressive mechanical properties of the material. Therefore, the volume content can be chosen up to 4% to change the microstructure of the composite. The fibres start acting once the matrix cracks. By performing the stitching of the microcracks, the creation of macro-cracks is delayed by the presence of micro-fibres (Lawler et al. 2002).

The workability of the mix results is strongly affected by the content and the aspect ratio of the used fibre. For a given volume content of fibres, the larger the aspect ratio the worse the workability.

Naaman (2003) found that the fibres, to be effective in the concrete mix, should have the following properties:

- a tensile strength significantly higher than the matrix (from two to three orders of magnitude);
- a bond strength with the matrix preferably of the same order as, or higher, than the tensile strength of the matrix;
- an elastic modulus in tension significantly higher than that of the matrix (at least three times);
- enough ductility so that the fibre does not fracture due to its abrasion or bending.

2.3.2 Mix design

The addition of fibres modifies the workability of the composite material. The creation of super-plasticizer helped the development of the self-placing concrete since the 1970s. The concrete compressive strength and the choice of the fibres have to be decided at the same time because the bonding properties depend on both. The bond stresses developed between fibres and matrix mainly depends on the compressive strength of the concrete. Commonly it is suitable to reach the slip of the fibre before reaching the maximum tensile stress of the metallic fibre. To predict the type of mechanism the critical length l_c of the fibre to be used can be individuated according to the matrix characteristics. The critical length could be determined through the pull out of a single fibre or a small group of steel fibres from the concrete matrix. Authors as Naaman (2004) and Seong-Cheol Lee et al. (2011) studied the pull-out phenomena for different surface roughness (smooth, hooked and twisted).

The steel fibres in the mix change the skeleton of the concrete and their dosage, length and diameter affect the workability. Kooiman (2000) underlines the importance of three factors in designing a SFRC mix:

- a minimum quantity of cement matrix is needed to give to the fibres the sufficient length to develop a correct anchorage;
- the length of the fibres and the diameter of the largest aggregate must be chosen together to avoid problems linked to the creation of fibre packets;
- a good workability must be reached.

The Baron-Lesage method described by Rossi (1990) is the preferred procedure to design a SFRC mix and has been used for the research projects at Polytechnique Montréal (Massicotte et al. 2000). This method consists in three phases:

1. according to the expected performance of the SFRC, the following quantities have to be fixed a priori: water/binder ratio, diameter of the largest aggregate, geometry and dimension of the fibres, desired workability and fibre percentage;
2. the best workability of the concrete mix has to be detected varying the mass ratio S/(S+G), where S refers to sand and G granulate masses;
3. if the workability found in the second phase does not correspond to the desired workability, the volume of the binder has to be changed trying to reach the workability requested, sometimes requiring the addition of superplasticizer.

2.3.3 Post-cracking tensile behaviour

The post-cracking behaviour may be described using two different approaches: stress-strain relation and the stress crack width relationship. A more particular attention will be given to the σ-w relationship (stress crack width relationship), especially because it can be easily retrieved and implemented in FE software. Mainly according to the volume content and the geometry of the fibres, the tensile behaviour can be "softening" or "hardening".

For the first case, the SFRC tensile behaviour can be divided in two different parts: pre-cracking and post-cracking behaviours. The pre-cracking segment is pretty much the same as for a plain concrete: between 0% and 40% of f_t' the concrete reacts linearly, between 40 and 90% of f_t' the relationships remains linear and the cement matrix begins to develop diffused micro-cracks, and at about 90% of f_t' macro-cracks start appearing. The matrix has to crack to allow fibres to develop bond stresses with the concrete and act as they are conceived for. Short fibres can start playing an active role – bridging micro-cracks – after the 40% of f_t', whereas long fibres need larger cracks to be able to start carrying tensile stresses. Once the matrix cracks, the concrete matrix can no more offer any tensile strength and the post-cracking behaviour of the SFRC is principally determined by the steel fibres action. The fibre contribution allows the mix to reach a softening behaviour in tension, as seen in the post-peak phase in Figure 2–2. The slope, the shape

and the strength values of the post-peak part of the curve depend on length, diameter, dosage and orientation of the fibres and it must be determined by experimental test as above described.

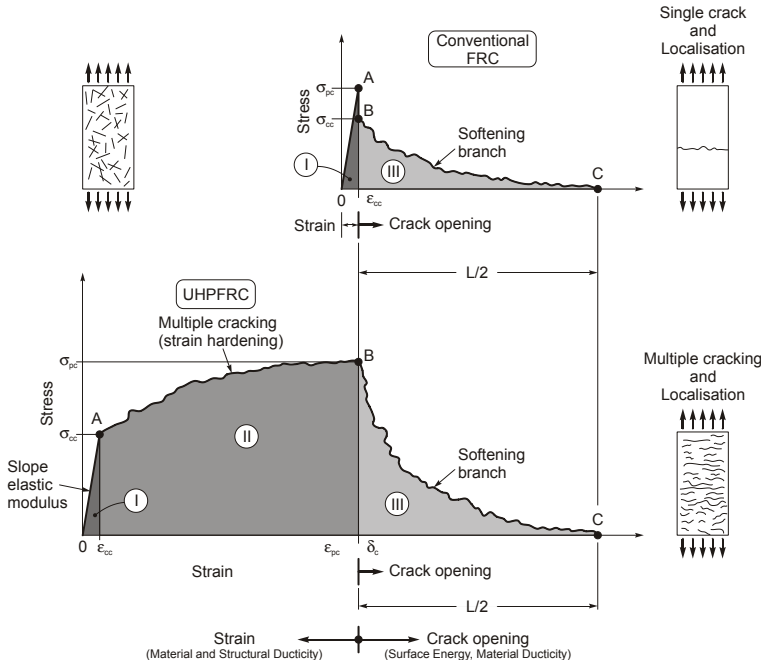

Figure 2–2: Softening and hardening tensile behaviours (Adapted from Naaman, 1996)

To obtain a “hardening” material the common dosage of fibres is higher than for the “softening” case. Typically shorter fibres are used, contribution to limit the micro-cracking of the matrix. A rather long micro-cracking phase allows the material to reach large tensile deformation and higher strength without crack localisation. In this phase the energy required to further open an existing crack is higher than the energy required to create another one. The composition of this kind of high-performance concrete – with very small water cement ratio, elevated doses of super-plasticizer, and high dosage of fibres etc. – permits to obtain very high compressive strength.

2.3.4 Aggregate and fibre bridging

The cracking behaviour of concrete mixes containing fibres is completely different than that of normal concrete. The flexural- or the shear- cracking pattern of beams made out of FRC is characterized by narrower and closer cracks than the corresponding beams without fibres. Depending on the fibre content, the brittleness of the failure can be reduced.

The tensile fracture mechanism of concrete is a complex phenomenon and still it has not been fully studied and detailed. The matrix-fibre mutual mechanism is mainly governed by:

- the aggregate bridging – that can be considered the same as for the plain concrete;
- the fibre bridging that contributes to energy dissipation in FRC concrete.

The fibre bridging can be considered always predominant for SFRC, but the final bearing in uniaxial tension is the combination of both mechanisms. Figure 2–3 shows the combination of the two mechanisms: aggregate bridging affects the tensile strength for a crack opening up to around 0.3 mm and the fibres start progressively acting once the matrix cracks. The work of fracture – individuated by the area under the stress-crack opening relation – is increased by adding fibres that dissipate energy from approximately 0.3 mm to half the length of the fibres.

The fibres act differently according to the geometry chosen. Long fibres, thanks to the elevated superficial area, develop bond stresses along the fibres. Preferred are the fibres with hooked-ends or corrugated. Their geometry permit to develop concentrated stresses that increase the bridging properties and allow reducing the fibre length to be adopted.

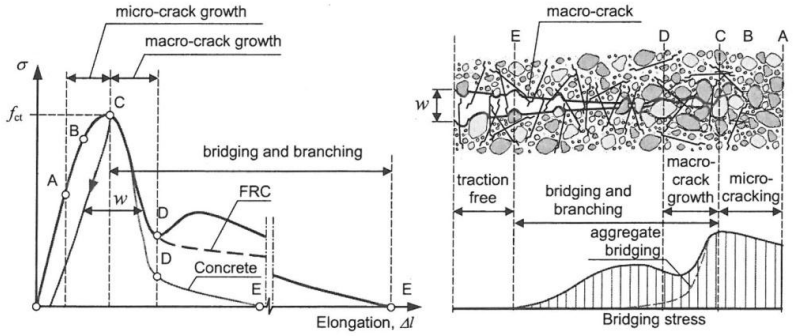

(a) Plain concrete vs. SFRC bridging stresses (b) Bridging stresses along the crack

Figure 2–3: Description of fibre and aggregate bridging mechanisms (Löfgren, 2008)

Figure 2–3 (b) shows a schematic description of the effect of the fibres on the fracture process in uni-axial tension; three distinct zones are pointed out:

- a traction-free zone, which occurs for relatively large crack opening;
- a bridging zone, where stress is transferred by fibre pull-out. For relatively small cracks even a aggregate bridging contribution can be taken into account;
- a zone of micro-cracking where the fibre contribution is quite irrelevant (for "softening" SFRC).

The contribution from fibre bridging comes gradually and it has any major influence until crack opening reaches, at least, 0.05 mm. Obviously, the kind, the mechanical characteristic, the percentage and the aspect ratio of the fibres can change the shape of this graph.

2.3.4.1 Aggregate Bridging

Aggregate bridging is the major toughening mechanism for plain concrete; an aggregate that bridges the crack until 0.3 mm works almost in the same way as fibres do. The concrete crack bridging is the coalescence of microcracks in the matrix due to the development of bond cracks between aggregate and matrix and the frictional pull-out of aggregates.

In plain concrete, in addition to aggregate bridging, many different mechanisms are involved:

- Crack shielding: the nucleation of many microcracks, around the tip of a propagating crack, has a significant influence on the propagation of the main crack. It reduces the stress intensity factors of the main crack;
- Crack deflection: at the interface of dissimilar materials the crack can arrest or advance by either penetrating the interface or deflecting into the interface (He et al., 1989);
- Crack surface roughness-induced closure: the mechanisms of crack closure arising from microscopic roughness of the fatigue fracture surfaces are not fully understood. It's known to strongly influence fatigue crack growth rates (Várkoly, 2001);
- Crack tip blunted by void;
- Crack branching: the tip of the crack shares in two different branches, the main and the secondary crack tip.

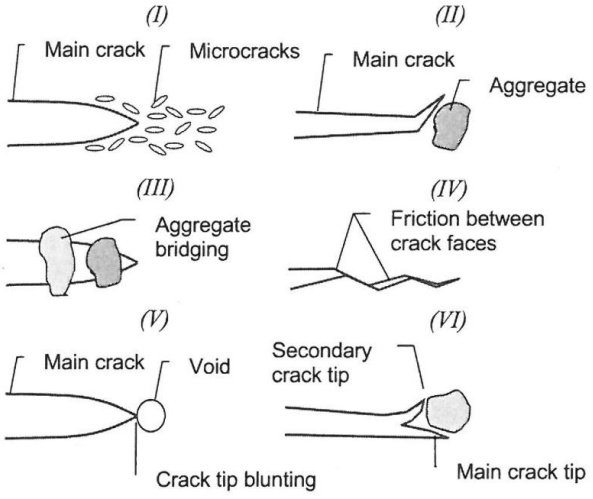

Figure 2–4: Some toughening mechanisms in plain concrete (Shah et al., 1995)

The major toughening mechanism – some of them are presented in Figure 2–4 – of plain concrete is the aggregate bridging and a lot of experimental and numerical observations support this hypothesis. In particular, several researchers have investigated the effect that aggregates play changing the type, the size, the shape and the volume fraction. It has been observed that, even before any stresses have been applied, pre-existing microcracks exist within the concrete, and this is due to the internal restrain caused by the aggregate and both shrinkage and thermal deformations.

2.3.4.2 Fibre Bridging

The fibre bridging, like the aggregate one, depends on many parameters and, for simplicity, an isolated fibre is investigated along a crack. The fibre contributes to dissipate energy through the following mechanisms:

- matrix fracture and matrix spalling;
- fibre-matrix interface debonding;
- post-debonding friction between fibre and matrix (fibre pull-out);
- fibre fracture;
- fibre abrasion
- plastic deformation (or yielding) of the fibre.

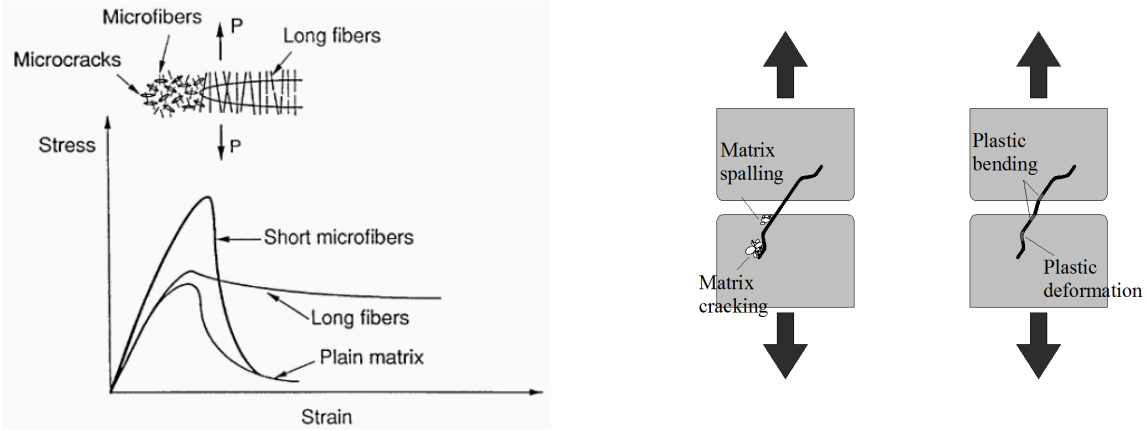

(a) Long and short fibre mechnisms (b) Different fibre bridging components

Figure 2–5: Fibre bridging mechanisms

The mechanical behaviour of SFRC mainly depends on:

- the amount of fibres;
- the orientation of the fibres;
- the pull-out versus load (or load-slip) behaviour of the individual fibres.

Orientation of fibres

The preferential orientation of steel fibres is due principally to two issues (Rossi, 1988):

- casting process of the SFRC;
- effects related to the flow of the concrete mix.

When the SFRC is cast into formwork, reinforcing bars or any potential obstacle to concrete flow, the shape of the formworks and the direction of the casting are the main factors affecting the orientation of the fibres in the structure. Rebars or stirrups can disturb the passage of fibres creating packets of fibres hardly covered by a sufficient quantity of concrete matrix. The vibration of the SFRC is not recommended because of the preferential direction of the fibres that its utilisation risks to cause. A problem of segregation caused by elevated specific weight of the fibres has to be eliminated with a rational choice of the fibre type (for example, a bigger specific

surface can increase the contact with the matrix and so limits the segregation of the fibres). The fibres tend to dispose parallel to the concrete flow.

For the specific case of casting a slender beam, the flow of the concrete has to be parallel to the length of the beam to try to arrange the fibres orthogonally to the development of the cracks. Behloul (1996) suggested slowing down the casting of the concrete to avoid any turbulence phenomena, which can provoke changes in the fibre preferential orientation. Mansur (1999) demonstrated that orientations of the fibres does not have any considerable effects on E, ν and f_c' in compression behaviour.

The behaviour in traction of a SFRC is however strongly influenced by the orientation of the fibres. Oesterlee (2010) and Van Mier et al. (2002) studied the stress crack opening relationships varying the angle of the bridging fibres in the crack.

Delsol (2012) pointed out the importance of the orientation of fibres in traction in both pre-peak and post-peak tensile behaviour. For the bending behaviour Behloul (1996) stated that fibres not correctly oriented might became defects of the structure causing a crack development along the fibre direction. Moreover, fibres well oriented orthogonally to the cracks might increase up to three times the final flexural bearing resistance. Behloul studied the bending behaviour of 5 beams with different preferential angle of fibre orientation. For a range between 45° and 90° – the angle is calculated between the direction of the fibre and the direction of the force causing the crack – the bending behaviour may be considered pseudo-brittle; for angles of about 45° a plateau in the SFRC tensile response starts being seen; and for higher angle values flexural strength and the hardening response increase.

Fibre pull-out

The fibre pull-out behaviour is the gradual debonding of an interface surrounding the fibre, followed by frictional slip and pull-out of fibres.

In particular, the pull-out depends on the type and the mechanical/geometrical properties of fibres, on the mechanical properties of the interface between fibre and matrix, on the angle of inclination of fibres with respect to the direction of loading and on the mechanical properties of the matrix. A large amount of literature covers this subject.

The bond (responsible of the forces transmission between fibre and matrix) has different components:

- the physical and/or chemical adhesion between fibre and matrix;
- the frictional resistance;
- the mechanical component (arising from the fibre geometry, e.g. deformed, crimped or hooked-end);
- the fibre-to-fibre interlock.

Several pull-out models exist, the simplest ignore the elastic stress transfer and the matrix deformation (Hillerborg, 1980 and Wang, 1989) while other models assume elastic interfacial shear bond stresses that gradually change into frictional forces because of the debonding of the interface. The debonding criterion can be described with two different approaches:

- strength-based criterion (or stress-based) where it is assumed that the debonding initiates when the interfacial shear stress exceeds the shear strength;
- fracture-based criterion that considers the debonding zone as an interfacial crack together with the evaluation of fracture parameters and energy consideration.

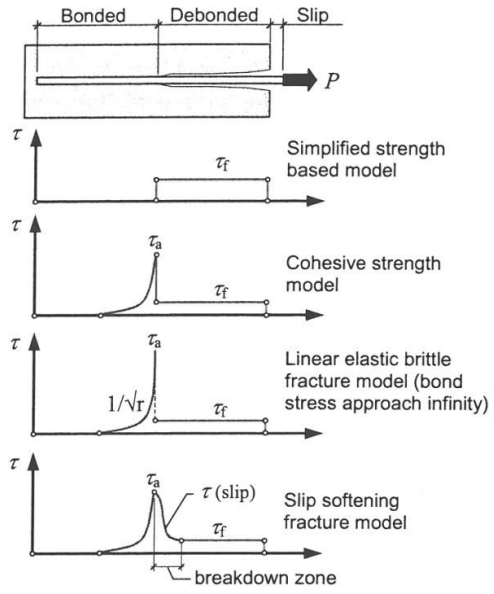

Figure 2–6: Different debonding models for fibre pull-out (Löfgren, 2008).

Once debonding has taken place, stress transfer develops owing to frictional resistance that, in its turn, can be described, as presented in Figure 2–6, with the following different relationships: constant friction, decaying friction (or slip softening) or slip hardening friction. In the literature, there can be found huge differences on the interfacial shear bond strength, ranging from 1 up to 10 MPa (Minelli, 2005); moreover interfacial shear friction capacity (ranging from 0,5 to 20 MPa) makes the correct interpretation of the pull-out test difficult (Löfgren, 2005). The dissipated energy is equal to the area beneath the load-displacement (slip) curve. The pull-out energy (both debonding and friction) increases with the embedment length, unless the embedment becomes too long and the fibre breaks, and depends on the end of the fibres (crimped, straight, hooked, etc.) as shown in Figure 2–7.

The behaviour of different fibres during the pull-out test depends on both their mechanical and geometrical properties, as well as on their chemical affinity to the matrix.

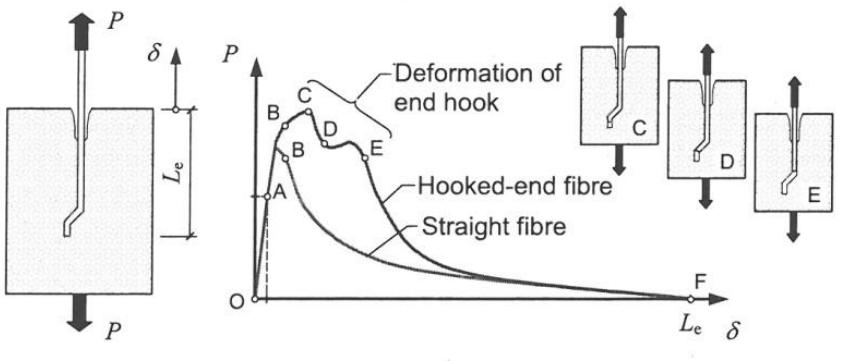

Figure 2–7: Typical fibre pull-out relationship between end-slip and load (Löfgren, 2005)

When the fibre is not perpendicular to the concrete block, the pull-out energy is also influenced by the angle of inclination, and, in this case, it is related to the matrix strength.

It is well known that a fibre-reinforced concrete consists of several fibres which, in most cases, have random orientation. Throughout this observation, Bentur and Mindess (1990) explained that the process of debonding and pull-out is quite different in an actual fibre-reinforced specimen compared to a simple pull-out test on a reinforcing bar. It is also important to note is that the pull-out behaviour and maximum load depend upon the spacing of the fibres.

2.4 Experimental characterisation of the mechanical properties of FRC

There is not any theoretical approach that can give the post-cracking behaviour of a SFRC knowing only the composition of the SFRC mix at issue. This is a big limitation that forces to determine tensile properties using different experimental tests. Even if the steel fibres mostly affect the post-peak tensile behaviour, the composition of the concrete matrix depends on several variables such as aggregates, cement, sand and the various other adding that avoid predicting the post-cracking relation with a sufficient level of accuracy.

1. The uniaxial tension test or direct tensile test (UTT) (RILEM, 2001) can retrieve directly the tensile behaviour in term of stress-crack opening. This test requires specialized equipment and most of the times it is difficult to control the stability of the specimen during the test. Moreover, this test requires highly trained and experienced personnel and it is rarely used.
2. Bending test are usually preferred due to the simplicity and the result reliability provided. Three point bending test or notched beam test was proposed by RILEM and describes the tensile behaviour by means of the relation "load mid-span displacement" of a notched prismatic beam. The results tend to overestimate the actual properties of the material due to the preferential orientation of the fibres and for the presence of the notch that focus the specimen to fail trough the reduced cross-section. The test provides: limit of proportionality, the residual and the equivalent flexural tensile strengths (EN 14651, 2005). Moreover, inverse analysis techniques allow determining the σ-w relation from P-CMOD results obtained (Nour et al, 2012).
3. Four-point bending test can be performed either on un-notched or notched beams depending on the guidelines followed. A 150 mm span between the two punctual loads permits to develop a constant bending moment in a larger zone at the centre of the beam. This mechanism makes the specimen fail in the actual weakest cross-section. With this test the calculation of crack openings present a lot of difficulties.
4. ASTM C1550 (2012) proposed a bending test on a centrally loaded round panel placed on three fixed supports. This test offers a little scatter in results. The 2D-random orientation of the fibres and the big volume of concrete involved lead to reliable results. Results are expressed in terms of P-Δ (central displacement) and the measurement of the crack openings

is feasible. Inverse analysis can be applied on resulting P-Δ relation to obtain σ-w properties (Nour et al, 2012).

5. Wedge splitting test does not require sophisticated equipment and has a good reproducibility. It might be carried out to evaluate fatigue crack growth, stress-crack opening relation or fracture properties of different concrete mix. The scatter showed in the results of this test is generally lower than the scatter of the previous two tests presented.
6. Double edge wedge splitting test has been proposed by di Prisco et al., 2013. The specimens needed to carry out this test present two wedge shaped grooves that accommodate the loading device. A compression load is applied and, due to the cut geometry of the two edges, a pure mode I fracture is produced.

Comparing the energy absorbed up to a predefined crack opening, Lambrechts (2003) studied the scatter exhibited by various tests. An average scatter of about 10% and 18% was found respectively for round panel and notched beam tests. Similar results were found for the notched beam tests by Bastien (2004) and Bélanger (2000). Results presented in the Appendix "A" of this document highlight the same average scatters.

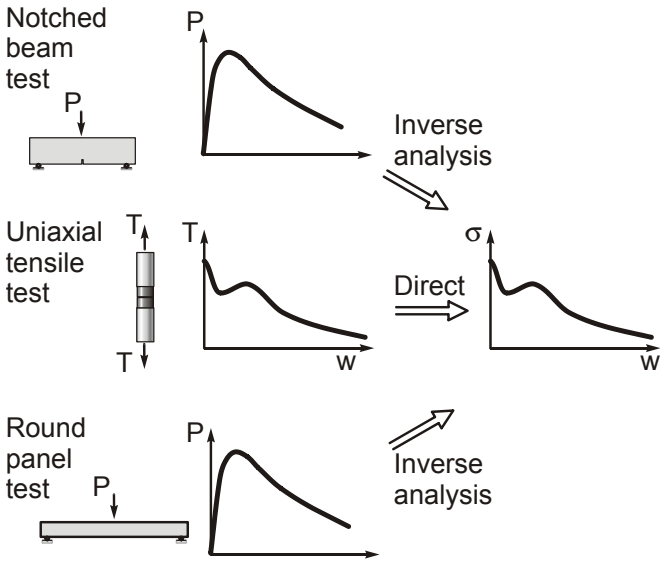

Figure 2–8: How to determine the σ-w relationship (de Montaignac et al, 2012)

2.5 FIB Model Code overview

2.5.1 Introduction

It has been said previously that the lack of an accepted design code for SFRC has limited the use of steel fibres for load-bearing structure. The technical groups FIB TG8.3 and FIB TG 8.6 have collaborated to the writing of new guidelines in the FIB Model Code 2010 (FIB, 2012) related to the design of SFRC structures. These design guidelines aim at synthesizing research findings, defining new research directions and producing design recommendations. The final goal of this model code is to develop a design code that will give to designers an easy and reliable guideline to follow.

In this paragraph, only principles related to SFRC with a softening post-cracking behaviour will be discussed. It will be presented: how FIB Model Code describes the constitutive law in uniaxial tension, the choice of the characteristic length l_{cs} and some basic aspects for design approach.

2.5.2 Tensile behaviour

The FIB model code, as the majority of other guidelines, has chosen to deduce the post-cracking behaviour by the notched beam test. From this bending test, it is possible to identify the residual flexural tensile strength f_{Ri} as the EN 14651 has defined: "f_R is the fictitious stress at the tip of the notch which is assumed to act in an uncracked mid-span section, with linear stress distribution, of a prism subjected to a centre-point load F_j corresponding to $CMOD_j$ (j=1,2,3,4)". Accordingly to the test, the different $CMOD_j$ correspond to 0.5, 1.5, 2.5 and 3.5 mm.

$$f_{R,j} = \frac{3\,F_j\,l}{2\,b\,h_{sp}^2} \tag{2.1}$$

where

$f_{R,j}$ is the residual flexural tensile strength corresponding to $CMOD_j$ $(j = 1,2,3,4)$

F_j is the load corresponding with $CMOD_j$ $(j = 1,2,3,4)$

l is the span length, in millimetres

b is the width of the specimen, in millimetres

h_{sp} is the distance between the tip of the notch and the top of the specimen, in millimetres

To determine the simplified strength-crack opening relation the model code chose to fix two crack openings corresponding to SLS and ULS. For serviceability limit state $CMOD_1$ will be considered and $CMOD_3$ controls the ultimate limit state. The values may be chosen differently from 0.5 and 2.5 (as suggested by EN test procedure) according to design considerations.

Two simplified stress-crack opening constitutive laws may be deduced: rigid plastic behaviour or a linear post-cracking behaviour.

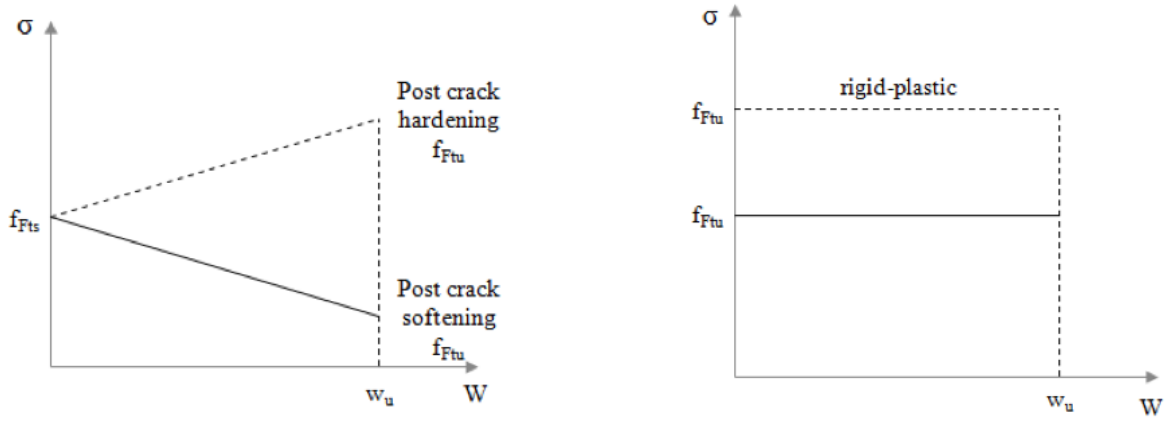

(a) Softening or hardening σ-w relations (b) Rigid-plastic σ-w relation

Figure 2–9: Post-cracking simplified models (FIB Model Code, 2012)

f_{Fts} represents the serviceability residual strength, defined for a crack opening value that represents a SLS analysis and the f_{Ftu} represents the ultimate residual strength for a ULS analysis:

$$f_{Fts} = 0.45\, f_{R1} \tag{2.2}$$

$$f_{Ftu} = f_{Fts} - \frac{w_u}{CMOD_3}\,(f_{Fts} - 0.5\, f_{R3} + 0.2\, f_{R1}) \quad \text{(Softening behaviour)} \tag{2.3}$$

where

f_{R1} is the residual flexural tensile strength corresponding to a $CMOD$ of 0.5 mm

$CMOD_3$ is the crack mouth opening corresponding to 2.5 mm

w_u is the maximum crack opening accepted in structural design and should not exceed 2.5 mm

$$w_u = \varepsilon_{Fu}\, l_{cs} \tag{2.4}$$

where

ε_{Fu} is assumed to be equal to 2% for variable strain distribution in cross section and 1% for only tensile strain distribution

l_{cs} is the structural characteristic length

$$l_{cs} = min\{s_{rm}, y\} \tag{2.5}$$

where

s_{rm} is the mean crack spacing

y is the distance between the neutral axis and the tensile side of the cross section

Two requirements have to be fulfilled if the fibre reinforcement partially or entirely substitutes the ordinary reinforcement in ultimate state:

$$f_{R1k}/f_{Lk} > 0.4 \tag{2.6}$$

$$f_{R3k}/f_{R1k} > 0.5 \tag{2.7}$$

where

f_{Lk} is the limit of proportionality.

2.5.3 Stress-strain relationship:

Considering softening material, the definition of the stress-strain law is based on the individuation of the characteristic length of the structural element l_{cs} (as introduced in the previous equation). Two stress-strain relations are proposed by FIB.

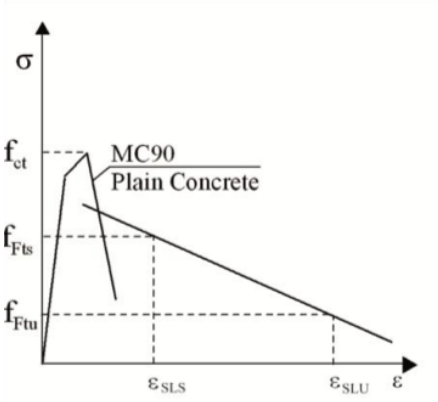

Figure 2–10: Simplified stress-strain relationship (di Prisco, 2009)

Up to the peak strength f_{ct}, the law follows the same relationship obtained for plain concrete. The post-cracking behaviour is simplified as a bilinear relation taking the strength, as defined previously, f_{Fts} and f_{Ftud} corresponding to strains ε_{SLS} and ε_{ULS}.

$$\varepsilon_{SLS} = {CMOD_1}/{l_{cs}} \tag{2.8}$$

$$\varepsilon_{ULS} = {w_u}/{l_{cs}} = min\left(\varepsilon_{Fu}\,, {2.5}/{l_{cs}} = {2.5}/{l_{cs}}\right) \tag{2.9}$$

with ε_{Fu} = 2% for variable strain distribution along the cross section and 1% for only tensile strain distribution along the cross section.

2.5.4 Classification of the SFRC following the FIB Model Code

The strength interval is defined by an acronym as the example presented in the Figure 2–11. The first number indicates the residual strength corresponding to a small value of crack width (0.5 mm) and the following letter *a*, *b*, *c*, *d* corresponds to the slope determined by f_{R3k}/f_{R1k} – where the f_{Rik} represents the characteristic value of the residual flexural tensile strength calculated by Equation 2.1.

- ***a*** if $0.5 \leq f_{R3k}/f_{R1k} \leq 0.7$;
- ***b*** if $0.7 \leq f_{R3k}/f_{R1k} \leq 0.9$;
- ***c*** if $0.9 \leq f_{R3k}/f_{R1k} \leq 1.1$;
- ***d*** if $1.1 \leq f_{R3k}/f_{R1k} \leq 1.3$;
- ***e*** if $1.3 \leq f_{R3k}/f_{R1k}$.

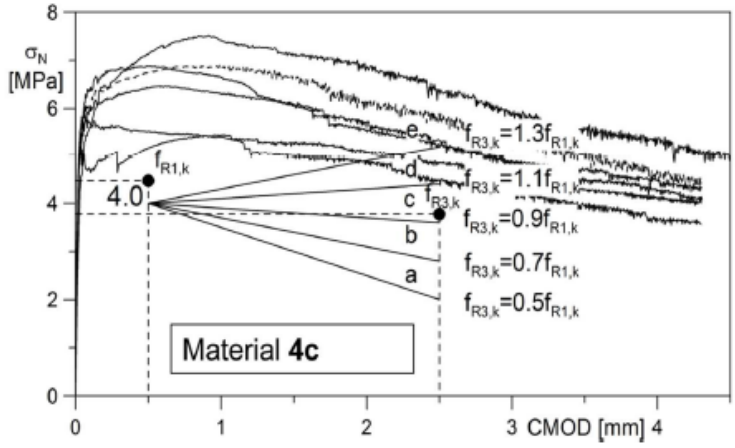

Figure 2–11: Classification of SFRC (Model Code 2010)

2.5.5 Partial safety factors

The choice of a safety coefficient should take into account (di Prisco, 2009):

1. the representativeness of the specimens used to characterize the mechanical response of the material, in relation to the structure considered;
2. the number of specimens used for mechanical characterisation;

3. the stress redistribution capacity of the structure under consideration;
4. the fractured volume involved in the failure mechanism.

For massive structure the fib model code, simplifies these aspects by considering a partial safety factor equal to 1.5 for cracked SFRC section. The volume of the specimen tested must be representative of structural member, if not, different tests have to be carried out.

$$f_{tsd} = {}^{f_{tsk}}/_{\gamma_s} \text{ and } f_{tud} = {}^{f_{tuk}}/_{\gamma_f} \tag{2.10}$$

2.5.6 Orientation factor

Generally isotropic fibre distribution is assumed for a structural member, so an orientation factor is taken equal to 1. The FIB model presents the possibility to take an orientation coefficient bigger or smaller than 1, but in both cases, the choice of the coefficient must be experimentally verified.

$$f_{Ftsd,mod} = {}^{f_{Ftsd}}/_{K} \text{ and } f_{Ftud,mod} = {}^{f_{Ftud}}/_{K} \tag{2.11}$$

2.5.7 Design approach in flexure

In load bearing SFRC structures, generally the use of steel fibres is accompanied by the rebars. In this case steel fibres provide only an additional reinforcement.

Referring to bending, ULS is reached when one of the following conditions is reached:

- attainment of the maximum compressive strain ε_{cu};
- attainment of the maximum tensile strain in the steel reinforcement bar (if present) ε_{su};
- attainment of the maximum tensile strain in the FRC, ε_{Fu}.

The ultimate bending moment can be evaluated by means of the rotation and translation equilibrium equations, under the following assumptions:

- sections remain plane;
- perfect bond conditions are assumed between steel bars and surrounding concrete;
- the tensile stress in SFRC are derived from the design stress–strain relationship;
- for the compressive stresses, the equations used for plain concrete can be also applied to SFRC.

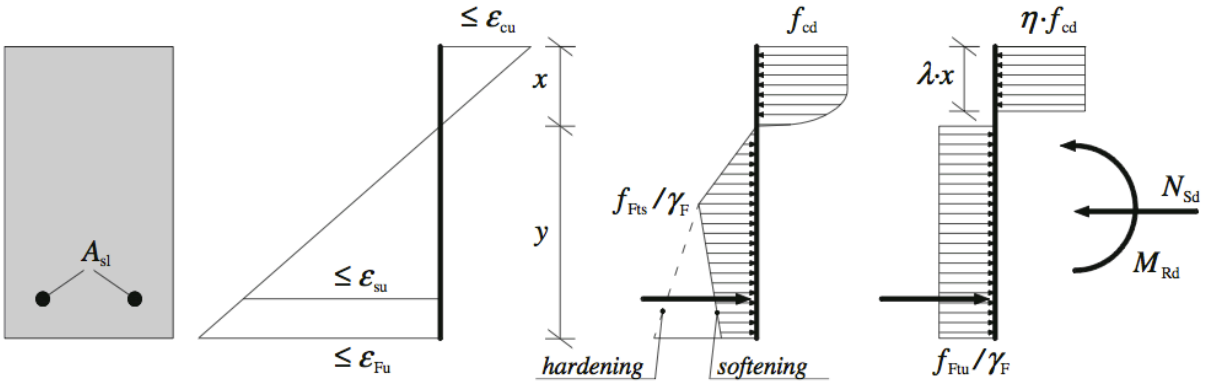

Figure 2–12: Design stress distribution according to fib MC 2010

2.5.8 Design approach in shear

The total shear resistance is calculated as the sum of the contribution of the concrete as well as the shear reinforcement. With respect to the design of a conventional concrete without fibre, the contribution given by shear reinforcement and concrete are the same; the steel fibres provide the new contribution V_{Rd}:

$$V_{rd,F} = \left\{ \frac{0.18}{\gamma_c} \cdot k \cdot \left[100 \cdot \rho_1 \cdot \left(1 + 7.5 \cdot \frac{f_{Ftuk}}{f_{ctk}} \right) \cdot f_{ck} \right]^{\frac{1}{3}} + 0.15 \cdot \sigma_{cp} \right\} \cdot b_w \cdot d \qquad (2.12)$$

where

γ_c is the partial safety factor for concrete without fibre

k is a coefficient that takes into account non-uniform self-equilibrating stresses leading to reduction of leading force

ρ_l is reinforcement ratio for ordinary rebar

f_{ctm} is the mean concrete tensile strength

$f_{ck,cyl}$ is the equivalent cylinder compressive strength

σ_{cp} is the average stress acting on the concrete due to loads or the prestressing force

b is the width of the cross section

d is the effective depth of the cross-section.

The code also defines a minimum value for the shear resistance:

$$V_{Rd,Fmin} = \left(v_{min} + 0.15\sigma_{cp}\right) \tag{2.13}$$

where $v_{min} = 0.035\, k^{3/2}\, f_{ck,cyl}^{1/2}$

2.5.9 Crack width

Design crack width can be specified to satisfy requirements according to functionality, durability or appearance. The condition to be satisfied is $w_d \leq w_{lim}$ where w_d denotes the design crack and w_{lim} is the nominal limit value of crack width. For SFRC the design crack is calculated as:

$$w_d = \frac{1}{2}\left(\frac{\phi_s}{\rho_{s,ef}}\right)\frac{(f_{ctm} - f_{Fts})}{\tau_{bm}}\,(\sigma_s - \beta\,\sigma_{sr})\,\frac{1}{E_s} \tag{2.14}$$

where

τ_{bm} is the mean bond strength between reinforcement bars and concrete

$\rho_{s,ef}$ is the effective steel reinforcement ratio

σ_s is the actual steel stress

β is an empirical coefficient for assessing the mean strain over the length over which slip between concrete and steel occurs

σ_{sr} is the maximum steel stress in the crack at crack formation stage

2.6 SFRC applications

2.6.1 Contributions to the structural behaviour

Steel fibres started to be used in bridge deck applications in the last few years. Steel fibres are used mainly prevent cracks, to reduce or simplify the steel reinforcement of the slab or to reduce the stress range in the reinforcement due to cyclic loads. Five bridge decks have been built in the last 15 years in Québec (Massicotte et al., 2014). Moreover, field-cast UHPC details connecting prefabricated structural elements used for bridge construction have proven to be a good solution for highway deterioration, repair and replacement (Graybeal, 2014).

In the last few years deeper and larger studies of the use of steel fibres for structural purposes have been conducted. The fib-ACI international workshop on the fibre reinforced concrete showed up the most recent innovative use of the FRC in the structural applications (Faggio, 2014).

- Steel fibres are used for the construction of footbridges, longitudinal joints between precast concrete beams, longitudinal joints connecting the concrete slab and steel beams in mixed bridge structures, and concrete barriers. The main advantages in this domain are: a better resistance to fatigue cyclic loads, a significant reduction of both crack spacing and openings, a simplification of the secondary steel reinforcement and an increased ductility of the structure.
- Steel fibres could offer a better confinement for rebars, a better ductility face to elevated seismic loads, and a reduction of the quantity of the reinforcement used. These are the main advantages the fibres could offer to beams, prestressed beams, columns, slabs and coupling beams used in civil constructions.
- Fibres used for foundations improve the post-cracking tensile behaviour, assure a better durability, better resistance to the plastic shrinkage and reduce the possibility of human errors during the casting process.

- Steel fibres are used for precast tunnel linings mainly to improve the tensile characteristics, to better control the cracking process and reduce the reinforcement.

(a) Museum of European and Mediterranean Civilisations

(b) Footbridge over the Ovejas (Serna et al., 2014)

(c) Wind towers

Figure 2–13: Existing fibre applications

In the last few years the use of SFRC has extended to many areas where high early strength and ductility are important. The large number of research works should be accompanied by design code that can be more easily used by civil engineers who still do not know the real performances and capacity of this new material. The works presented during the International Workshops held

in Montreal in 2014 (FRC 2014) showed the great knowledge of the capacities of FRC and the need to put it into a design code in the next years.

2.7 EPM3D

2.7.1 Introduction

Numerical analyses represent a good alternative to predict structural behaviour and failure mechanisms face to the elevated costs for experimental tests. If properly used and implemented a finite element analysis could provide more and essential information to integrate and strengthen the calculation done in the design phase.

Concrete is a complex material that exhibits nonlinear behaviour even under small stresses level, so the development of a robust constitutive model requires elevated experience and competences. Massicotte et al. (1990) developed a nonlinear constitutive model for concrete structure limited to biaxial state of stresses and in 1995 Bouzaiene and Massicotte extended that model to triaxial state of stresses. The constitutive model has been made portable for the first time in FORTRAN language for educational software NISA and MEF. Ben Ftima in 2004 made the constitutive model portable for software ANSYS (v 7.1), ADINA (v 8.1) and ABAQUS (v 6.4). The tension stiffening implemented has been improved after the works made by Nour et al, 2005. Since then various versions have been developed (*figure* 2-14): EPM-v1.0 was implemented for both standard and explicit nonlinear computations, EPM3D v2.0 and EPM3D v3.0 were developed only for explicit version. The third version of EPM3D v2F has introduced the possibility to study SFRC structures, but both normal concrete and fibre reinforced concrete can be analysed in the same model only with the last version v3.3.

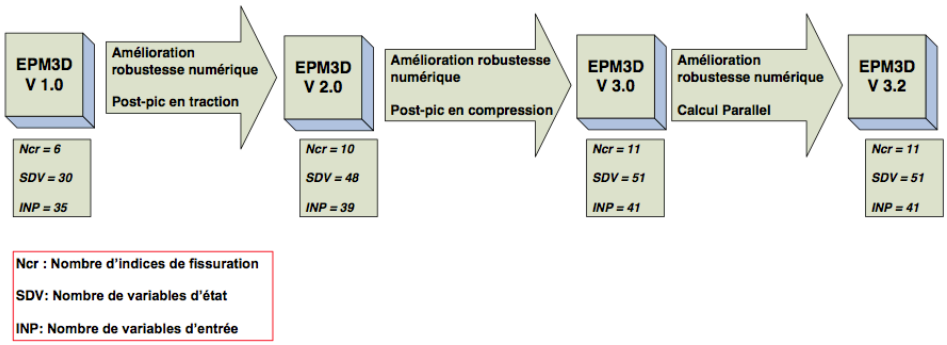

Figure 2–14: EPM3D versions (Ben Ftima, 2013)

2.7.2 ABAQUS/explicit

The first version of EPM3D was implemented both for standard and explicit resolution approaches. The model demonstrated immediately to be reliable and high performing and its use was expanded to structure with high-level of complexity in terms of materials, contacts and dimensions. The standard solution method demonstrated to have problems in memory space cost and time of solution, so that, it has been decided to develop the following of EPM3D versions only for explicit procedure. Explicit resolution considers the entire process dynamically; even a static analysis is processed through the evolution of a virtual time that might be considered not real. This procedure was born, and it is still well performing, for the study of dynamic processes and it is based on the resolution of Newton's equation:

$$M\ddot{u} = P - I \tag{2.15}$$

where M is the mass matrix, P is the vector of external forces, I is the vector of internal forces, and $\ddot{u}$ is the vector of node accelerations; $M\ddot{u}$ represents the force vector due to material inertia. The inversion of mass matrix does not cost a lot in terms of time and memory because it is a diagonal matrix. After having inverted M, the calculation of the nodal acceleration vector is done and the dynamic analysis can take place by successive integrations using a prearranged time interval chosen in order to allow the stability of the calculation. The absence of iterations makes

this procedure different from standard one. In sequence vectors representing velocity and displacement are calculated using central difference integration without any iterations. This integration rule is only conditionally stable and the convergence of the solution depends on the time interval. A time increment too big would lead to the instability of the solution. Consecutively the increments of deformations, stresses and internal forces at $t + \Delta t$ can be calculated.

The maximum stable time increment is $\Delta T_{stable} = {}^{2}/_{\omega_{max}}$, where ω_{max} is the largest natural circular frequency of the structure. Its value is not easy to determinate. Assuming that ω_{max} is smaller than the maximum natural frequency of the smallest finite-element of the model, the stable time interval can be computed as $\Delta T_{stable} = {}^{L_e}/_{C_d}$, where L_e is the length of the smallest element of the model and C_d is the wave propagation velocity within the material.

The choice of the time increment might be made either automatically by the software or user-defined if the analysis has special computational needs.

2.7.3 Analysis quasi-static

The analyses done in this thesis are not dynamics and the explicit procedure requires the definition of loads, constraints and boundary conditions according to a virtual time. During the analysis, loads and boundary conditions have to be applied to the structure to not cause any dynamic instability. To succeed in keeping a quasi-static analysis Abaqus proposes to do a preliminary frequency analysis of the structure. Using an analysis time 10 times bigger than the largest natural frequency of the structure – determined by the frequency analysis – would enable a quasi-static analysis. A dynamical instability could be identified looking at the resulting values of energy ratio ${}^{E_c}/_{E_I}$, where E_c is the kinetic energy and E_I is the internal energy. A user-defined limit value equal to 5% must not be exceeded throughout the whole analysis. Also the application of the loads must be done smoothly, avoiding concentration of waves that propagate along the structure disturbing the significance of results.

Figure 2–15 represents the standard evolution of the energy during a finite-element analysis of a concrete structure such the ones studied in this thesis. The user defines the total virtual time T_C. From 0 to t_1 the analysis begins dynamically and the waves of the applied loads propagate

through the structure up to reach the boundary conditions; in this phase it is important to maintain a linear behaviour of the structure. After the first phase the energy ratio might be considered equal to zero up to the first cracking in the structure, the appearance of multiple cracks causes few peaks in energy ratio that have to be maintained below the ratio limit chosen. This phase evaluates till the failure of the structure, which causes a sudden increasing of the dynamic energy making the analysis completely unpredictable. Every peak in the second phase of energy diagram may be used to individuate the values of loads that correspond to the appearance of cracks in the structure. It is important to note that the value of energy limit of 5% is only a suggestion.

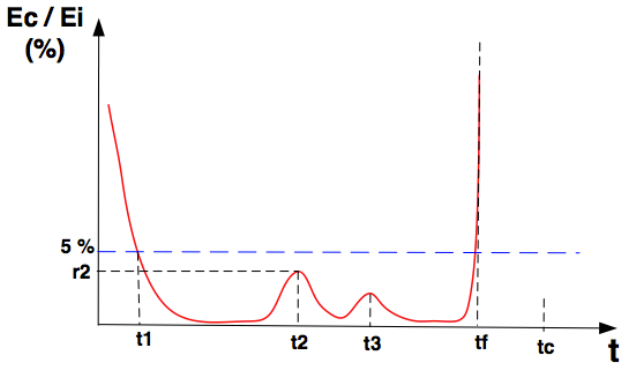

Figure 2–15: Energy evolution

2.7.4 Choice of finite-element

The explicit procedure limits the choice between the possible finite element types. Ben Ftima (2013), implementing the constitutive model, individuated two kind of element as the most adapt for concrete structure analyses: C3D8R and C3D10M. The first kind of element is the one used for the analyses of this thesis and it is a 8-node hexahedral element with reduced integration, with the relaxed stiffness as hourglass control technique activated. With this element type is important to keep constantly the energy ratio E_H/E_I under 5%, where E_H is the energy consumed by hourglass control and E_I for the total internal energy. The second kind of element has tetrahedral form with 10 nodes and complete integration system.

For modelling the reinforcement elements, ABAQUS gives the possibility to use 2D or mono-dimensional elements. The analyses in this thesis have been realized using mono-dimensional finite elements. This choice allows modelling separately concrete and reinforcement without the necessity to have all the coincident nodes of elements.

2.7.5 INPUT parameters

All the information presented herein refers to the version v-3.2. EPM3D manages the introduction of concrete characteristics by a worksheet that resumes about 61 different factors to characterise the concrete material to be directly modelled in ABAQUS. Most of them are related to the reinforcement (conventional or fibre). Concrete parameters can be defined only with f_c'. Only the topics that had a crucial importance during the cases of this thesis will be discussed in this section.

2.7.5.1 Post-peak in compression

The post-peak behaviour in compression is linearly described by two user-defined parameters: the slope of the relation and the residual concrete strength – expressed as a % of the characteristic f_c'.

- Aubrée (2014) permitted to determine a reliable value for the post-peak slope.
- The suggested value for the residual compressive strength is 0.2 f_c'

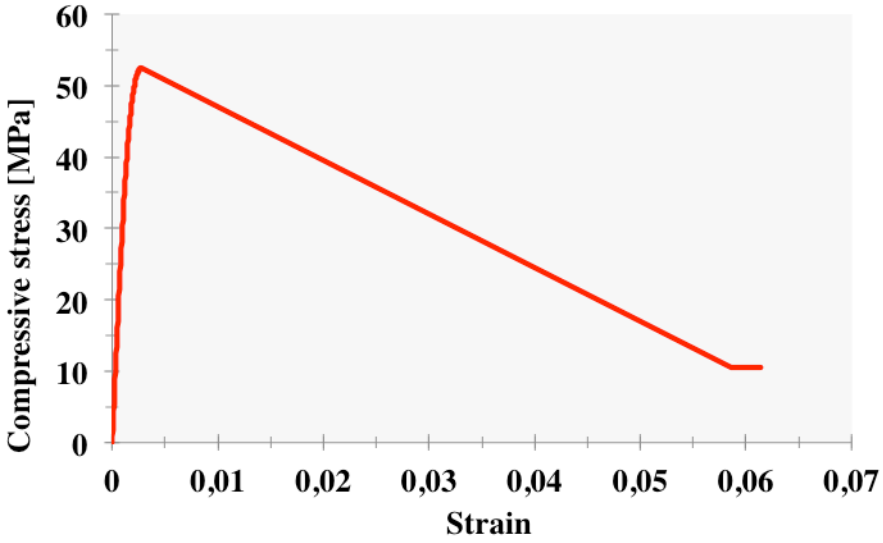

Figure 2–16: Compressive post-peak evolution

2.7.5.2 Tensile behaviour

Plain concrete

Constitutive model developed for a continuum could follow different approaches: micro-plane model, smeared crack models, discrete crack models, elasto-plastic models like Willam-Warnke model, damage models or non-linear models calibrated with experimental results from tension and compression tests.

The tensile behaviour of the concrete is described using the smeared crack approach, used for the first time by Rachid (1968). This model permits a simpler implementation in finite element software than the one needed for discrete crack approach. This technique is based on the energy concept and model cracks providing a stress-strain relation. Hence, the cracks are supposed to be uniformly propagated in the concrete. A quasi-linear relation up to the cracking stress provides to plain concrete the tensile behaviour in pre-cracking phase, a softening exponential relation represents the post-cracking behaviour up to the ultimate strain state for which the crack cannot transmit any tensile stress.

$$\sigma_t = f_t \cdot exp\left(-\frac{\varepsilon - \varepsilon_e}{\varepsilon_a}\right) \tag{2.16}$$

$$\varepsilon_a = \frac{G_{f1}}{h_t \cdot f_t} \; ; \; G_{f1} = G_f - \frac{h_t \cdot f_t^2}{2 \cdot E_0} \; ; \; \varepsilon_e = \frac{f_t}{E_0} \tag{2.17}$$

G_f represents the fracture energy consumed by crack per unit of surface, h_t is the representative dimension of the mesh chosen for the model and is the equivalent tensile length for which the displacement due to cracking propagation is uniformly distributed. G_f is a user-defined variable and h_t is automatically given by Abaqus.

The smeared approach used does not allow detecting directly the actual crack opening, but it only permits to represents the average behaviour of the concrete structure in tension.

Steel Fibre Reinforced Concrete

Constitutive models for SFRC can be classified in macro-models and micro-models according to the scale in which they are defined. The model implemented in EPM3D is a macro-model and the SFRC is represented as a unique material with average properties. The tensile post-cracking behaviour is determined by using a $\sigma - w$ relation. This relation can be obtained carrying out a direct traction test or indirectly obtained through an inverse analysis from bending test results.

The advantage of this phenomenological approach is the use of material information at the relevant scale for the analysis of the structure. The main drawback is the need of extensive and costly experimental tests.

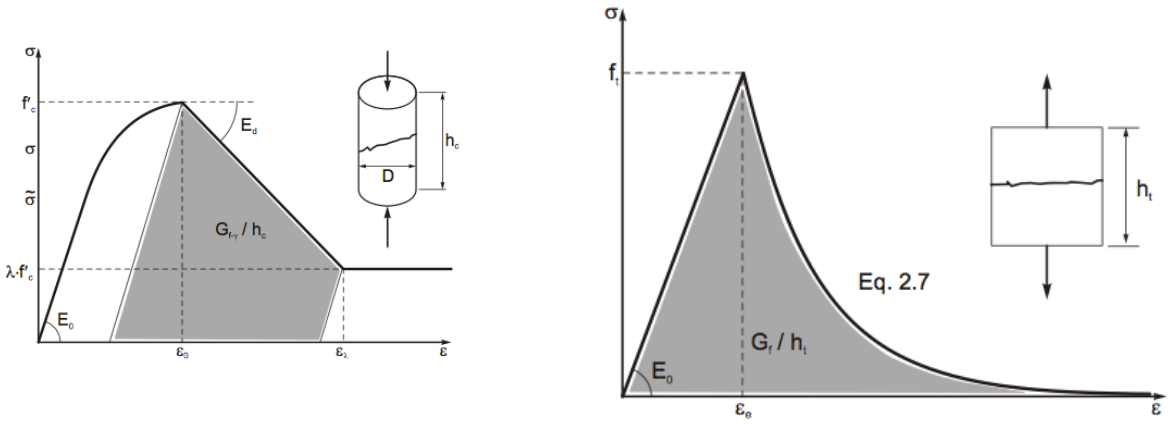

(a) Typicall stress-strain curve for an element in compression

(b) Typicall stress-strain curve for a plain concrete element in tension

Figure 2–17: Compressive and tensile typical fracture energies

The tensile behaviour of a SFRC concrete might be divided into two different phases: the pre-peak part and the post-cracking phase. The first part is described as for a plain concrete by a quasi-linear behaviour. It is modelled by introducing directly the values E_c and f_c'; it is assumed that fibres do not have any relevant contribution up to the cracking stress. After reaching the maximum tensile strength, EPM3D allows the user to introduce the crack width-stress relation. The $\sigma - w$ retrieved from the experimental tests can be simplified choosing between three possible relations – two of the three are represented in Figure 2–18.

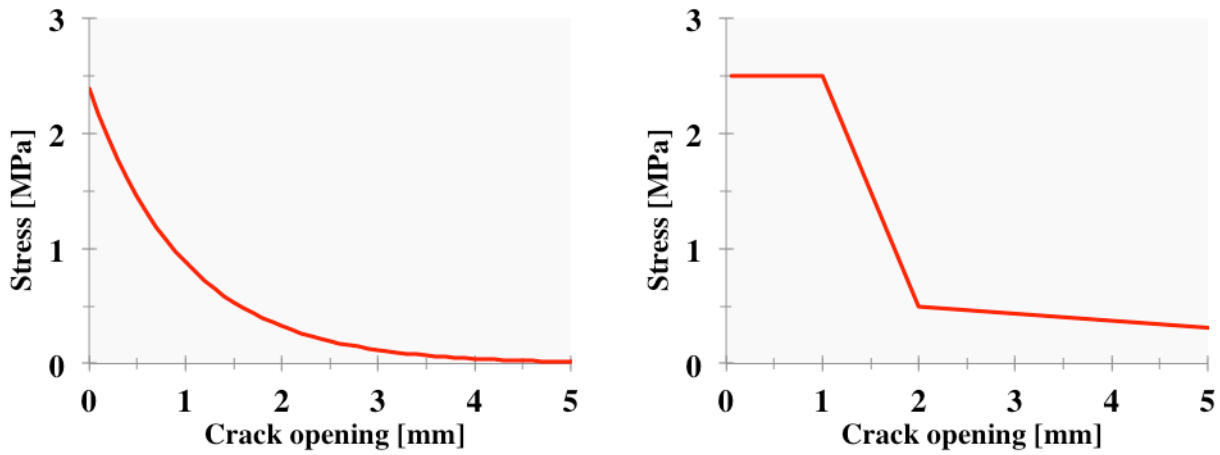

(a) Exponential law (b) Linear simplified relation

Figure 2–18: Self-user simplified post-cracking tensile models

The transformation of the $\sigma - w$ relation into a $\sigma - \varepsilon$ curve is done by the characteristic length L_r as explicated previously. The value of L_r is automatically taken equal to the average element size chosen to model the SFRC structure.

2.7.6 Tension stiffening modelling

In presence of reinforcement the interaction with the concrete leads to enhance the concrete tension resistance and it has to be adequately represented by modifying appositely the tensile performances of the plain concrete. This interaction permits concrete to resist tensile stresses better than a cracked section but less than an uncracked one, this is owing to the possibility to transfer tensile stresses from concrete directly to rebars. In the model implemented the behaviour of both reinforcement and concrete is modified; the user could choose among five different kind of tension enhancement: Fields and Bischoff (2004), Belardi and Hsu (1994), CEB-FIB (1993), Mitchell and Collins (1991) and AIJ (1986). In the case of fibre reinforced concrete, the post-cracking behaviour is taken into account using the σ-w relation introduced.

2.7.7 Output variables

EPM3D permits to detect 51 State Defined Variables (SDV) after each finite element analysis. Only six variables are presented here, they are the variables that detect the cracking state in the structure. From SDV13 to SDV15, it is possible to detect the tensile stresses for every finite element of the structure in the three principal directions of the model and similarly SDVs 16 to 18 represent the corresponding strains. It is not possible to detect directly the values of the crack openings from some output variables, but from the evolution of tensile stresses and the σ-w relation introduced the crack widths are easily determinate.

Other important output variable is the energy diagram. It is fundamental to check the energy state of the structure constantly during the analysis, as it is said before, the kinematic and hourglass energy values have to represent less than 5% of the total energy to be able to consider valid the finite-element results.

CHAPTER 3 EXPERIMENTAL AND NUMERICAL STUDIES OF RECTANGULAR SFRC BEAMS

3.1 Introduction

The aim of this chapter is to present the validation of EPM3D concrete model based on results of the experimental campaign carried out by William De Broucker (2013). To better understand the numerical validation, the first part of the chapter presents a review of the most important information of the experimental program. The experimental program (De Broucker, 2013) was divided into three different phases:

- fabrication of large scale specimens in a precast concrete plant;
- determination of material properties of the different SFRC batches, namely the compressive strength, obtained from cylindrical specimens, and post-cracking tensile strength, determined using inverse analysis from the bending tests carried out on both notched beams and round panels;
- testing of 9 large scale rectangular prestressed beams.

3.2 Optimized concrete mix

The Group for Research in Structural Engineering of Polytechnique Montréal has been studying SFRC mix optimisation for several years (Massicotte et al. 2000). The mix design retained for the prestressed beams started from a previous similar concrete mix formulation called “BRF70-HOL” (Voisin et al., 2011). With respect to this previous concrete mix some changes were necessary to suit the precast plant usual products and project objectives:

- the cement from “Lafarge Canada” replaced the cement produced by “Holcim Canada”;
- the plasticizer Plastol 6400 was used in a larger volume to stabilize and get more fluidity to the concrete mix;
- the fibres Dramix 65/35 were used in a volume equal to 80 kg/m^3 (≈1,0%);
- a reduced water/cement ratio was used to increase the compressive strength.

For the concrete mix used for this campaign the following properties have to be fulfilled:

- a self-placing concrete;
- a minimum of 80 MPa compressive strength, for a design strength of 70 MPa;
- a minimum of 2,5 MPa for the residual tensile strength up to 1 mm of crack opening.

The optimization process went through 12 different concrete mixes (Androuët et al. 2013) and the final concrete formulation is given in the Table 3-1.

Table 3-1: Concrete mix components

Component	Identification	Mass (kg/m^3)
Cement	Gub-SF (Lafarge)	685
Water	-	186
Plasticizer	Plastol 6400	9.8
Total water (adj. included)	-	195.8
Sand	St-Félix	855
Stone	5-10 St-Donat	630
Fibres	Dramix 65-35	80

The elevated amount of concrete needed for each beam, the space required for applying the prestressed stresses and the use of a single formwork lead to manufacturing the beams through nine different casts. The properties of each concrete mix have been investigated and verified. A total of 36 cylinders (203 mm high and 102 mm in diameter) were tested with the 4480 kN AMSLER universal testing machine using a loading rate equal to 2.2 kN/s (500 lbf/s). Table 3-2 summarises the mechanical properties reached for each concrete batch.

Table 3-2: Compressive test results

Characteristic	R01	R02	R03	R04	R05	R06-1	R06-2	R07	R08
f'_c (MPa)	84	86.1	86	92.5	98.7	80.7	79.6	80.6	68.1
E_c (GPa)	36.9	37.8	39.3	39.1	38.1	39.0	34.5	37.2	32.8
ν	0.265	0.245	0.275	0.241	0.201	0.231	0.209	0.212	0.219

As it could be verified in Table 3-2 the minimum compressive strength was reached for all the 8 concrete batches produced. Specimen R08 was made of HP concrete without fibres.

3.3 Characterisation of the tensile post-peak properties

Bending tests both on notched rectangular beams and round panels were performed. The inverse analysis was then used to determine the σ-w properties from the P-Δ relations measured by the bending tests. De Montaignac (2012) stated the good reliability of the inverse analysis techniques applied on bending test results. So no direct tensile tests were required to determine the tensile characteristics of the SFRC batches. A more detailed explanation of the test procedures can be found in the "Appendix A" where the same tests have been performed to characterize a different SFRC mixes.

3.3.1 Notched beam test

The casting and the loading processes followed the procedure presented in European Standard EN 14651 (2005). The wood moulds used for this experimental campaign (Figure 3–1a) were manufactured at Polytechnique Montréal following the geometrical dimensions Figure 3–1b indicated by EN standard.

a) The mould

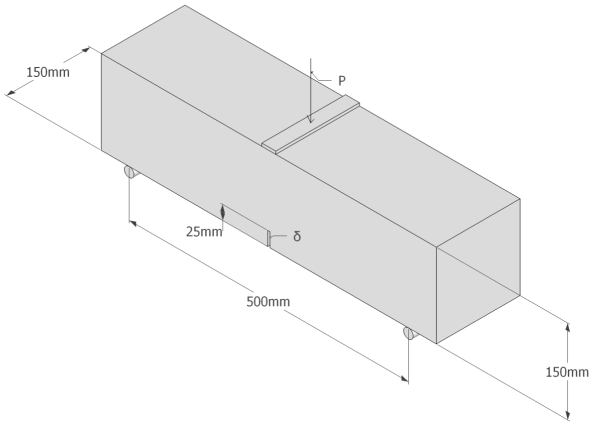

b) Specimen dimensions

Figure 3–1: Geometry of the notched beam to be tested

Each side of the mid-span section was equipped by an extensometer gauge (Figure 3–2) to measure the crack opening during the test. A LVDT was also installed – as showed in the Figure 3–2 – on each side of the specimen in order to measure the vertical displacement at the centre of the beam.

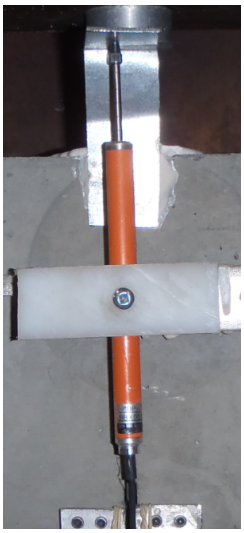

LVDT for deflection measurements

CMOD measurement device

Figure 3–2: LVDT placed for notched beam tests

From these measurements two different relations are retrieved:

- P-Δ relationship showing the vertical displacement related to the applied load;
- P-CMOD relationships showing the crack mouth opening displacement according to the applied load.

To apply the inverse analysis method, a single crack must occur on the specimen (Figure 3–3). Results from multi-cracked specimens have been rejected.

Figure 3–3: Rupture of a notched specimen

Three notched beams were tested for each concrete batch. Using the average P-Δ response measured for each concrete mix, the post-cracking tensile relation was retrieved for each concrete batch using the inverse analysis procedure developed by Nour et al. (2012).

The results were processed through five steps to obtain a normalized average relation from all the valid P-Δ curves measured (Tordjman, 2012):

- the noise of experimental curves is eliminated using a software developed by Conciatori (2012), providing a smoothed curve that can be analysed and treated easier in the following steps;
- the average values of the peak-load and the corresponding displacement are then determined;
- the displacement and the load of each prism are normalized with respect to the average peak-load and average peak-displacement;
- the average load-displacement curves are finally calculated.

This four-step procedure is used to retrieve the average load displacement relationship for each SFRC batch – an example in Figure 3–4. Inverse analysis is then applied to determine the σ-w relation (Figure 3–4).

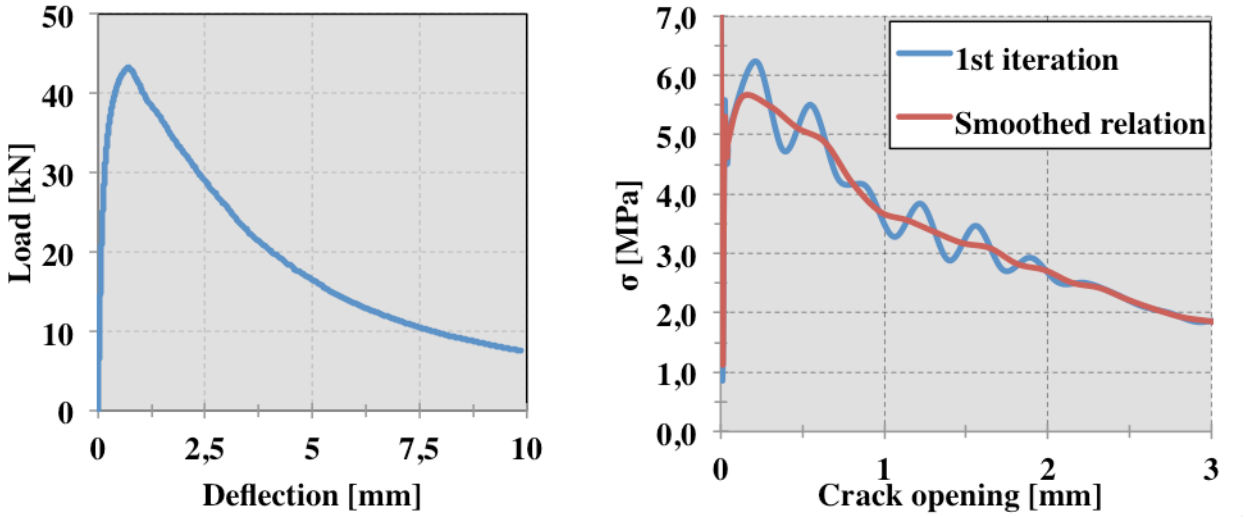

Figure 3–4: Example of the notched beam *P*-Δ response and corresponding σ-*w* relationships

The resulting post-cracking relationship presents a short hardening phase and a smooth softening response for every curve obtained. The notched beam test, due to the preferential fibre orientation associated with its fabrication process, generally gives higher post-cracking tensile strength than expected in a real structural member. Predictions are optimal in terms of small crack width, whereas they tend to overestimate the measured properties for large crack widths (de Montaignac, 2012).

3.3.2 Round panel tests

Three round panel tests have been carried out for each concrete batch manufactured. Following the hypothesis of the inverse analysis procedure developed by Nour et al. (2012), the round panel tested must fail with three cracks (Figure 3–5 (b)). The panels with fewer cracks (Figure 3–5 (a)) would tend to overestimate of the tensile properties and must therefore be rejected.

(a) Two-crack failure (b) Three-crack failure

Figure 3–5: Round panels tested. Two and three crack failures

The test setup for round panel specimens requires using a LVDT located underneath the specimen for measuring the vertical displacement at the centre of the circular panel. As done for the notched beams, the inverse analysis procedure is applied to retrieve the post-cracking relationship (Figure 3–6).

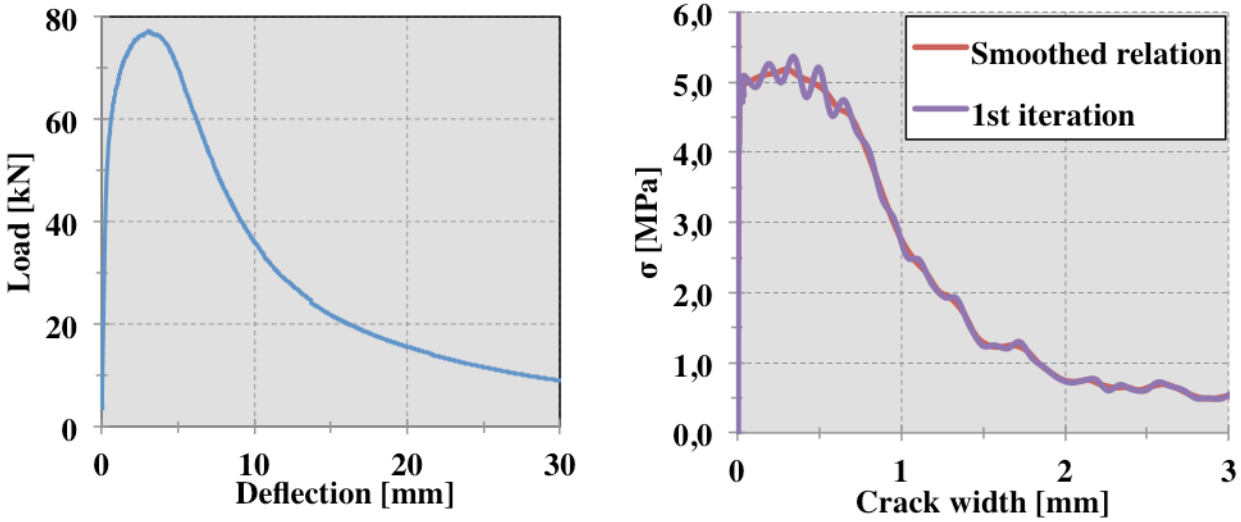

Figure 3–6: *P-Δ* response and σ-*w* relationships from round panel tests

The post-cracking curve was calculated for the manufactured specimens. Relationships from one-crack-failure panels and from notched beams with multi-crack failure were rejected – following the assumptions of the inverse analyses adopted. Based on the study by Torjdman (2012) with which notched beams, round panels and dog bone specimens were compared for various SFRC mixes, it has been considered that the notched beams generally overestimate the tensile properties of the SFRC studied. So that, for the numerical analyses carried out herein, the results from the round panels are used. Table 3-3 presents the post-cracking values for each concrete batch investigated. An average relation has been calculated.

Table 3-3: Inverse analysis results from Round panels

	R01	R02	R03	R04	R05	R06-1	R06-2	R07	Average
f'_t	3.94	4.18	-	4.27	4.07	-	-	4.38	4.2
$\sigma_{0.02}$	4.82	4.28	-	4.55	4.39	-	-	3.71	5
$\sigma_{0.1}$	4.66	4.67	-	4.86	4.52	-	-	4.12	4.5
$\sigma_{0.3}$	4.75	4.72	-	4.82	4.48	-	-	4.34	4.5
$\sigma_{1.0}$	2.1	3.11	-	3.68	1.74	-	-	3.22	2.9
$\sigma_{2.0}$	1.39	1.23	-	0.86	0.32	-	-	0.85	0.78

The batches corresponding to specimens R03, R06-01 and R06-02 have no values because only one-crack formed in round panels. The results were rejected.

To conclude on the characterisation of the SFRC studied, the tensile strength at cracking is calculated in Table 3-4 using different approaches. The values retained for the numerical analyses are shown in bold. They correspond to the stress calculated from round panel tests for a crack opening equal to 0.005 mm. For the three batches without reliable panel tests, the tensile strength is taken equal to the peak values obtained by the notched beam tests before cracking or using the simplified formula $f_t' = 0.4 \cdot \sqrt[2]{f_c'}$.

Table 3-4: Tensile strength

	Source	R01	R02	R03	R04	R05	R06-1	R06-2	R07	R08
$f_t' = 0.4 \cdot \sqrt[2]{f_c'}$	Compression	3.67	3.71	3.71	3.85	3.97	3.59	3.57	3.59	3.30
$f_t' = \sigma_t(w = 0)$	Beam	3.18	3.36	5.37	4.22	5.73	-	-	5.64	-
$f_t' = \sigma_t(w = 0.005)$	Beam	5.61	7.5	8.36	7	6.5	-	-	7.06	-
$f_t' = \sigma_t(w = 0)$	Round panel	5.82	6.74	-	6.94	5.87	-	-	7.17	4.52
$f_t' = \sigma_t(w = 0.005)$	Round panel	3.94	4.18	-	4.27	4.07	-	-	4.38	-
$f_t' = \sigma_t$	-	**3.94**	**4.18**	**5.37**	**4.27**	**4.07**	**5.0**	**5.0**	**4.38**	**4.52**

Dispersion of results obtained by bending tests is in accordance with the considerations made in previous research works (de Montaignac, 2012). For the round panel specimens, a randomly planar distribution of fibres and the larger volume of concrete involved caused a smaller dispersion in load-displacement relationships than the equivalent results obtained from notched beams bending tests. Nonetheless, for notched beam specimens the preferential orientation of the fibres along the main direction – possible presence of multiple cracks at the notch – lead to an overall overestimation of the actual σ-w relation. For that reason, for the NLFEA the average stress crack width relation retrieved from round panel was used for each batch (Table 3-3).

The post-cracking relationships used for the numerical analyses followed the results obtained from the inverse analyses applied on round panel bending tests. EPM3D allowed the use a simplified relation determined by 7 different points. Simplified curves are so used to represent the tensile characteristics retrieved experimentally.

The tensile resistance f_t' is introduced as the largest value between the maximum stress retrieved from the post-cracking relationship and the tensile strength (bold values from Table 3-4).

From both bending tests performed, a reduction of the tensile strength right after the beginning of the cracks can be highlighted (Table 3-5). This reduction might be ascribed to the development of the crack opening necessary for the fibres to start performing their anchorage mechanisms. For each beam analysis it has been decided to introduce a reduction of the tensile properties, as it might be seen in the zoomed area for small crack widths in Figure 3–7. This reduction follows

experimental results obtained from direct tensile tests (de Montaignac et al. 2012). The tensile strength is so reduced by 80% of the f_t' for a crack opening of 0.02mm. It has been found that this reduction in terms of tensile strength affects correctly the cracking mechanism of the beam.

The good results obtained by the numerical study presented later in this document demonstrated the accuracy and the reliability of the post-cracking properties obtained.

It has not been possible to use a specific post-cracking relation for each beam, as it can be seen from Table 3-4. For R03 and R06 the average relationship has been used Figure 3–7 or Table 3-5. The adopted relationships for the other beams are presented in Appendix C.

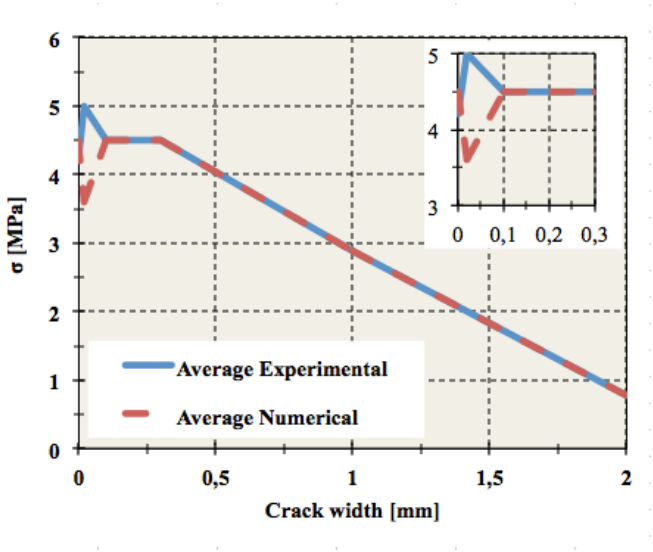

Figure 3–7 : Average Numerical σ-w relationship

Table 3-5 : σ-w relationship retained in the numerical analyses

Identification	Crack width (mm)	Experimental stress (MPa)	Retained stress for analysis (MPa)
f'_t	0.0	4.20	4.50
$\sigma_{0.02}$	0.02	5.00	3.60
$\sigma_{0.1}$	0.1	4.50	4.50
$\sigma_{0.3}$	0.3	4.50	4.50
σ_1	1.0	2.90	2.90
σ_2	2.0	0.78	0.78
σ_{10}	10	0	0

3.3.3 FIB Model Code

For using the FIB Model Code, crack mouth opening displacements (CMOD) are required, as indicated in Eq.2-1. These values can be measured or calculated as indicated by EN14651 standard. In the tests carried out by De Broucker, the CMOD were measured (Figure 3–2) but not reported in the thesis. Treatment of the measured values allowed determining the average load-CMOD response of the notched beams and computing the equivalent bending stresses associated to $CMOD_1$ and $CMOD_3$ for the purpose of the present project, as shown on Figure 3-8.

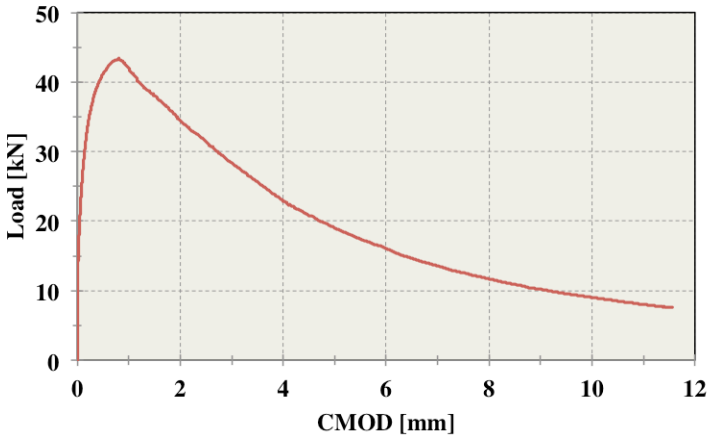

Figure 3–8 : Average F-CMOD relationship

Table 3-6 presents the post-cracking stress values obtained from the notched beam tests results following FIB Model Code recommendations. According to the classification of FIB (see Section 2.5.4), the ratio $f_{R3}/f_{R1} = 0.68$ which indicates this SFRC mix is of class a. Moreover, the equivalent bending stress corresponding to the limit of proportionality f_L is equal to 6,62 MPa. The f_{R3}/f_{R1} and f_{R3}/f_L ratios of the characteristics properties are used by the FIB Model Code to determine if the SFRC mix can replace conventional reinforcement. The ratio of the average properties would meet the limits indicated in Section 2.5.2.

Table 3-6 : Average post-cracking stress values from the notched beam test

$CMOD_i$	w (mm)	f_{Rj} (MPa)
$CMOD_1$	0.5	12.50
$CMOD_3$	2.5	8.49

3.4 Experimental campaign

The nine beams were all manufactured at the precast plant of Béton Préfabriqué du Lac "BPDL" in Saint-Eugène-de-Grantham. The dimensions were equal for all the nine large-scale specimens as showed in Figure 3–9.

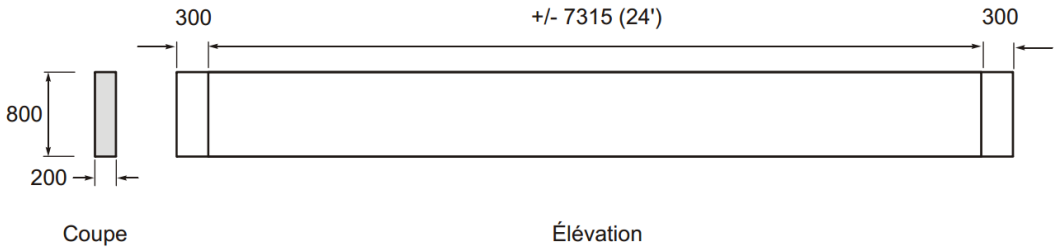

(a) Transverse dimensions of the beams

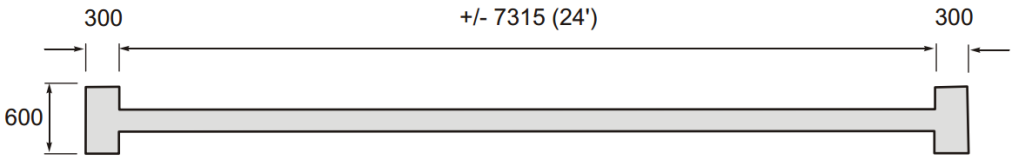

(b) Longitudinal dimensions of the beams

Figure 3–9: Geometry of the specimens

Because the huge volume of concrete needed, the production of the concrete was done directly in a ready-mix truck. The concrete mix was first prepared in the wet-batch plant while the fibres were added in the truck afterward. The Abram's cone test was carried out before and after the addition of the fibres to verify the consistency of the concrete mixes. L-box test was also done for the SFRC mix only. Admixtures were adjusted until satisfactory characteristics were obtained. The pouring of the concrete was made from one end of the formwork, letting the concrete flow along the formwork walls up to the opposite extremity. The dimensions and the volume quantity of the steel fibres introduced and the disposition of the reinforcing strands and stirrups did not seem to affect the correct flow of the concrete. Hence the concrete manufactured was able to fill the whole formwork without the creation of remarkable congestions and without any vibration,

confirming the industrial feasibility of such a self-placing concrete for this kind of application. A layer of polythene covered the top of the beams and all the other specimens for 24h.

The tension force was applied to each strand before the concrete casting. After three days of moist curing the strands were cut, applying the prestressed force to the beam. The two extremities of the cables have been cut simultaneously to avoid any possible different stress transitions between the two sides of the specimen.

All the prestressed strands used for the beams were T15 with the mechanical properties indicated in Table 3-7.

Table 3-7: Prestressed strand properties

Diameter (mm)	Area (mm^2)	f_y (MPa)	f_{pu}(MPa)	Ultimate load (kN)	Maximum traction force (kN)
15.2	140	1675	1860	260,4	209

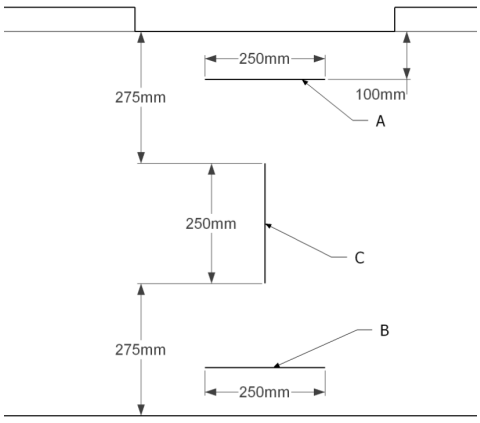

(a) DEMEC point locations

(b) Example of a DEMEC point

Figure 3–10: DEMEC points installed

Three pairs of DEMEC points (Figure 3–10) were installed to measure the prestressing losses. The disposition of those points are indicated in Figure 3–10. The two horizontal measures

allowed determining the evolution of the strain diagram over the member depth while the measurements in the vertical direction enabled measuring mostly shrinkage strains.

The distance between the different points was measured before and after the release of the prestressing force to calculate the prestressing loss in the cables – knowing the Young's modulus equal to 200 000 MPa. The initial length L was measured before the application of the prestressing force whereas the deformation, $\Delta\varepsilon = {\Delta L}/{L}$, was determined from measurements of ΔL after the application of the prestressing force and before testing the beams. The prestressing loss at the various stages is then computed by $\Delta\sigma = E_p \cdot \Delta\varepsilon$.

3.4.1 Bending tests

The first five large-scale beams have been tested with a symmetrical load disposition for performing a bending test. The main goal of these tests was the investigation of the different behaviour of the beams using different types of reinforcing bars for the lowest layer.

The failure mode, the crack openings, the crack spacing, the ultimate load at failure and the ductility of the beams will be the main results to be discussed. A comparison of the results obtained from the beams R01, R02 and R03 will be done in the next chapter. The two beams R04 and R05 had the same reinforcing arrangements of the beams R01 and R02 respectively. Those specimens have been loaded with cyclic loads before reaching the failure. Ten load cycles between 100 kN and 400 kN – total load – were applied. The upper bound load is equal to the total force that had resulted necessary to crack the R01 beam. This is not the load variation to be followed for investigating a fatigue limit state, but it is a great indicator of the ability of such a specimen to sustain cyclic loading.

The disposition of the prestressed strands used for these 5 beams followed the scheme from Figure 3-11 to Figure 3-14. All the prestressed strands have to be considered bonded, except for the lowest layer of strands of specimens R02, R03 and R05. A tensile stress equal to 1300 MPa was applied to each cable. The distance of 50 mm between the strands in the bottom part of the beam is the minimum necessary to apply the prestressing force with the industrial equipment used. The two strands placed at the upper part of the section would avoid cracks at the top of the beam, which would not represent the real mechanism in the actual application.

The presence of two enlargements – one for each extremity of the specimen – prevented the instability of the beam during the tests and the transportation.

As shown in Figure 3–11, the R01 and R04 beams have 6 prestressed strands acting as the main reinforcement at the bottom of the specimen. The lowest layer of cables is made using bonded prestressed cables as all the others for these sections. Two stirrups 10M are located at each extremity 50 mm apart.

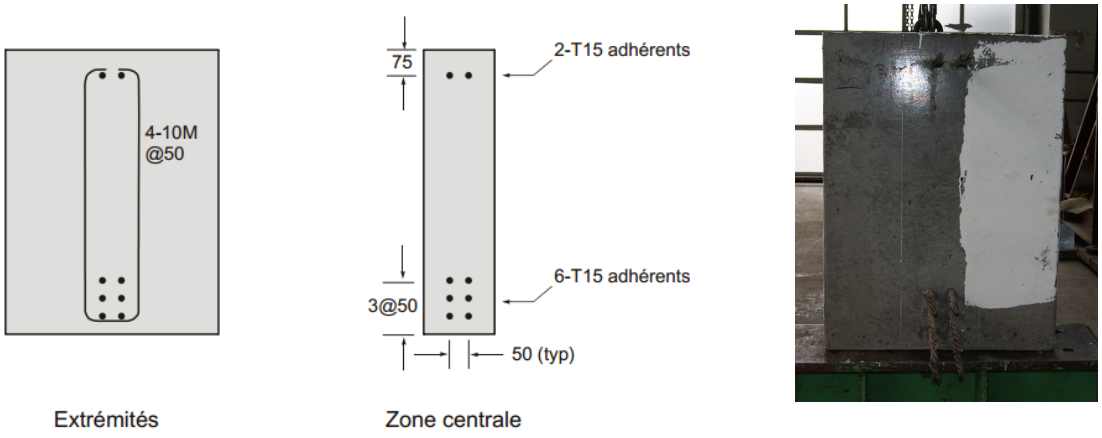

(a) Reinforcing strand location (beams R01-R04) (b) Extremity of the beam R01

Figure 3–11: Reinforcing bars for the specimens R01 and R04

The reinforcing disposition for specimens R02 and R05 is the same as R01 and R04 with T15 cables used for all the prestressed strands. For the bottom layer of the reinforcement, two un-bonded strands for 4 m at the centre of the beam are used to enable the movement between the cables and the covering concrete. This option was taken to limit the stress ranges due to the cyclic loads to which such structures are often subjected.

The bottom layer of reinforcement of specimen R03 consists in two reinforcing bars 30M. The other 4 prestressed strands and the two strands at the top of the section are bonded cables (

Figure 3–12). The transverse reinforcement is the same as previous specimens. (Figure 3–11 (a))

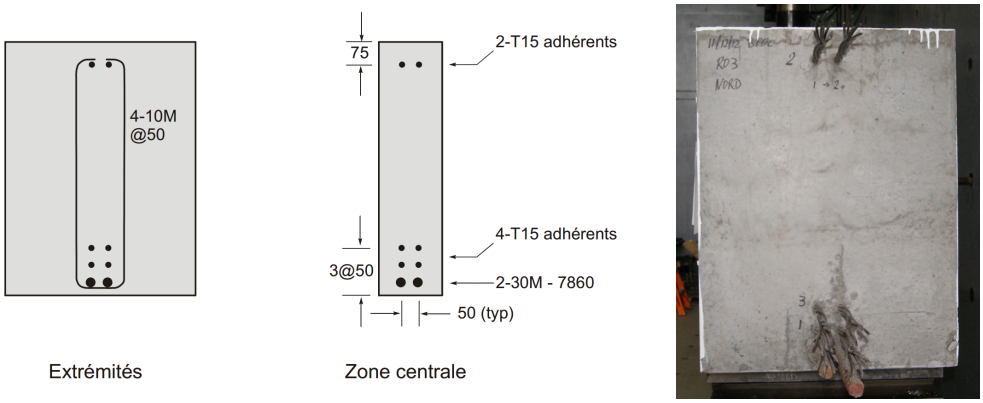

(a) Reinforcing strand location (beam R03) (b) Extremity of the beam R03

Figure 3–12: Reinforcing bars for the specimens R03

Table 3-8: Reinforcing bar properties

Area	700	mm^2
f_y	464	MPa
f_u	635	MPa

3.4.2 Shear tests

The remaining 4 beams have been tested to investigate the shear failure. An asymmetric load disposition was considered to enable a shear mechanism. The reinforcement configuration was increased to eliminate bending failure while keeping the same total prestressed force applied to the specimen. The reinforcement strands configuration and the prestressed stress applied to each cable are shown in Figure 3–13. Two design parameters were changed for the shear capacity: the addition of shear reinforcement for two specimens and the use of HP concrete without fibres for one specimen:

- the different transverse reinforcement configuration between the two R06 specimens (without stirrup) and R07 specimen (with stirrup) will show the different mechanism using or not the stirrups to prevent a shear failure mechanism;

- the absence of steel fibres for the R08 specimen will get reliable results to investigate more in detail the strength offered by the fibres for the appearing of shear cracks.

The two R06 specimens (Figure 3–13) did not have any transverse reinforcement. Only two simple stirrups 10M at each extremity are located.

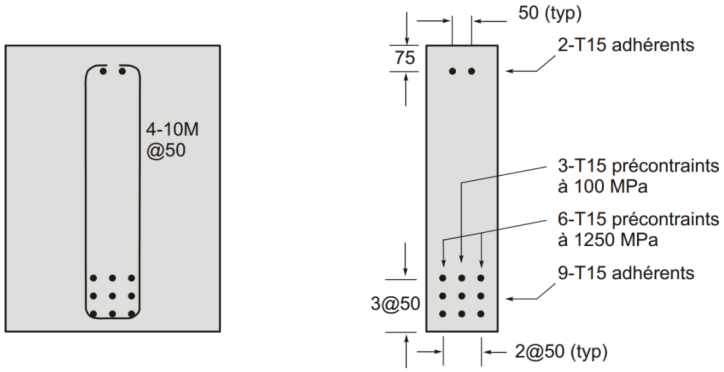

Figure 3–13: Reinforcing bars for the specimens R06-1 and R06-2

The reinforcement configuration for beams R07 and R08 follows the scheme in Figure 3–14. Simple stirrups 10 M are used along the specimens (Figure 3–15). Specimen R08 specimen was made of plain concrete without the addition of steel fibres. The R08 would act as a reference model to be compared with the SFRC ones.

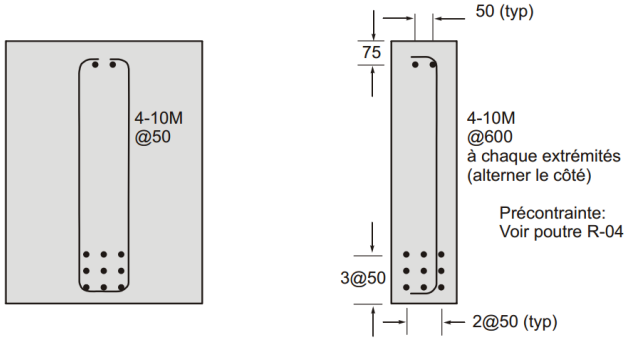

Figure 3–14: Reinforcing bars for the specimens R07 and R08

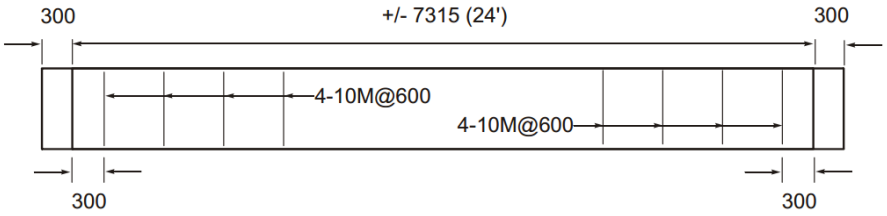

Figure 3–15: Transverse reinforcement for R07 and R08

3.4.3 Test set-up and instrumentation

Simple supported conditions at both extremities of a 7315 mm span were reproduced for each specimen and two actuators were used for loading. The two actuators performed as a master-slave system – tests were carried out fixing at 0.02 mm/s the displacement rate of the master actuator – the slave load device was automatically controlled consequently. Two different configurations of the load system were necessary (Figure 3–16 and Figure 3–17): bending tests required positioning the actuators symmetrically with respect to the specimen mid-span with a constant moment region of 1500 mm. For shear tests, R06-1 was the first specimen tested and the two actuators were placed to obtain a shear span of 2500 mm close to the southern extremity, maintaining a distance of 1500 mm between the two loads. Due to a bending/shear failure of the beam, it was decided to move the two load devices 500 mm closer to the south extremity for the following tests. Tests were stopped every 100 kN to allow the identification of the cracks appearing on the specimens at each load interval.

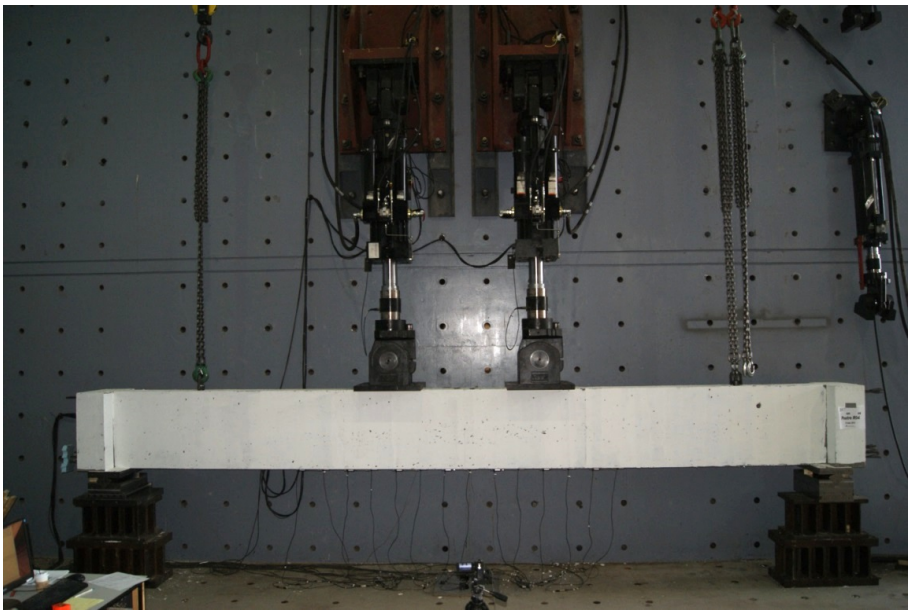

(a) Photo of the bending test set-up before the test

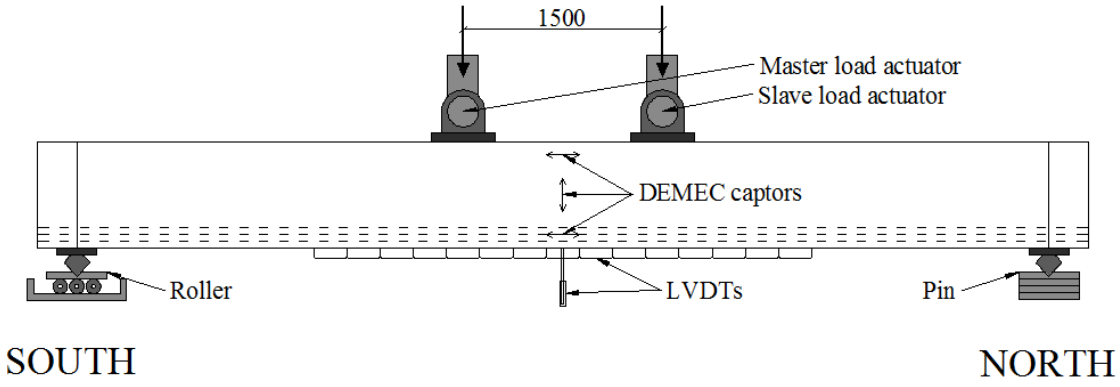

(b) Sketch of the bending set-up

Figure 3–16: Bending test set-up

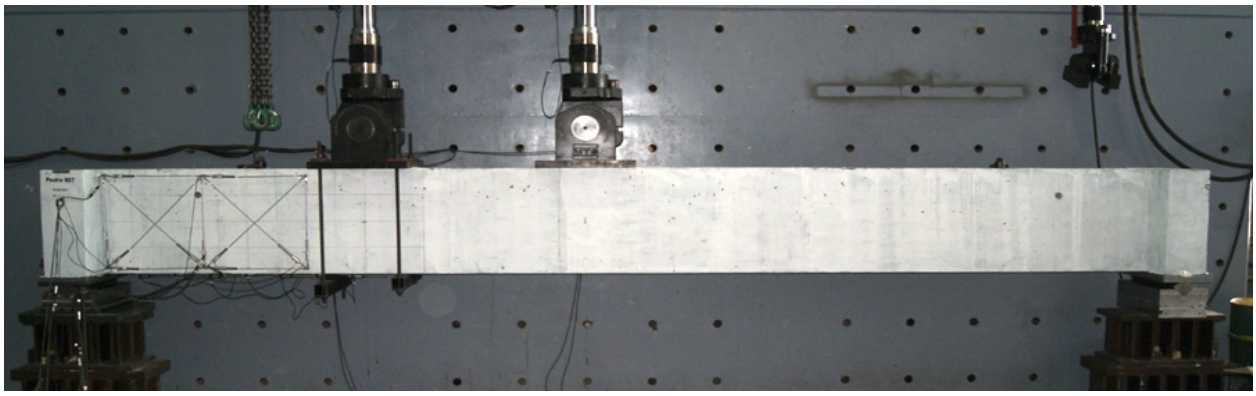

(a) Photo of the shear test set-up before the test

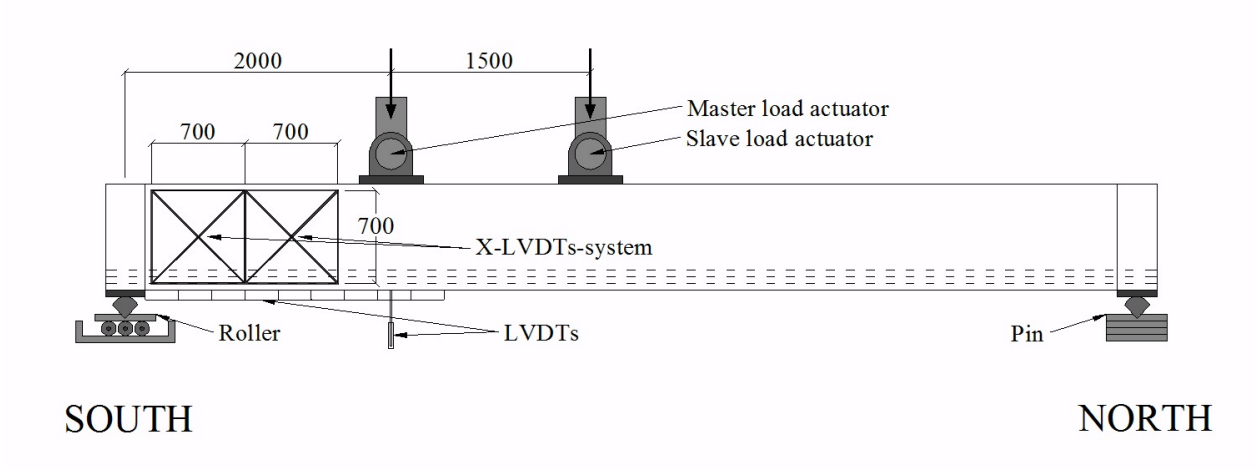

(b) Sketch of the shear set-up for specimens R06-2, R07 and R08

Figure 3–17: Shear test set-up

One of the main goals of the experimental program was to investigate any difference of the crack pattern – mainly crack distance and openings – produced by using different reinforcement configurations. For this reason each beam has been equipped by a system of LVDTs to measure the crack openings during the experimental campaign. Each LVDT device has a length of 250 mm. According to the different loading configuration adopted, different failures were expected. For bending test a flexural failure at the mid-span cross-section was expected and for shear tests the reinforcement configuration should have enabled a shear failure close to the south extremity of the beams.

For bending tests seventeen LVDTs have been installed symmetrically with respect to the mid-span section, underneath each beam to measure the development of the flexural crack pattern, numbered incrementally from left to right. For the shear tests a system composed by 11 LVDTs (Figure 3–18) was placed close to the South extremity where a shear failure was expected to occur. This measuring system (Figure 3–18) should have enabled to investigate an expected diagonal crack along the line between the load device and the south extremity. Nine other LVDTs were placed underneath the specimen close to the south (left) extremity as shown in the Figure 3–17, numbered from left to right.

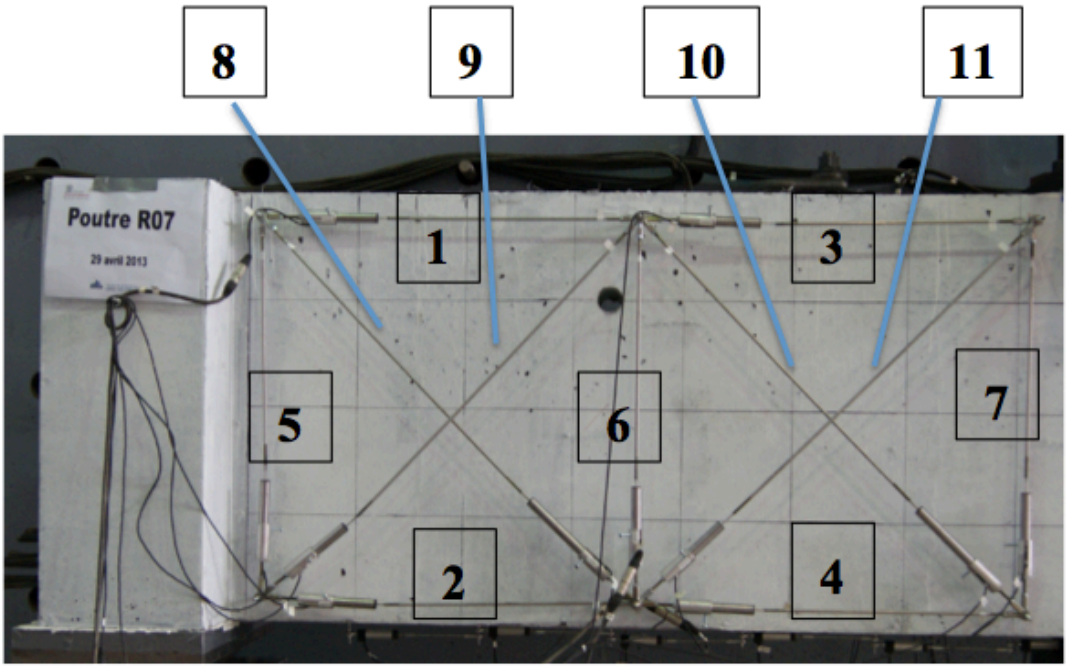

Figure 3–18: LVDTs located close to the south extremity for R06, R07 and R08

3.4.4 Pre-design of the rectangular beams

As part of this thesis, the bending capacities calculated with AIS and the FIB Model Code simplified method are calculated with the safety factors ϕ or γ equal to 1 in order to reproduce the same quantities measured experimentally.

3.4.4.1 AIS

The bending capacity of the rectangular specimens tested can be provided by some simplified calculations. The software AIS is able to compute the sectional bending capacity, allowing the user to introduce the real properties of the material. For the specimens presented in this chapter the bending capacity will be calculated for the beams R01, R02 and R03 (Table 3-9), which are tested with symmetrical loads. The input data are:

- material properties – the mechanical and geometrical properties of the strands and the reinforcements used for this application as presented above (Table 3-7 and Table 3-8) – and the tensile properties of the SFRC used taken from the average relationship from the round panel tests (Figure 3–6);
- geometry of the section – in this case the location of the reinforcement and the dimensions of the cross-section are those presented from Figure 3–11 to Figure 3–14
- the tension applied to the strands;
- the bounding properties of the strands.

The values corresponding to the total load in the Table 3-9 – the sum of the two punctual loads applied to the specimen – are calculated with a simple equilibrium equation knowing the geometry of the applied loads in the Figure 3–16.

Table 3-9: Bending moment calculated with software AIS

Beam	Bending capacity	Total load
R01 – R04	1110 kN-m	764 kN
R02 – R05	1018 kN-m	700 kN
R03	1235 kN-m	806 kN

3.4.4.2 FIB Model Code

The rigid-plastic stress distribution is chosen to represent the tensile stresses along the section (Figure 3–19). The safety factor and the factor for the orientation of fibres are taken equal to 1.0.

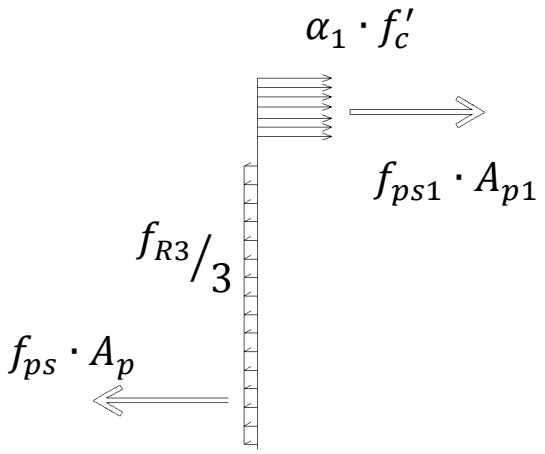

Figure 3–19: Stress distribution fib model Code 2010, for beams R01 and R04

For specimens R01 and R04, the force equilibrium on the section allows computing the height of the compressive zone – it is an iterative process shows the final values – because the f_{ps} is not known:

$$\boldsymbol{f_{ps}(2) = 1719\ MPa} \text{ and } \boldsymbol{a(2) = 126\ mm}$$

The rotational equilibrium allows computing the resisting moment in the mid-span section:

$$\underline{\boldsymbol{M_u = 1070\ kN \cdot m}}$$

This values can be compared with the more accurate value of 1110 kN-m obtained with AIS.

3.4.5 Experimental results

In order to better understand the experimental results, the measurements from the first five beams will be presented first, and the remaining 4 beam results will be discussed next separately.

Respectively the Table 3-10 and Table 3-11 summarise the main results from bending and shear tests.

3.4.5.1 Bending tests

The two specimens R01 and R02 (bounded and unbounded bottom strands) exhibited the same behaviour in terms of ultimate bending moment. The first beam demonstrated a better performance in terms of displacement at failure – 8 mm more than R02 displacement, equivalent to a percentage improvement of 15.5%. Both specimens failed in flexion and the crack pattern was truly similar with average crack spacing respectively of about 75 mm and 85 mm. On approaching the ultimate resisting load a widespread micro-cracking pattern in the top part at mid-span started developing. As expected for both specimens, the ultimate compressive strength was reached close to the center of the beam. Load – deflection results are presented in Figure 3–20 and the different failures occurred in Figure 3–21.

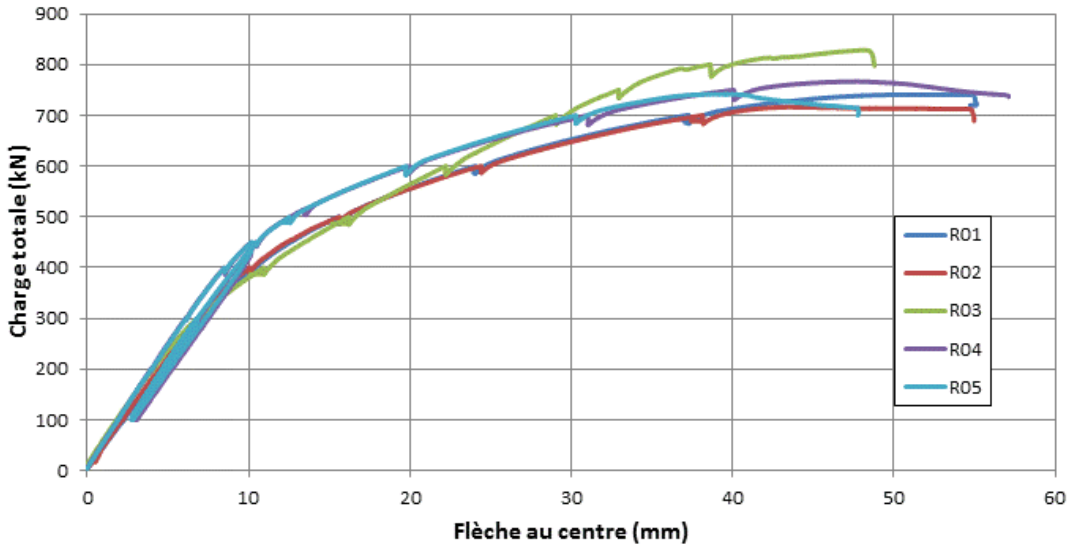

Figure 3–20: Load-deflection response of specimens R01 to R05 (De Broucker, 2013)

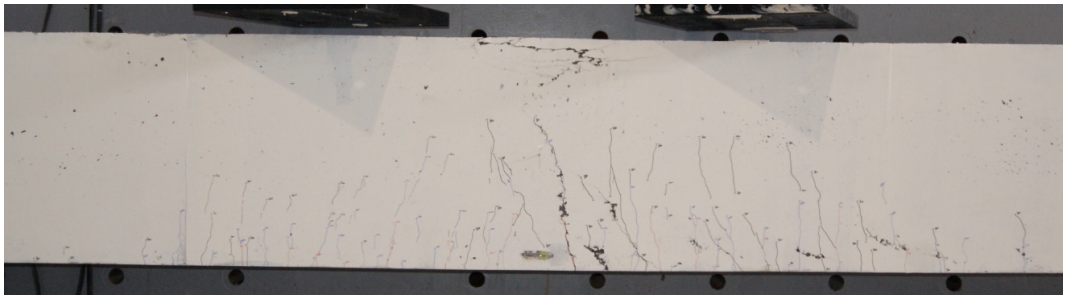

(a) Bending failure of specimen R01

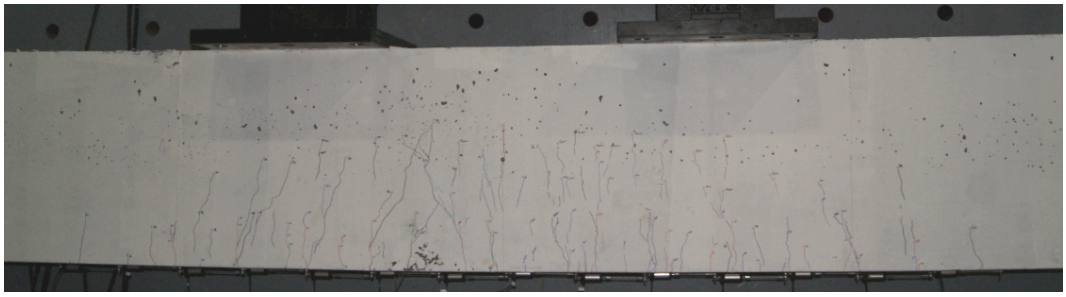

(b) Bending failure of specimen R02

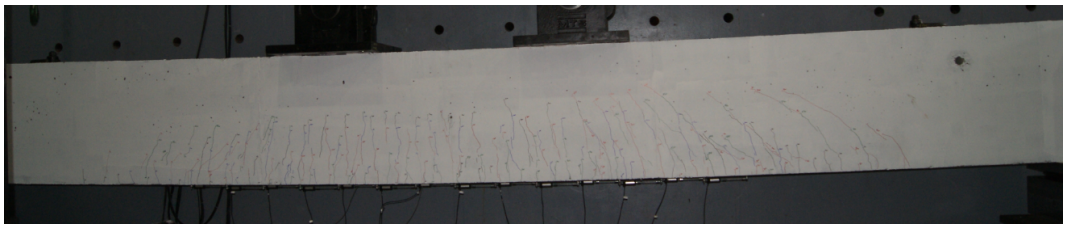

(c) Cracking pattern of specimen R03 before failure

(d) Shear failure of specimen R03

Figure 3–21: Failure modes of specimen R01, R02 and R03 (De Broucker 2013)

Specimen R03 exhibited an increase of 11% and 14% in ultimate bending moment compared respectively to R01 and R02 results. However, the displacement at failure showed in all these three tests remained comparable. Although a bending failure was expected, R03 exhibited a different failure mode. The R03 specimen developed a typical flexural crack pattern similar to that of the two previous beams up to approaching the ultimate load. At failure the beam presented a brittle diagonal crack (Figure 3–21 d). As the Figure 3–21d shows, the diagonal crack that caused the failure of the specimen occurred on the northern part of the specimen and simultaneous microcracks appeared at the top of middle cross-section – typical indicator of the attainment of the maximum compressive strength. For that reason, in Table 3-10 the failure mode is considered to be a combination of both failures: shear and flexural. R03 showed also narrower cracks at failure than the two previous beams – an average crack spacing of about 65 mm was measured.

In Figure 3–20 the relationships between the total applied load and the displacement at the center of the beam are presented for the five beams. The curves corresponding to the first three beams showed few discontinuities at every 100 kN. As explicated previously, the tests were stopped at each 100 kN to highlight with different colours on the beam the development of the cracks – Figure 3–21 is an example.

In Table 3-10 the total load applied is the sum of the two loads applied simultaneously by both actuators on the beams. Because of the symmetrical loading scheme, the maximum shear force is taken equal to half of the total load applied – equal to the reaction at the simple support. The maximum resisting moment is simply calculated using the symmetry of the loading system: $M_{max} = V \cdot a$; where "V" is the half of the maximum total load applied and "a" is the distance between the applied load and the beam support. The displacements calculated in Table 3-10 refer to the vertical displacement measured at the peak resisting load. After reaching the peak-load a "plateau" is highlighted by the different relationships (Figure 3–20). This behaviour shows the capacity of the fibres and prestressing strand combination to provide a ductile behaviour.

Table 3-10: Bending test results

	Results				
Beam	R01	R02	R03	R04	R05
Total load [kN]	737.7	716.6	828.6	766.9	741.9
Peak – Displ. [mm]	51.6	43.6	48.2	47.8	38.9
Max. Moment [kN·m]	1073	1043	1206	1116	1080
Max. Shear Force [kN]	368.9	358.3	414.3	383.5	371.0
Crack # w > 0.2 mm	14	14	14	14	14
Crack # w > 1 mm	10	6	6	9	4
Crack # w > 2 mm	1	1	1	2	1
Crack spacing [mm]	±70	±85	±65	±85	±80
Failure mode	Bending	Bending	Shear	Bending	Bending

The cracking patterns of each specimen is shown in Figure 3–21. For specimen R01 the cracks at the top of the middle-cross section indicate the attainment of the maximum compressive strength of the concrete. In the bottom part of specimen R01 (Figure 3–21 a) and of specimen R02 (Figure 3–21 b) the cracks are orthogonal to the lines of development of the tensile stresses induced by the applied loads.

Figure 3–21c and Figure 3–21d highlight the failure mechanism of the beam R03. The first one refers to an applied load equal to 700 kN corresponding to the previous step before the failure. A typical flexural cracking pattern is highlighted. Figure 3–21 d shows the brittle failure mode of this specimen. This failure must be studied in detail for to explain its unexpected occurrence in a bending test.

Specimens R01 and R02 exhibited basically the same flexural behaviour. Load-displacement responses, crack patterns and failure mechanisms of the two tests are comparable. The choice between bonded or un-bonded strands does not seem to have an important role in the overall bending behaviour. The choice between these two solutions might be governed by other considerations such as cost, industrial feasibility or stress ranges in the strands. Globally, the combined use of prestressed strands and steel fibres in the concrete mix revealed excellent behaviour in terms of bearing capacity and maximum displacement.

The use of two 30M bars permitted to obtain closer and finer cracks while a larger bending capacity was also obtained. The ribbed surface of both bars increased the bond stresses at the

contact surface with the surrounding concrete producing closer cracks than what obtained for the R01 and R02 beams. A higher ultimate bearing load is the direct consequent of the better adherence developed between bars and concrete. The better bending performances obtained with the use of reinforcing bars and the imperfectly proper orientation of fibres in the northern part of the beam caused the development of the diagonal crack for this specimen. It is interesting to see that the flow of SFRC from one end contributed to orient the fibres at the North side of the beam in a slightly inclined plane, parallel to the main compression force. This particularity is such that the steel fibres where not correctly oriented to bridge the diagonal crack with a consequent reduction in the shear resistance. The unexpected behaviour of specimen R03 leads to state three important remarks:

- the orientation of steel fibres could hardly be handled in such applications and the possibility of the presence of a weaker unanticipated plane shall be something to be aware of;
- the shear crack occurred for the R03 specimen suggest to consider – in the design phase – a variable post-cracking relation for SFRC along the beam depending on the industrial casting technique used;
- the presence of a minimum transverse reinforcement should be taken into account even if the shear contribution given by steel fibres can totally cover the shear resistance needed.

3.4.5.2 Shear tests

The shear test results are presented in the Table 3-11. Specimen R06-1 was manufactured first. Few geometrical imprecisions lead to the fabrication of a second specimen –R06-2. Specimen R06-2 was tested first with a shear span of 2500 mm. The first applied load was located at a distance of 2500 mm from the extremity and a distance of 1500 mm between the two loads was chosen. The specimen tested had an un-expected bending failure. Consequently specimen R06-1 was tested with a modified position of the loads.

Specimen R06-1 had a shear failure, but the diagonal failure occurred on the North part of the beam, on the opposite side where it was expected. For this reason the measurements of the crack openings cannot be considered because the beam was equipped with LVDTs on the South part only.

The crack spacing presented in the Table 3-11 refers to the LVDTs located underneath the beams as represented in the Figure 3–17 close to the south extremity.

The presence of transverse reinforcement in specimen R07 did not change the performance compared to specimen R06-1. These two beams exhibited almost the same bearing performance showing similar values of ultimate bending moment and displacement at the peak-load. Moreover they showed identical P-Δ relationships up to an approximate load of 800 kN. The crack pattern differed in number and spacing – beam R07 showed more and closer cracks than what beam R06 did. A shear failure took place for both specimens but R06-1 showed a final diagonal crack in the Northern part of the beam even if it was supposed to occur on the opposite side as the for specimen R07.

The only difference between specimens R07 and R08 was the presence of steel fibres. The absence of steel fibres in the specimen R08 caused a substantial drop in load bearing capacity – 35% less in terms of ultimate carrying load and 52% less for the displacement at load-peak than beam R07. A shear diagonal failure occurred in the southern part of the beam as expected. Due to the small deflection that occurred for specimen R08, narrower and closer cracks than R06 and R07 specimens were detected.

Table 3-11: Shear test results

	Results			
Beam	R06-1	R06-2	R07	R08
Total Load [kN]	950.6	858.6	900.1	585.6
Peak – Displ. [mm]	42.3	53.0	45.6	20.0
Max Moment [kN-m]	1413.8	1243.0	1239.0	806.1
Crack # w > 0.2 mm	8	12	14	9
Crack # w > 1 mm	3	4	5	2
Crack # w > 2 mm	1	1	2	1
Crack spacing [mm]	±145	±65	±100	±85
Failure Mode	Shear	Shear / Flexion	Shear	Shear

Specimen R08 provided about half of the bearing capacity of the corresponding SFRC beam – specimen R07. The maximum displacement exhibited by R08 was the 44% of the one measured for beam R07. Concrete without steel fibres demonstrated, as expected, to carry a shear response less performing than the SFRC with 1% of amount of fibres. The presence of a minimum quantity of transverse reinforcement – as done for the specimen R08 – seems to be insufficient in

order to meet the required bearing capacity and adequate crack pattern evolution. The comparison between specimens R07 and R08 confirmed the improvement in shear bearing capacity brought by the presence of fibres. The addition of steel fibres is therefore highly recommendable to provide thinner and closer cracks, thereby preventing damages to the prestressed strands and improving the durability of the structure.

R06 and R07 showed the same behaviour in terms of ductility and bearing capacity regardless the presence of stirrups in R07 beam. However, the crack pattern of R07 was constituted by closer and narrower cracks and more ductility has been detected in the specimen response. The presence of stirrups permits to obtain a certain certitude in the answer expected, in fact the shear failure occurred in the shortest part of the beam as manually anticipated before the test, which was not the case for R06 where shear failure occurred in the slender part of the specimen. As the consideration done for the specimen R03, a minimum use of transverse reinforcement is still recommended in order to avoid part of the incertitude caused by a possible incorrect fibre orientation.

3.4.5.3 General comments

The good the concrete mixes and the quality of the beams obtained demonstrated that the industrial personnel and procedures could totally fulfill the production requirements. The transverse dimensions of the formwork did not seem to represent any difficulty to the casting phase and the self-placing concrete designed did not have problems to fill all the voids along the entire length. The distance between the longitudinal strands did not represent a bottleneck to fibres to pass through them and correctly cover the bottom part of specimens. The casting of the concrete was made from the southern part for all the beams holding the back chute steady and leaving the concrete flow along the formwork. The concrete tended to stagnate in the southern part of the beam and then moving on filling the formwork up to the opposite side. This behaviour caused a diagonal flow of the concrete along the formwork with the consequent most likely orientation of the steel fibres parallel to the concrete flow. This is probably the reason that caused a diagonal crack as occurred for R03 and R06 beams in the northern part. The different orientation of the fibres probably caused a reduction in fibre contribution and then an unexpected shear crack. The unexpected failures of the R03 and R06 specimens highlighted the need of precision, attention and quality on the industrial fabrication and casting of SFRC beams.

3.5 Numerical analyses

3.5.1 Finite element model

All the specimens were modelled and analysed using the finite-element software ABAQUS (Hibbit et al., 2010). The SFRC behaviour was modelled by the user-defined subroutine EPM3D (Massicotte et al., 2012). EPM3D is a general and portable constitutive model for nonlinear analysis of plain and fibre-reinforced concrete structures. It is based on three-dimensional hypo-elastic smeared crack approach. Originally implemented either for standard or explicit resolution techniques, the last version EPM3D v-3.2, with which all the analyses presented herein were made, was implemented only for explicit approach principally to reduce the solution time. Furthermore, version 3.2 allows modeling SFRC structures assuming an isotropic post-cracking behaviour with the value of the characteristic length L_R equal to the average size of the finite-element mesh chosen.

The main objective of the numerical analyses was to guarantee the correct use of the constitutive model EPM3D for such structures. This model should be able to predict the performances of a SFRC beam with a satisfactory level of accuracy. To accomplish this goal, numerical analyses shall be able to: predict different failure modes as happened in real tests, detect accurately crack width and spacing, and provide a load displacement relation in agreement with the experimental responses.

Simple-supported boundary condition and eight-node solid elements with reduced integration were considered for all the analyses. Load configuration, boundary conditions and geometry of specimens authorized considering some symmetry expedients: transverse symmetry along the main direction (Figure 3–22) was taken into account for all analyses to reduce the time of solution. A longitudinal symmetry with respect to mid-span cross-section was considered for the specimens loaded symmetrically. A perfect bonded contact between concrete and steel reinforcement was considered. To replicate numerically the unbounded contact of the lowest strands in the specimen R02, the modeled beam was cut horizontally in correspondence of the plane where the lowest strands were placed. A “hard contact” was forced between the two concrete surfaces and the continuity between the two parts was restored. This solution enabled

the relative motion between the strands and the concrete. A finite-element mesh size of 50 mm enabled to obtain a good convergence of the results within a reasonable time.

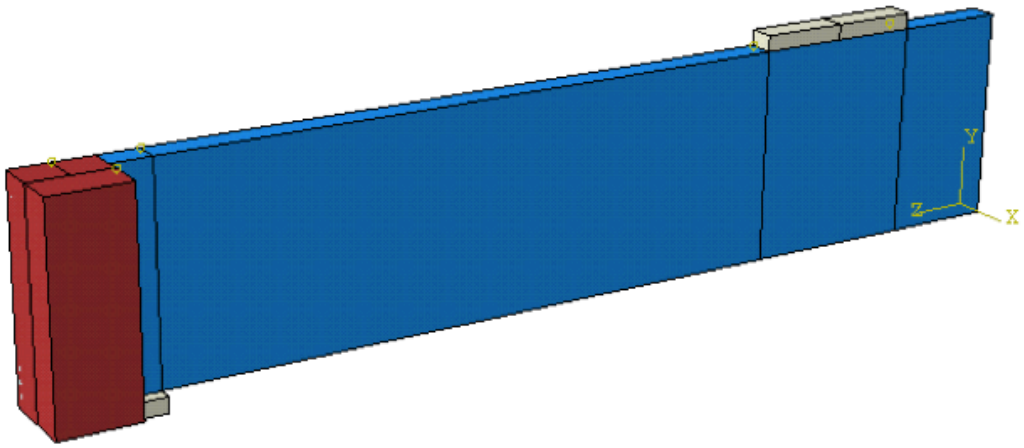

Figure 3–22: Different material of the numerical beam

Load and support plates were modelled with 25 mm elements and steel reinforcements were discretized with linear truss elements with a length equal to 25 mm. All material properties used in the numerical models followed the results obtained from the experimental characteristic tests.

Therefore, EPM3D follows a phenomenological approach allowing the direct introduction of the σ-w curve retrieved by characterisation tests. For each concrete batch the average post-cracking relationship retrieved from round-panel bending tests was used. The simplified σ-w relations used to model the tensile behaviour are 7-points curves that simplify the curves obtained applying the inverse analysis on P-Δ results from the corresponding round-panel tests (Table 3-3).

To avoid the development of cracks in the transfer zone of the prestressing force, which would have not represented the responses obtained in laboratory tests, a linear and elastic behaviour was assigned to the enlarged extremities of all beams.

3.5.2 Numerical results

3.5.2.1 Global behaviour

The excellent concordance between load-displacement relationships obtained by experimental and by NLFEA is shown in Figure 3-23. The numerical results reproduced with a high degree of accuracy the experimental results. Good results were expected because the flexural behaviour is governed by the strands. But near perfect match indicates that the assumptions used for modelling the SFRC are adequate. It has been determined that the post-cracking relationships used to model the beams govern the cracking behaviour of the specimens. Numerically the σ-w relationship used for the model change notably the slope of the P-Δ response after the beginning of the cracking. The reduction of the tensile properties for very small crack openings, which is confirmed by a common direct tensile test (de Montaignac et al, 2012), has been calibrated to give a better match between numerical and experimental results. The results in Table 3-12 highlight the difference in terms of values and percentages for the maximum forces and the maximum displacement measured experimentally and calculated numerically.

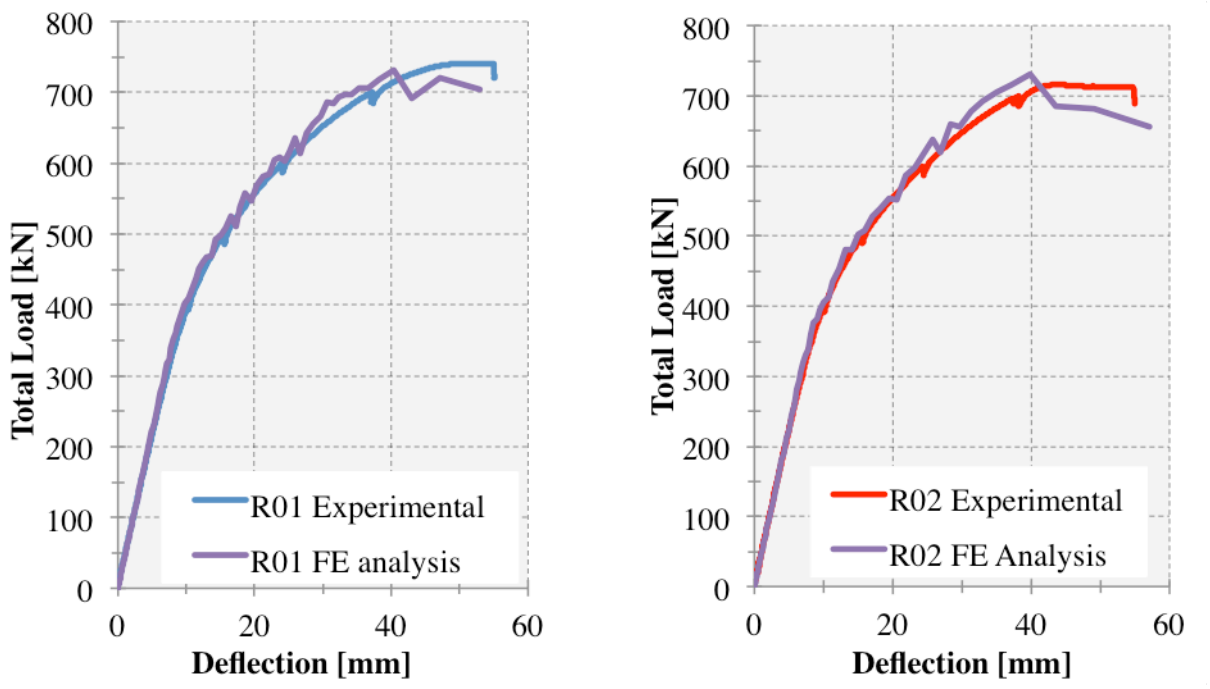

(a) P-Δ of beam R01

(b) P-Δ of beam R02

Figure 3–23: Experimental and numerical P-Δ relationships.

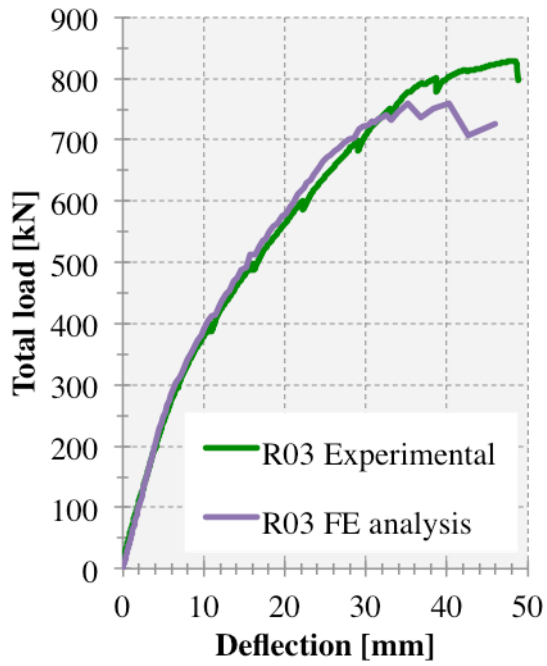

(c) P-Δ of beam R03

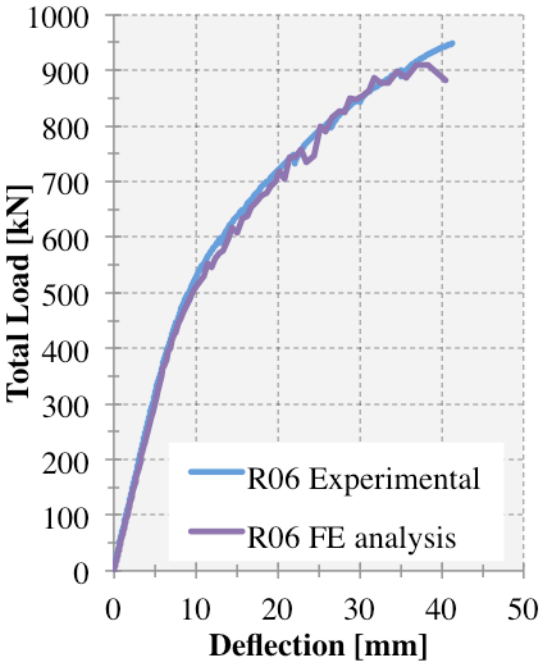

(d) P-Δ of beam R06

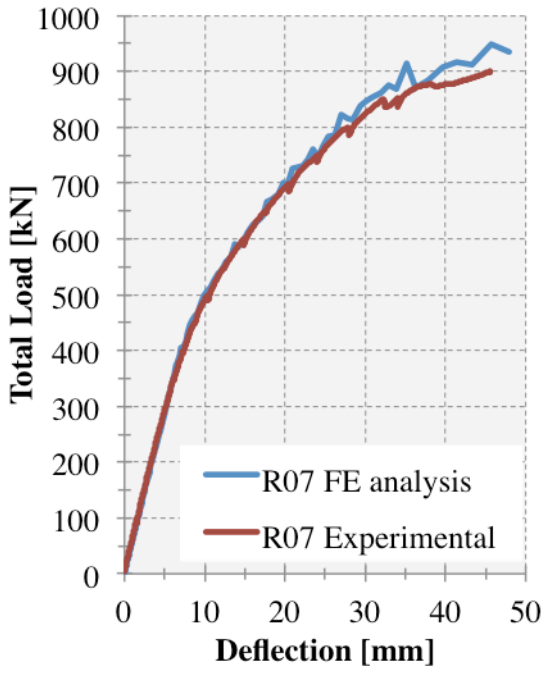

(e) P-Δ of beam R07

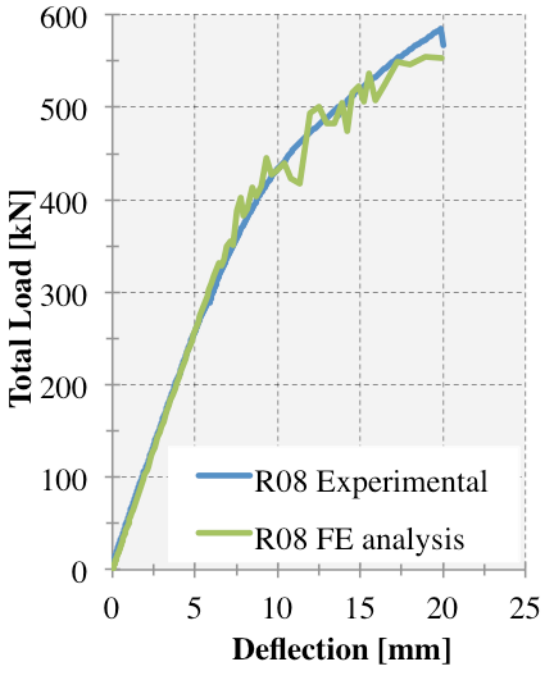

(f) P-Δ of beam R08

Figure 3–24: Experimental and numerical P-Δ relationships (continued)

Table 3-12: Comparison between numerical and experimental results

	Experimental		Numerical		Difference		Failure mode
Beam	P [kNm]	Δ [mm]	P [kN-m]	Δ [mm]	P [kN-m] (%)	Δ [mm]	
R01	737.7	51.6	730.8	40.3	-6.9 (-0.9)	-11.3	Bending
R02	716.6	43.6	731.5	39.9	+14.9 (+2.1)	-3.7	Bending
R03	828.6	48.2	760.4	40.3	-68.2 (-8.2)	-7.9	Shear/Bending
R06-1	950.6	42.3	910.2	40.5	-40.4 (-4.2)	-1.8	Bending
R06-2	858.6	53.0	/	/	/	/	Shear/Bending
R07	900.1	45.6	917.8	41.4	+17.7 (+2.0)	-4.2	Bending
R08	585.6	20.0	555.0	19.0	-30.6 (-5.2)	-1.0	Bending

The initial linear part of all P-Δ curves is well represented by numerical outcomes. Moreover FE analyses provide a correct trend of the load-displacement curves through the cracking phase up to failure. When the first crack appears on the specimen modeled, all P-Δ curves show a slight instability due to the progress and the development of the crack pattern in the model. Maximum loads and displacements at peak-load are predicted with a high level of precision considering the variability of the concrete characteristics introduced in the model that should be taken into account.

The numerical analysis of specimen R03 reproduced the failure for lower values of the maximum bending moment (-8.2%) and displacement (-7.9mm) than experimental measurements. The shear/flexural failure attained by R03 beam was well represented – numerical results reproduced the appearance of a diagonal crack before whether concrete or cables failed for bending stresses. Both for R01 and R02 beams, FE analyses predicted a clear flexural crack pattern with failure due to compressive stresses in concrete as occurred experimentally. A shear diagonal crack was also anticipated for the R06, R07 and R08 models.

The crack-smeared approach used in the EPM3D gives the possibility to follow the evolution of the tensile stress for each element of the beam. This enables determining an average crack spacing according to the finite element size chosen. Consequently the accuracy reachable in determining the crack spacing is equal to the element size chosen. Within this approximation range, the FEM analyses provided reliable crack spacing ranges for each beam analysed. Figure 3–27 shows the cracking pattern at failure for each beam. A comparison between experimental and numerical failures is presented for three specimens in the Figure 3–27.

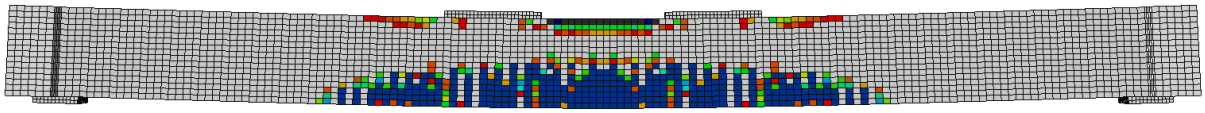

(a) Crack pattern of the beam R01

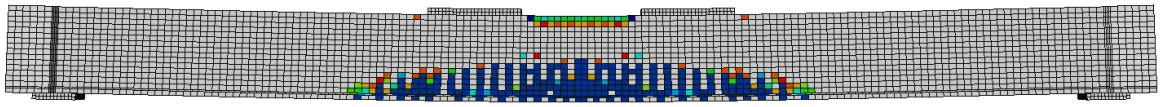

(b) Crack pattern of the beam R02

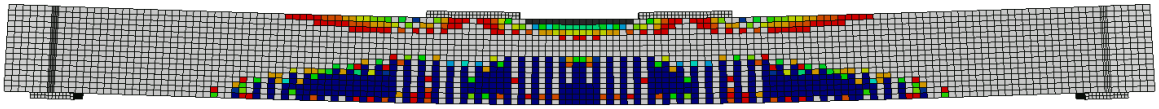

(c) Crack pattern of the beam R03

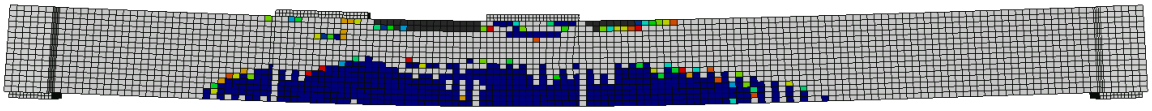

(d) Crack pattern of the beam R06

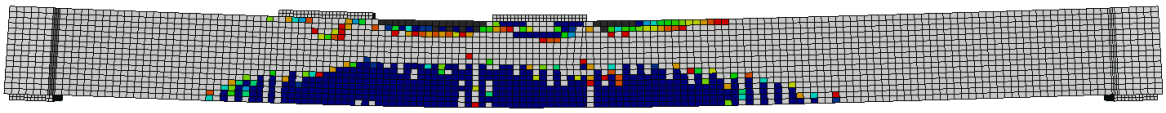

(e) Crack pattern of the beam R07

Colour legend: blue represents cracked concrete, red and green represent the beginning of cracking, and grey is for uncracked concrete

Figure 3–25: Different failure obtained numerically

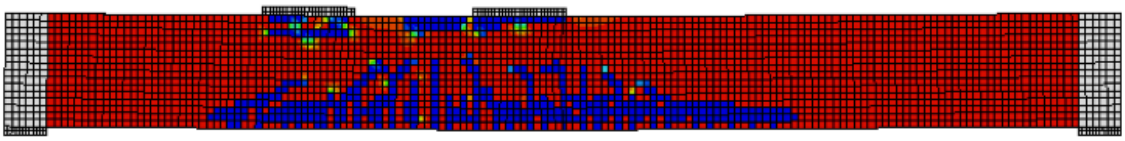

(f) Crack pattern of the beam R08

Colour egend: blue represents cracked concrete, green stands for the beginning of cracking, and red colour is for uncracked concrete

Figure 3–26: Different failure obtained numerically (continued)

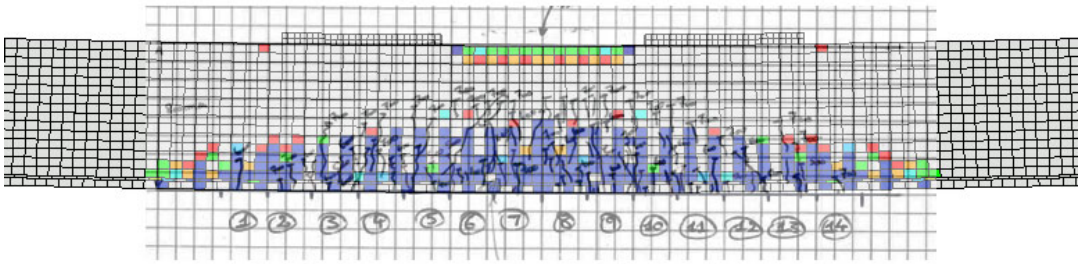

(a) Beam R01

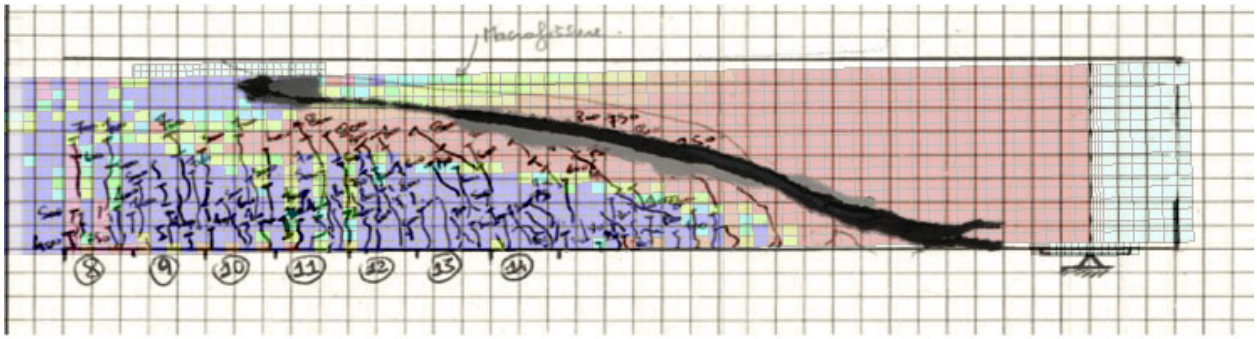

(b) Beam R03

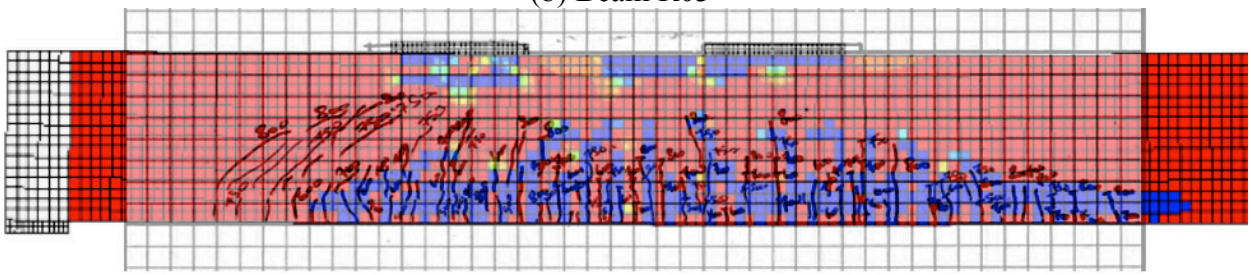

(c) Beam R08

Figure 3–27 : Comparison between the experimental and the numerical failures

The quality of the numerical results obtained confirmed the validity of the constitutive model and the reliability of the inverse analysis hypothesis applied on the round panel results. Numerical analyses well anticipated the overall bearing capacity, the cracking pattern and the failure mechanism occurred for specimens R01, R02, R06 and R08.

Longitudinal prestressed strands mainly determine the bending capacity of each beam tested. The numerical model used to represent the cables and their interaction with the surrounding concrete demonstrate to be consistent in anticipating correctly the bearing capacity.

The agreement of R01 and R02 numerical results with the corresponding experimental outcomes showed the good capacity of the model in modelling bond properties between the concrete and both bonded and un-bonded strands.

The good results retrieved from the beam R08 showed the capacity to study the behaviour of both plain concrete and SFRC with the same constitutive model. The absence of fibres caused a more marked instability in the numerically response of the structure. This is caused by the quicker crack propagation that is no more controlled by the presence of fibres – the final P-Δ relation still excellently approximates the actual behaviour and a shear failure can be easily identified.

Numerical analysis tended to underestimate the capacity of specimen R03. This could be explained by several causes: a higher tensile strength of SFRC than assumed, a better adherence offered by the ribbed bars in the experimental test leading to more closely spaced cracks. Indeed it is possible that the presence of large ribs on the 30M bars created more closely spaced cracks than obtained with de 3D model, as illustrated on Figure 3–27b. A 3D representation of the reinforcement bars could probably overcome the problem and offer a better approximation of the analysis results. Even though the model is not capable to predict the occurrence of this brittle shear failure, the P-Δ relation is still well reproduces up to the earlier propagation of the shear crack.

The displacements found at peak-load are every time slightly lower than the displacement experimentally measured. This is principally due to the difficulties of the numerical analyses in handling the increasing of the internal energy for load values close to the failure. When structure strains are large enough to get the beam to the failure, the energy inside the model becomes too high and the analysis cannot reproduce correctly the post load-peak mechanism. Changing the load rate in proximity of the failure load could be a solution even if the time cost might be

excessively high. Finally the numerical analyses showed an acceptable ability to anticipate the mechanical behaviour, the crack pattern and the failure mode. Either for plain or fibre reinforced concrete EPM3D could offer reliable and necessary information in the design of prestressed beams.

3.5.2.2 Crack opening measurements

The experimental program enabled to calculate the displacement of some strategic points on each beam. For the 4 beams tested in shear conditions two different systems were adopted: 11 Linear Variable Displacement Transformer (LVDT) – as shown in Figure 3–18 – were placed in the zone where a diagonal shear failure was expected (Figure 3–17). In the same part of the beam – close to the support – 8 more LVDTs at the center of the bottom surface were placed to detect the propagation of the crack. Moreover for all the beams tested in flexural conditions, 15 LVDTs were installed symmetrically on the beam bottom face. The length of all the LVDTs placed underneath the beams was equal to 250 mm.

The LVDTs, measuring the displacement between two points, are a great indicator of the crack width evolution with the increasing load. The knowledge of the crack width at each different load values would allow determining the fibre contribution to the shear and bending resistances. Moreover it is not easy to predict the crack width without experimental tests. Too many factors influence the cracking pattern: type and volume of fibres, geometry of the structure, matrix strength, load level etc. To overcome this incertitude in predicting the crack width, a numerical study on each beam aimed to reproduce the crack pattern obtained from the experimental campaign. Only few of the relations calculated will be presented herein to show the overall accordance of the results achieved. Results for specimens R01, R02 and R03 are presented to investigate the use of different types of longitudinal reinforcement. Specimen R06 results also aims to validate the prediction of the crack pattern evolution for a shear load configuration. The measured and modelled crack opening for these four specimens are presented in Figure 3–28 to Figure 3–34.

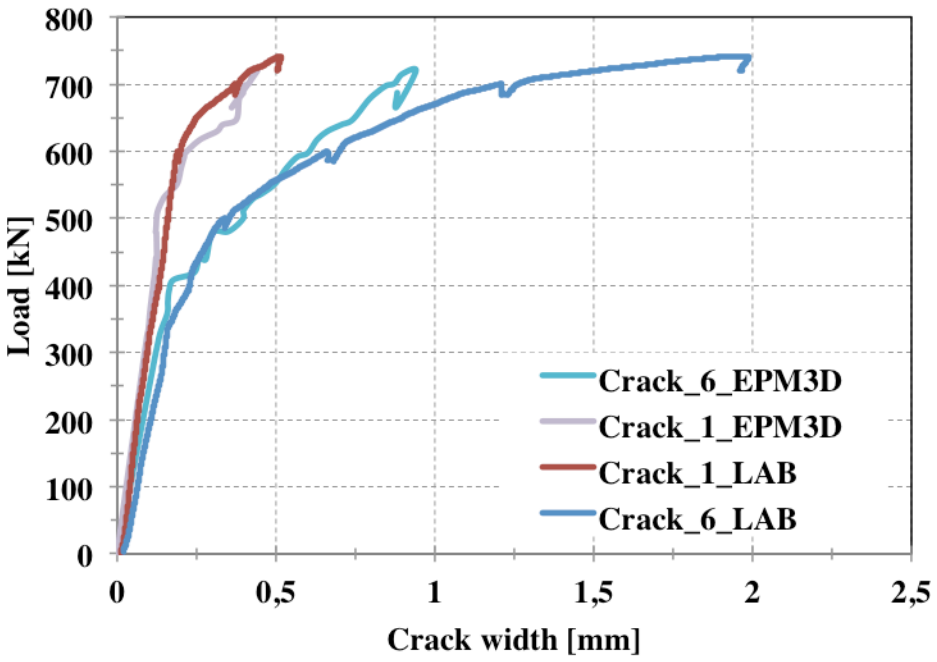

Figure 3–28: Experimental and numerical displacement measurements of LVDTs 1 and 6 for R01

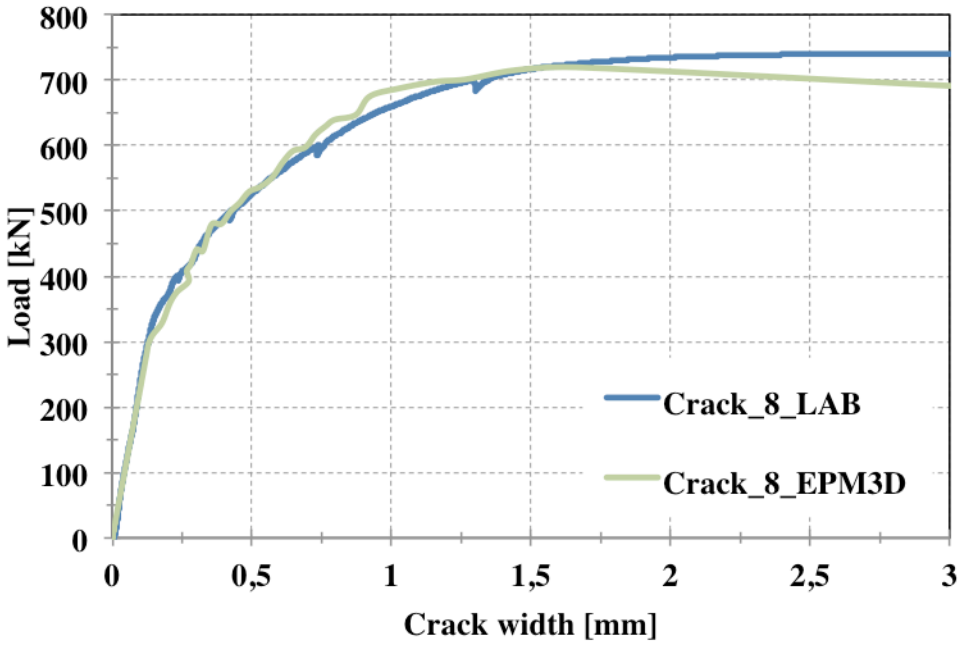

Figure 3–29: Experimental and numerical displacement measurements of the LVDT 8 for R01

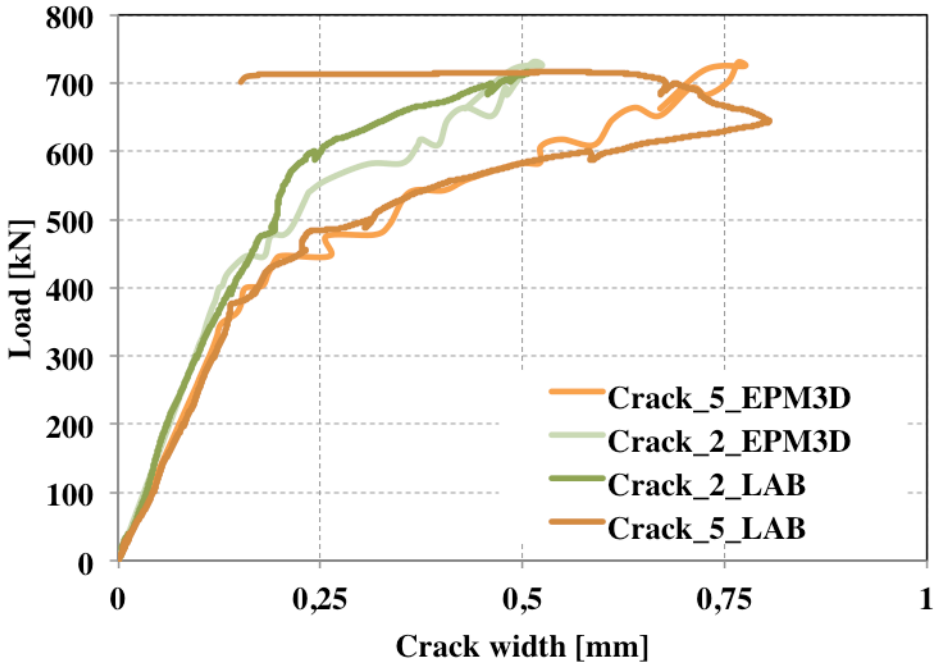

Figure 3–30: Experimental and numerical displacement measurements of LVDTs 2 and 5 for R02

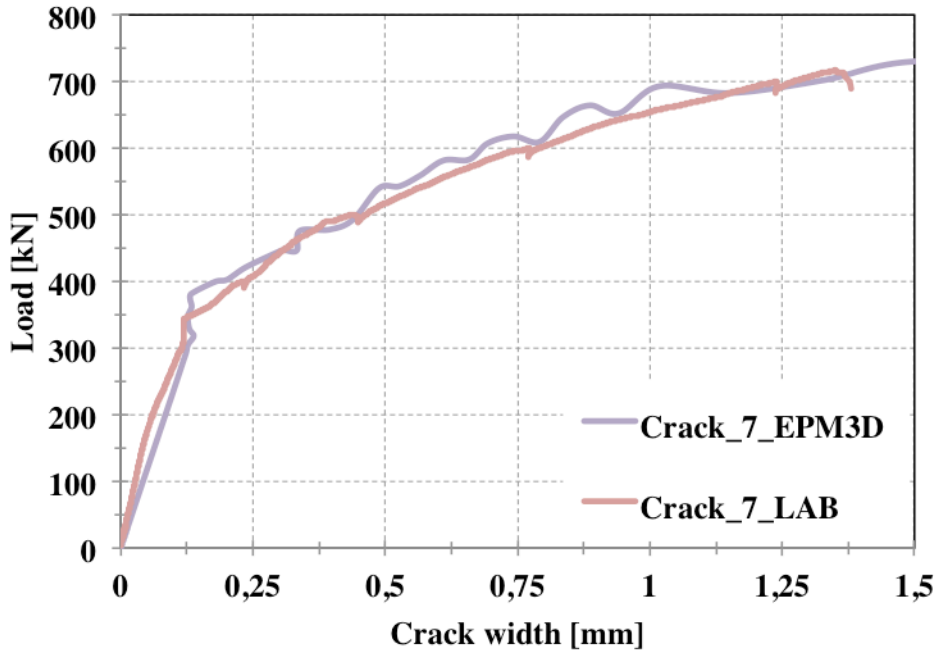

Figure 3–31: Experimental and numerical displacement measurements of LVDT 7 for R02

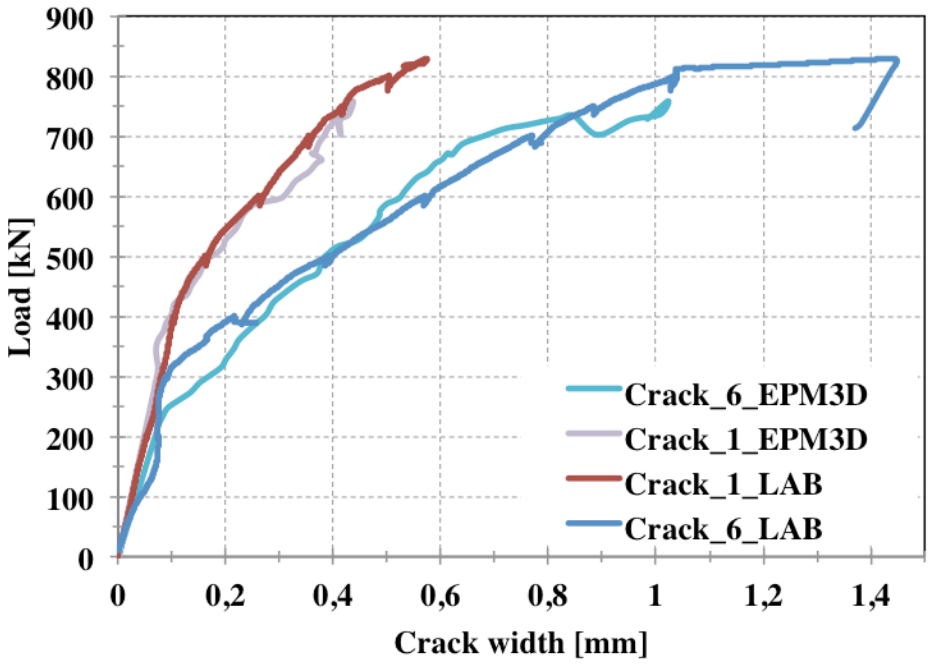

Figure 3–32: Experimental and numerical displacement measurements of LVDTs 1 and 6 for R03

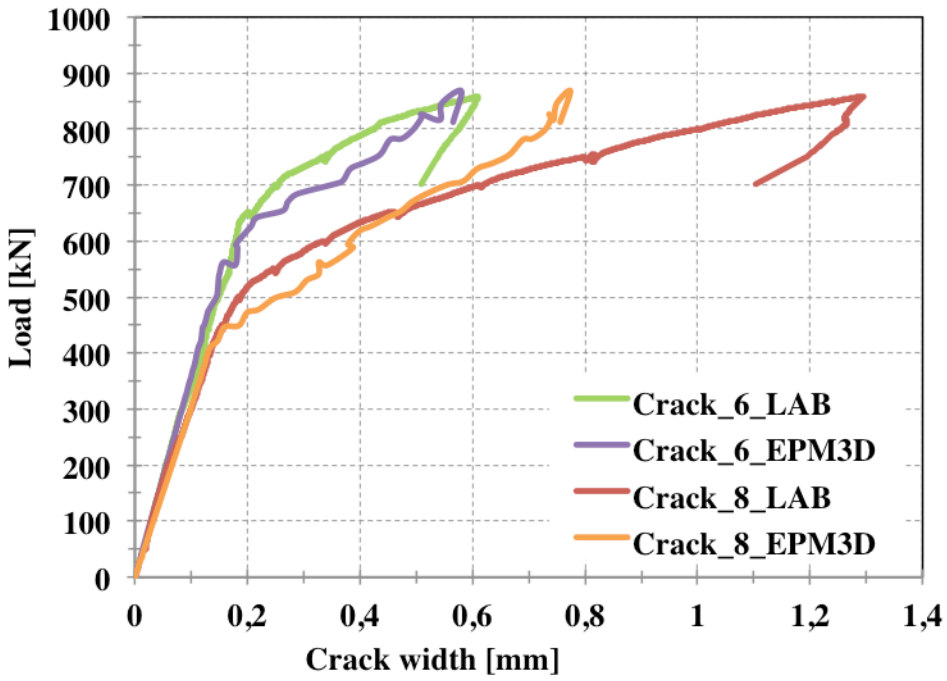

Figure 3–33: Experimental and numerical displacement measurements of LVDTs 6 and 8 for R06_02

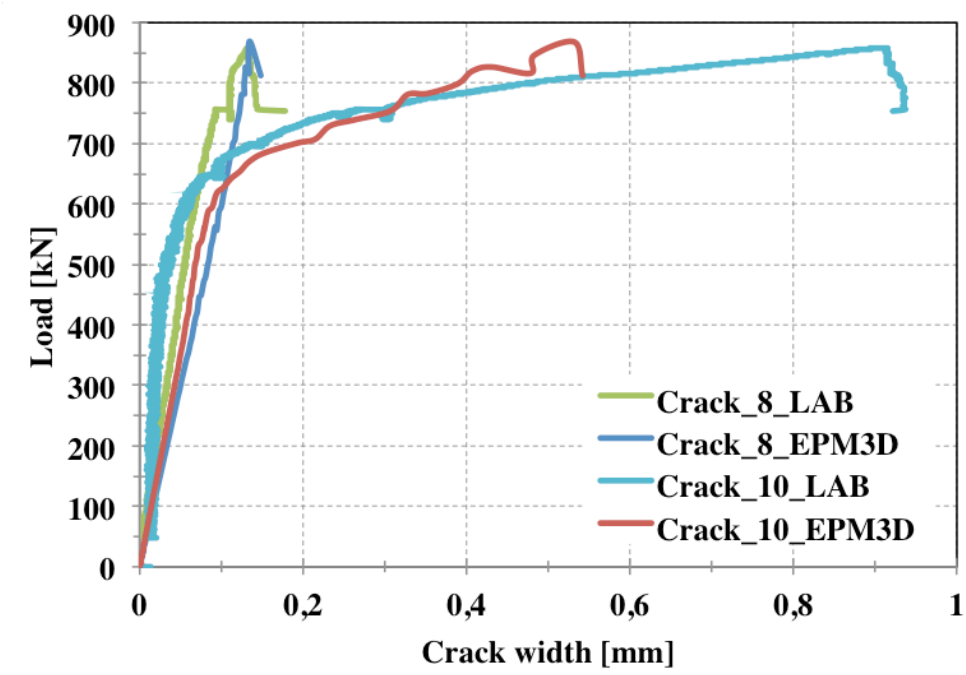

Figure 3–34: Experimental and numerical displacement measurements of LVDTs 8 and 10 of the X-LVDT system for R06_02

In the interest of readability, for each of the beams presented above not all crack measurements are presented. For each case, the most representative results are shown. From Figure 3–28 to Figure 3–33, the measurements of the LVDTs located under the beam are shown. Figure 3–34 presents the crack measurements corresponding to the LVDTs located close to the R06_02 south extremity – the numeration of the measuring devices follows Figure 3–18.

The NLFEA clearly demonstrated – as seen for every crack measurement – to be able to detect the correct evolution of the cracks from the beginning up to the failure of each beam tested. The initial linear relation is adequately identified. The load that corresponds to the first crack is easily recognised at the end of the linear relationship for all crack measurements – FE models retrieved those loads values with a great level of accuracy. Moreover, the FE relationships follow the trend of experimental results up to the failure of the structures with a good prevision of the maximum displacement at the failure point.

The first graph of the R06 beam represents two crack measurements from the LVDTs placed below the beam; the second graph shows the crack evolution measured by two of the X-LVDT-

system as numerated in the Figure 3–18. Even for the shear failure case, the constitutive model EPM3D offered a great level of accuracy in providing the progress of the diagonal crack.

Globally, the constitutive model used ensures a great accuracy in crack prediction for such a structures. SFRC beams with different kind of longitudinal reinforcements either for flexural or shear ultimate state are well represented by numerical analyses.

3.5.2.3 General comments

All along this chapter, the concepts of crack width and of relative displacement are considered as the same notion. Even if the LVDTs did not measure exactly crack opening values, they measured the relative displacement between two points probably taking into account more than one crack in the same measurement. Anyhow the measurements done are considered to be the most valuable parameter to determine reliable values for the crack width. The validation of the model EPM3D in predicting relative displacements between the same points is considered satisfactory because the model measures the same physical parameter as done for the experimental campaign. It is however difficult to clearly conclude on the actual opening of individual cracks.

The capacity of EPM3D to predict the crack evolution, as presented just above, provides even more evidence of the capabilities offered by this constitutive model. Using a σ-w design approach, knowing the crack width evolution according to the load applied, would allow determining the fibre contribution with accuracy for each load level up to the failure. For example, to calculate the shear capacity, the Casanova's approach (Casanova, 1995) needs the knowledge of the average crack width w_m to compute the fibre contribution. A numerical analysis could provide this necessary information with a certain level of accuracy.

The constitutive model EPM3D demonstrated to provide a valid, solid and reliable prevision of the actual behaviour of the large-scale specimens tested. Moreover, the model allows a direct introduction of the σ-w relation, which enables an easier management control by users – who merely entry the curve obtained from the characteristic tests. The post-cracking tensile relation could be retrieved by a direct traction test or applying an inverse analysis approach to one of the available bending tests. The use of the second technique has been previously validated.

3.6 Conclusion

The main objective of this chapter was to established the appropriate approach for modelling prestressed SFRC beams and to validate the model predictions for flexural and shear failures. Through these analyses, another objective was to provide a detailed analysis of the experimental results obtained in a previous work, including a global analysis of the technical feasibility of fabricating SFRC prestressed girder for bridges. In that context, the following conclusions can be made.

- The industrial prefabrication of large SFRC beams ensures to obtain high-quality products. The thickness of the cross section and the distance between prestressed strands did not interfere with the SFRC flow.
- The casting phase was found to be crucial for the fibre orientation. The shear/bending failure occurred for the beam R03 could have been caused by a diagonal weaker plane as a consequence of the directional flow of the SFRC during the casting process;
- Inverse analysis applied either to round-panel or notched-beam tests revealed to be consistent. Post-cracking relation retrieved from notched beam tends to overestimate the real tensile properties. The excellent results obtained with FEM analyses validate the choice of using the σ-w average relationships from round-panel tests.
- The use of bonded or un-bonded strands did not reveal any significant difference in terms of crack pattern, bearing capacity and ductility. Moreover, the use of two 30M bars showed a larger bearing capacity than specimens with bonded and un-bonded strands. This is possibly due to the better adherence offered by the ribbed surface of the bars. Closer cracks were also observed – the improved adherence between concrete and reinforcement could explain this phenomenon.
- The simultaneously increase in bending capacity, due to the better adherence offered by the rebars, and the reduction of the shear contribution provided by steel fibres, probably caused by the incorrect fibre orientation on one side of the specimen, resulted in a shear/flexural failure of the beam R03. Thus a minimum quantity of transverse reinforcement is highly recommended in SFRC structures to avoid any incertitude related to the orientation of fibres.

- The comparison between the specimens R07 and R08 pointed out that steel fibres can increase the shear ultimate bearing capacity (+35%) and the ductility (+44% in terms maximum displacement at failure) of the specimen.
- EPM3D provided excellent numerical results of such concrete structures. Bearing capacity, displacement and cracking pattern are provided accurately for any load level. Moreover bending and shear failure modes can be both reproduced. Its use might be a reliable resource to be exploited in design analyses.

CHAPTER 4 DESIGN OF SFRC T-GIRDERS

4.1 Proposed bridge system

The main idea of the entire project is to give the possibility to build a bridge superstructures with precast beams connected by UHPFRC joints as in Figure 4–1. The single prestressed T-beam represents the structural module of the bridge system. The number of the beams that constitute the bridge would vary according to the required width. The precast of the entire set of beams before their positioning would save time and guarantee a better control of the mechanical properties of the material. Once all the beams are placed, the UHPFRC joints will be cast to connect transversally the beams.

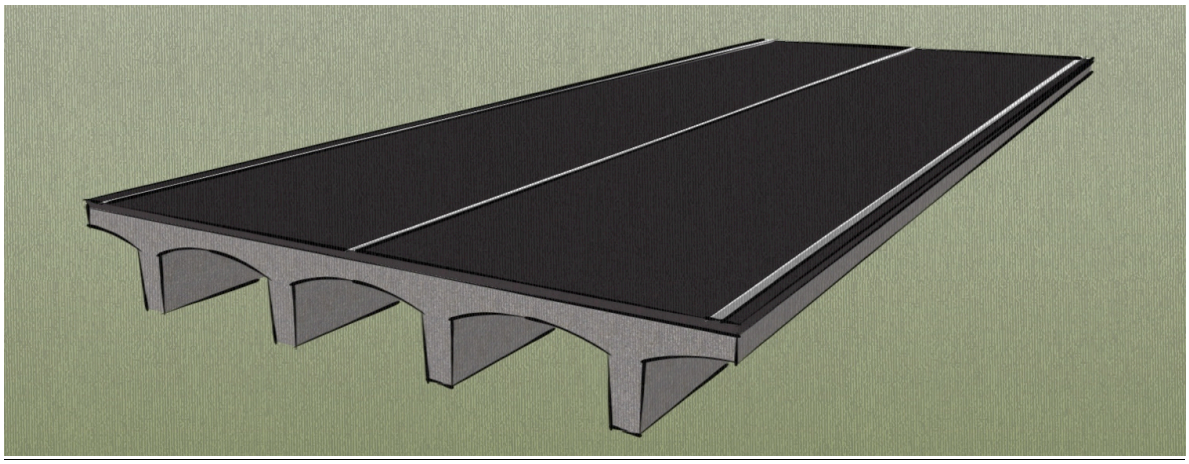

Figure 4–1: Sketch of the final deck configuration

The design of the whole modular cross-section is divided into three different phases: the fabrication of the precast prestressed SFRC T-beams, their connection in the field with lapped conventional reinforcement joined with UHPFRC, and the installation of asphalt (and membrane if required) and precast barriers. The typical shape of the T-girders is illustrated in Figure 4–2. As described later, only one layer of transverse conventional reinforcement is considered in the deck.

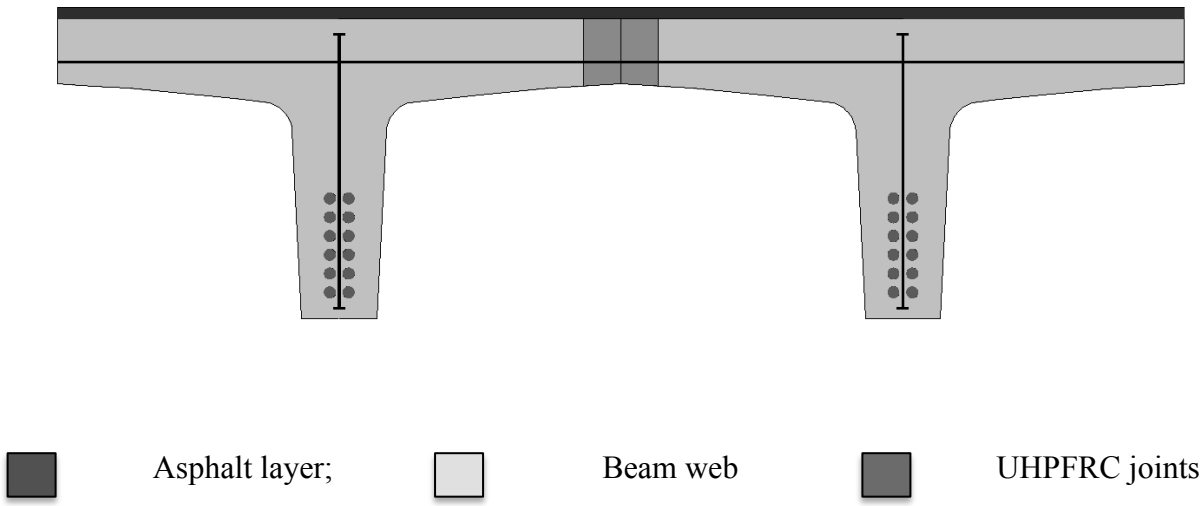

Figure 4–2: Sketch of the double-T-beam cross-section

The experimental study conducted by De Broucker (2013) aimed to investigate:

- the mutual behaviour between steel fibres and prestressed strands;
- the industrial feasibility of such precast structures;
- the cracking pattern obtained using different longitudinal reinforcements;
- the shear strength contribution offered by steel fibres.

Analytical and experimental studies by Faggio (2014) aimed to provide the geometrical section and the quantity of the transverse reinforcement of the integrated slab. The UHPFRC connections are chosen to carry the positive transverse moments at the cold joint between the longitudinal beams and contribute to the negative bending moment resistance over the beams.

To investigate the longitudinal resistance of the beam a numerical study is done in this thesis. The following phases can be identified:

- determination of the design criteria to be fulfilled;
- determination of the geometry of the cross-section;
- investigation of the flexural and the shear behaviour of the section chosen for different span lengths.

4.2 Design criteria

4.2.1 Background information

There is no code covering the design of SFRC prestressed beams yet. The results from previous research studies – mainly Massicotte et al., 2012 and the thesis project presented in De Broucker (2013) – combined with some requirements demanded by the MTQ allowed determining the design criteria. In this thesis the study of three sections corresponding to three different spans will be done with the support of nonlinear constitutive model EPM3D (Massicotte et. al. 2013) used with FE analysis software ABAQUS (Hibbit et al., 2010). The pre-design of the beams is divided into two phases: in the first one the loads applied to the structure and the design criteria to be fulfilled are determined; the second step deals with the non-linear study of the beam – flexural and shear load configurations are studied in order to provide a proper cross-section.

The following points summarise the most important conclusions of the previous studies:

- steel fibres can improve significantly the ultimate shear strength;
- the presence of metallic fibres provides more and closer cracks than in plain concrete structures which enables the structure to control and reduce the crack development in service conditions;
- industrial procedures demonstrated to be appropriate to manufacture SFRC mixes with high-standard mechanical performances using admixtures to obtain a self-compacting concrete without segregation which enabled a correct and quick casting of the concrete;
- the post-cracking tensile behaviour of the mixes produced reached the requested minimum values in term of compressive strength and post-cracking characteristics;
- two different level of longitudinal reinforcement shall be used – the first level of prestressing aims to avoid the curvature caused by the self-weight of the beam to simplify the storage of the prefabricated beams – and the second level is needed to allow the beam to attain the ultimate capacity required;
- the use of bonded prestressed strands, un-bonded prestressed strands or reinforcing bars as longitudinal reinforcements did not give significant differences in term of crack openings and crack spacing and any combination can be considered;

- the un-expected failures obtained from experimental tests suggested the presence of a minimum amount of stirrups to avoid the incertitude linked to the fibre orientation and cold joints;
- an optimum fibre volume ratio equal to 1% is suggested in order to obtain a more uniform distribution of the fibres over the entire cross-section;
- the total height of the beams was indicatively chosen equal to *L*/25;
- the slab profile is determined to reduce transverse stresses of the section and the same final geometric profile was used for the sections of all the different girders.

4.2.2 SFRC

The mechanical characteristics of the SFRC follow the results obtained in the experimental campaign. The fabrication of a SFRC mix attaining a minimum compressive strength of 70 MPa did not presented any feasibility issues. Moreover all the mixes manufactured provided a minimum post-cracking tensile strength equal to 2.5 MPa up to a crack opening of 1 mm as expected. The experimental campaign carried out by De Broucker (2013) highlighted the industrial feasibility of such a SFRC mix. Previous studies (Tordjman, 2011; Androuët et al, 2012) reached similar results in terms of mechanical properties. The same studies showed that an optimum volume content in fibres equal to 1% – this percentage provides a more uniform distribution of the fibres in the whole structure and consequently a reduced scatter in terms of tensile properties. This elevated amount of fibres reduces the workability of the mix which must be adjusted. The Baron-Lesage design method was adopted to design the final mix. To achieve a correct orientation of the fibres along the beam, a self-compacting concrete is necessary. The use of superplasticizer is needed to achieve the workability required. The $\sigma - w$ relation describes the post-cracking behaviour of the SFRC used for the design of the beams.

To make a conservative choice of the retained $\sigma - w$ for design purposes, the average relationships retrieved from notched beam and round panel tests carried out for the experimental campaign (De Broucker, 2013) have been considered. Inverse analysis prediction on the notched beam tests tends to slightly overestimate the post-cracking properties, especially for small crack width (de Montaignac, 2012).

To determine the characteristic $\sigma - w$ relationship the Student's rule – equation 4-1 – must be applied:

$$\sigma_{ch} = \bar{\sigma} \cdot (1 - t \cdot V) = \bar{\sigma} \cdot \mu \tag{4.1}$$

where *t* is the Student's factor and in the case of using the inverse analyses method the coefficient of variation *V* must be calculated with the statistical distribution of the area under the load-deflection curves up to a prescribed displacement (de Montaignac, 2012). The coefficient of variation could be rather high, especially considering SFRC with low fibre volume. Therefore, to take into account a larger number of different possible SFRC mixes, the post-cracking properties chosen for the characteristic relation are half the average properties reached by the inverse analysis applied on round panel tests up to a crack width equal to 1 mm. For larger crack width the results from round panel tests tend to underestimate the actual pot-cracking properties of the SFRC mix. So that, the characteristic relation chosen for w > 1 mm has not been reduced. The real post-cracking properties could be likely identified between the notched beam and the round panel results. For design purposes the lower bound – round panel test results – has been chosen to represent the post-cracking properties for crack width higher than 1 mm as the Figure 4-3 illustrates.

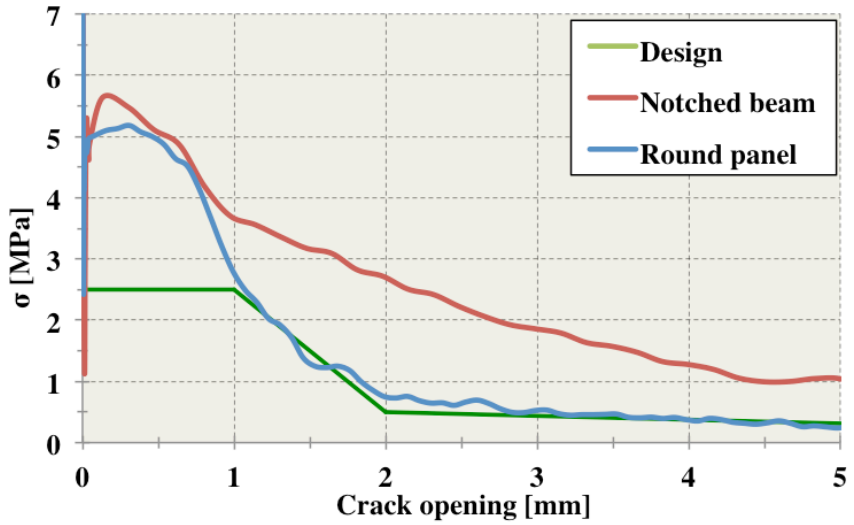

Figure 4–3 : $\sigma - w$ relations respectively retrieved from experimental campaign (De Broucker, 2013) and the simplified one used for design purposes

4.2.3 Longitudinal reinforcement

De Broucker (2013) experimental results did not highlight differences between the use of bonded or un-bonded prestressed tendons in terms of crack pattern, ultimate resistance and ductility. The use of 30M bars showed a better adherence between concrete and reinforcement due to the ribbed surface of the bars. For this reason narrower and closer cracks appeared and a higher ultimate resistance was attained. Finally, the results obtained are not considered to be relevant to privilege any type of longitudinal reinforcements. Even if bonded prestressed tendons constitute the final choice – object of the nonlinear analysis study – a preliminary study carried out using of different types of reinforcement will be presented. Thus, horizontal prestressed bonded strands are used as the primary longitudinal reinforcement for all sections studied. The possibility to use parabolic strand profile or adopt inclined strands has not been considered to adopt simple and economical concept to optimise the fabrications costs. Two different levels of prestressing tendons characterize the longitudinal reinforcement of the beams. The first level aims to avoid the curvature caused by the self-weight forces of the beam after its fabrication. Providing a zero-curvature after the fabrication, would allow creep and shrinkage strains to induced only axial deformation, enabling to store the girders for long periods without concerns with the development of long term deflection. The second level of prestressed strands would be applied at the time of construction, at the precast plant or on the construction site. The adherence between the strands and the concrete could be provided by high-pressure injections of mortar into ducts pre-installed before casting the SFRC. The prestressed stress imposed to all strands in the design phase is equal to 1300 MPa (0.70 f_{pu}).

4.2.4 Crack opening

In the previous study (De Broucker, 2013), an uncracked section was envisaged for permanent load at serviceability limit state. A maximum crack opening of 0.5 mm was permitted considering moving loads at the serviceability limit state. In this study it was decided to not allow any crack at the serviceability limit state. The main reason in so doing is to ensure a better protection of the prestressed wires providing the best conditions possible for the durability of the beam. Although cracks will not appear at the bottom of the beam at the SLS, steel fibres are necessary to control and avoid the crack development in the integrated slab. They contribute also to simplify the reinforcement in the anchorage zone of the prestressing. As seen previously, fibres improve

significantly the shear strength of beams. Nonlinear FE analyses will be able to predict the evolution of the cracking pattern in service conditions and up to the failure.

4.2.5 Stress range of reinforcement stresses

In the examples studied by Braike (2007), the stress range limitation was the most critical criterion for the design of prestressing tendons. This criterion requires some expedients to overcome the excessive variation in reinforcement stresses. The use of unbounded strands for the lower level of the longitudinal reinforcement configuration reduces significantly the stress range at the fatigue limit state – the relative movement between the concrete and the strands is allowed and no transmission of stress is provided at the contact surface. The Canadian Code CSA-S6 imposes a limit value for the stress range in the steel reinforcement equal to 125 MPa for both reinforcing bars and prestressed strands and 70 MPa for prestressed bars. Using bonded tendons the limit to be respected will be: $\Delta\sigma_{FLS} < 125MPa$. Contrary to Braike, adopting an uncracked condition would significantly reduce the stress variation due to moving loads.

4.2.6 Material resistance factors

The material resistance factors for both types of reinforcement are chosen following the Canadian Bridge Code CSA S6-06 (CSA, 2006). The SFRC factor is determined from Bélanger (2000) for SFRC deck application. It is the same used for concrete in the bridge code. Bélanger's findings indicated that the proposed value is lower than the results obtained from her study.

Table 4-1: Material resistance factors

Concrete	$\boldsymbol{\phi_c = 0.75}$
SFRC – post-cracking	$\boldsymbol{\phi_f = 0.75}$
Reinforcing bars	$\boldsymbol{\phi_s = 0.90}$
Prestressing strands	$\boldsymbol{\phi_p = 0.95}$

4.2.7 Material mechanical properties

Concrete: compression

The concrete properties chosen to design the different beams are the following:

- $f_c' = 70\ MPa$;
- $E = 36000\ MPa$;
- $\upsilon = 0.2$.

These characteristics came from the experimental study carried out by De Broucker. The tests demonstrated the industrial feasibility of such a SFRC mix.

Concrete: traction

The tensile cracking strength resistance of the SFRC mix is calculated with the equation (4.2) used in the implementation of EPM3D:

$$f_{cr} = 0.33 \cdot \sqrt[2]{f_c'} \tag{4.2}$$

For a 70 MPa concrete, this equation gives a cracking strength of 2.75 MPa.

The post-cracking behaviour is retrieved from the results obtained from the experimental campaign. The average $\sigma - w$ obtained applying the inverse analysis to the round panel test results is used. The designing relation used in the tests is the simplified relation illustrated in Figure 4-3.

Strands

Bonded strands T-15 are used throughout the nonlinear analyses on the different beams. The strands used have exactly the same characteristics of the ones used in the experimental campaign:

- $A_p = 140\ mm^2$;
- $f_{py} = 1680\ MPa$;
- $f_{pu} = 1860\ MPa$.

4.2.8 Summary of design criteria:

The selected design criteria are summarised as follows:

- SLS: no cracks at the bottom part of the beam;
- SLS: $\Delta_{SLS} < {}^{L}/_{800}$
- FLS: stress range in the tendons $\Delta\sigma < 125\ MPa$ and displacement;
- ULS: $M_r > M_f$ and $V_r > V_f$.

4.3 Reference cross-section

4.3.1 Introduction

A T-cross-section was been chosen to meet all criteria required. The previous study fixed approximately the height of the beam equal to ${}^{L}/_{25}$ – 600, 800 and 1000 mm respectively for spans equal to 15, 20 and 25 m. In this thesis a more detailed study aims to determine the section characteristics starting from the geometry investigated previously. Although this is the outcome of the design, presenting the final design helps following the different steps followed in the entire design procedure.

The width of the integrated slab is fixed to 1500 mm. The slab thickness is fixed at 175 mm at both extremities of the T-section and the bottom profile must be designed to limit the stresses caused by the transverse bending due to live loads. The longitudinal strand configuration must meet certain distance requirements: a minimum distance of 50 mm between the strands must be respected in both directions to allow the application of the prestressing force. Also minimum distance of 70 mm from the bottom edge is required to ensure proper fibre flow underneath the prestressing strands. The reduced width of the web obliges to arrange the longitudinal strands on two vertical rows at the center of the web. The lateral profile of the web is inclined: a width equal to 250 mm at the top and a width of 200 mm at the bottom is kept constant for each beam size. The cable configuration and the geometrical limitations for the beam web are chosen to minimise any issues related to the fibre flow and optimise their orientation. Moreover the geometrical characteristics were chosen to standardise the profile of the section to reduce the costs related to the production process – mainly associated to the formworks.

The use of a minimum transverse reinforcement is envisaged: simple stirrups at the center of the web between the two rows of strands or conventional stirrups might be used. The proposed cross-section profiles are shown in Figure 4–4.

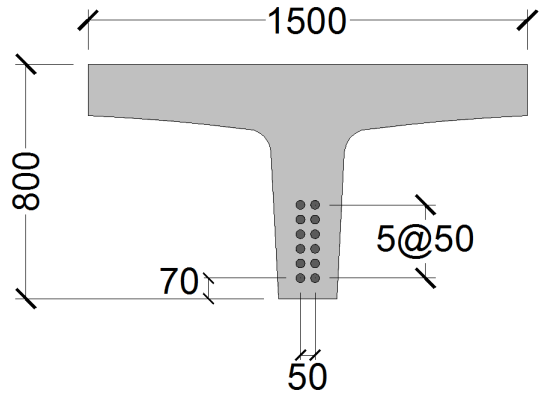

(a) Cross-section for L = 15 m

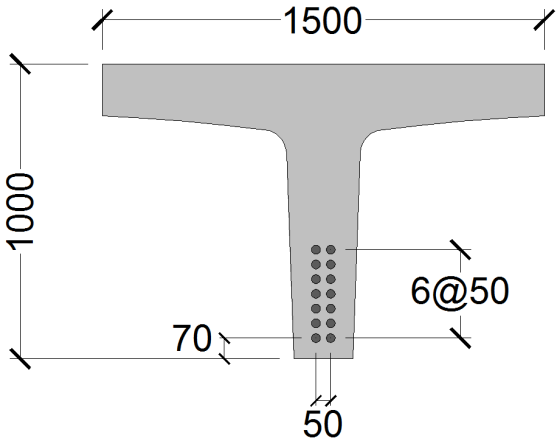

(b) Cross-section for L = 20 m

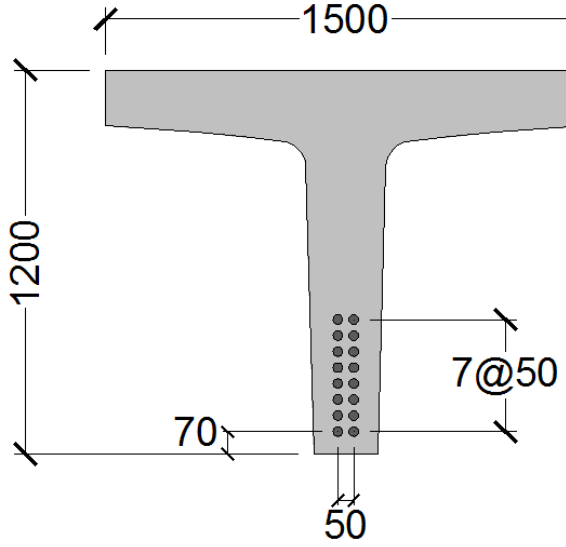

(c) Cross-section for L = 25 m

Figure 4–4: Transverse cross-sections for spans equal to 15, 20 and 25 m

As indicated above, the slab configuration is common to all spans considered. This solution would allow the use of the same formworks for every span considered. The parabolic profile (Equation 4.3) was optimised by Léa Faggio (2014) with the objective of minimising tensile stresses in both positive and negative moment regions allowing the use of only one layer of transverse reinforcement.

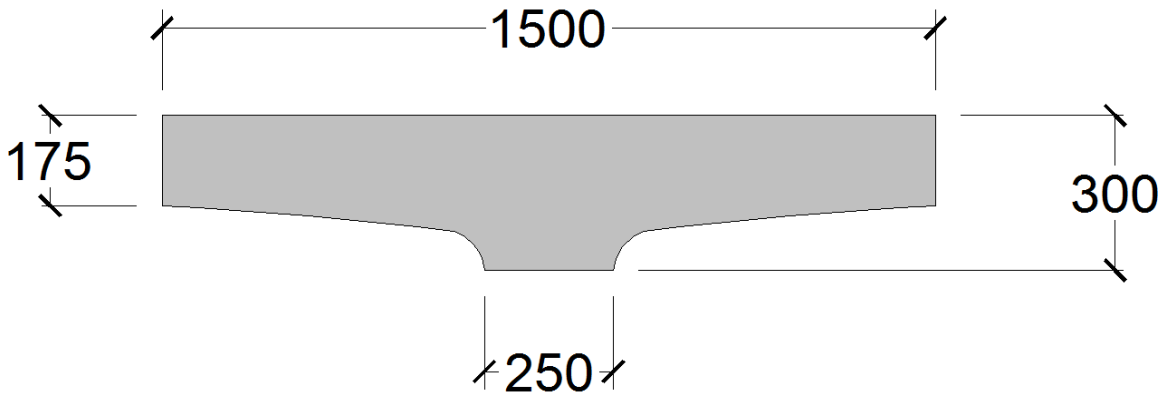

Figure 4–5: View of the integrated slab profile

The curve describing the bottom profile of the slab is determined to limit the forces caused by transverse loads. Placing the origin of a hypothetical $x - y$ plane at the top right extremity of the web, the profile follows that relation:

$$y = h \cdot \left\{1 - \sin\left(\frac{\pi}{B} \cdot \left(x + \frac{B}{2}\right)\right)\right\}^{n} \tag{4.3}$$

Where the geometrical properties chosen are:

h = 125 mm;

B = 1200 mm;

n = 0.43842.

The application of the prestressed force on the section induces curvature on the beam opposite to that of applied loads. Creep associated with this curvature causes problems during the girder storage before the bridge construction. To avoid this problem, it is suggested to apply the prestressing in two different stages. The first one (e_1) – applied after the attainment of a specific predefined resistance for the concrete – aims to provide the necessary force to equal the curvature caused by the self-weight of the beam. Trying to attain an overall curvature close to zero would simplify the stacking of the beams after their fabrication. The second level of prestressing force (e_2) would be applied before the transportation phase or directly on the construction site, depending on how the site is equipped. The total prestressing force allows the beams to attain the capacity to meet serviceability and ultimate design criteria.

The total height of the section and the number of longitudinal strands are the parameters to be determined with respect of any design criteria. Details are indicated in Table 4-2.

Table 4-2: Main geometrical characteristics of the three designed sections

	15m	20m	25m
Section	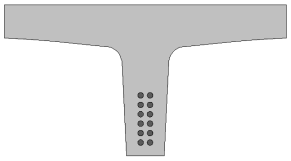	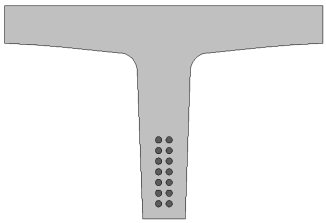	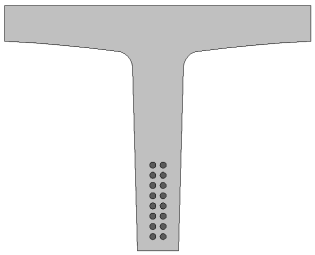
Height [mm]	800	1000	1200
# strands	12	14	16
e_1 (# strands)	310 (6)	425 (8)	540 (10)
e_2 (# strands)	460 (6)	600 (6)	740 (6)

Due to the required height of the 25 m beam, it has been decided that 30 m spans would require too deep cross-section, not effective for this type of beam, and was therefore not considered. A section with a large bottom flange is necessary for longer spans, which is outside the scope of this project.

4.4 Flexural strength with AIS

4.4.1 Flexural response

A preliminary study of the sections is done using the software AIS (Massicotte et al, 2014). This numerical tool allowed the calculation of the nonlinear flexural strength at all loading stages of a cross section. The use of different kind of longitudinal reinforcement is investigated. Three types of longitudinal reinforcement are studied: bonded T15 tendons, un-bonded T15 tendons and 30M reinforcing bars. The case of reinforced concrete without fibres is also presented. As done in the experimental campaign in the chapter 3, the different reinforcement used refers only to the lowest row – all the other tendons are bonded.

The moment crack-width behaviour of all girders are illustrated in Figure 4–6 to Figure 4–8. Results are summarised in Table 4-3 to Table 4-5. Only the final design configurations that satisfy the design criteria are presented.

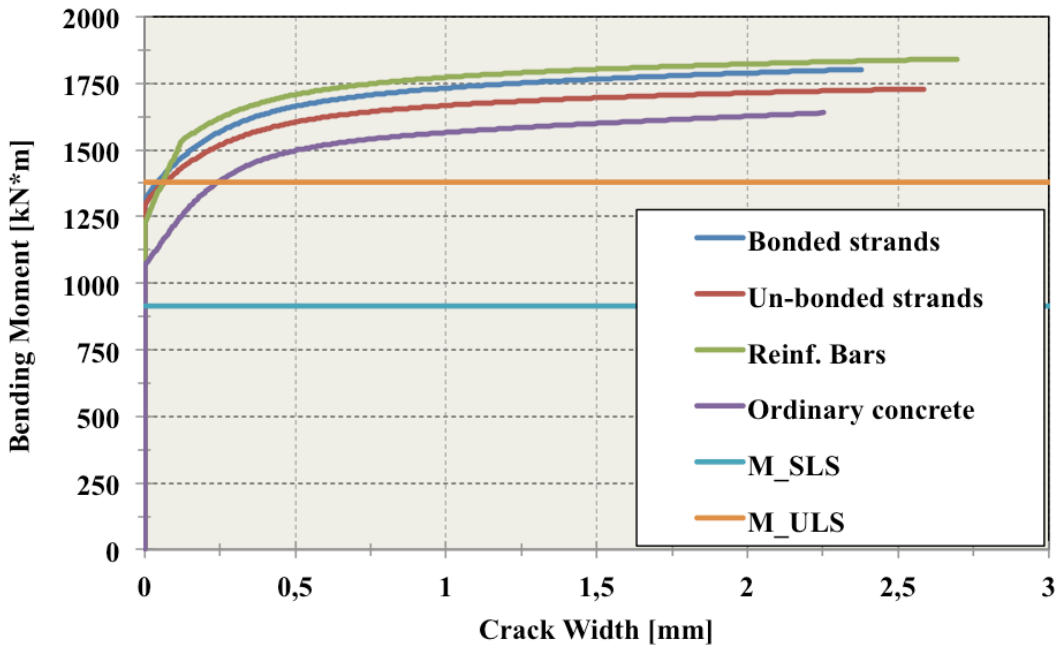

Figure 4–6: $M - w$ relations using different longitudinal reinforcements for a 15 m span

Table 4-3: Values of the cracking moment, resistant moment and stress range using different longitudinal reinforcements for the 15 m span

	Bonded strands	**Un-bonded strands**	**Reinf. bars**	**Ordinary concrete**
$\boldsymbol{M_{crack}}$[kN m]	1318	1299	1222	1072
$\boldsymbol{M_r}$[kN m]	1802	1729	1841	1639
$\boldsymbol{\Delta\sigma_{reinf}}$ [MPa]	63	0	64	63

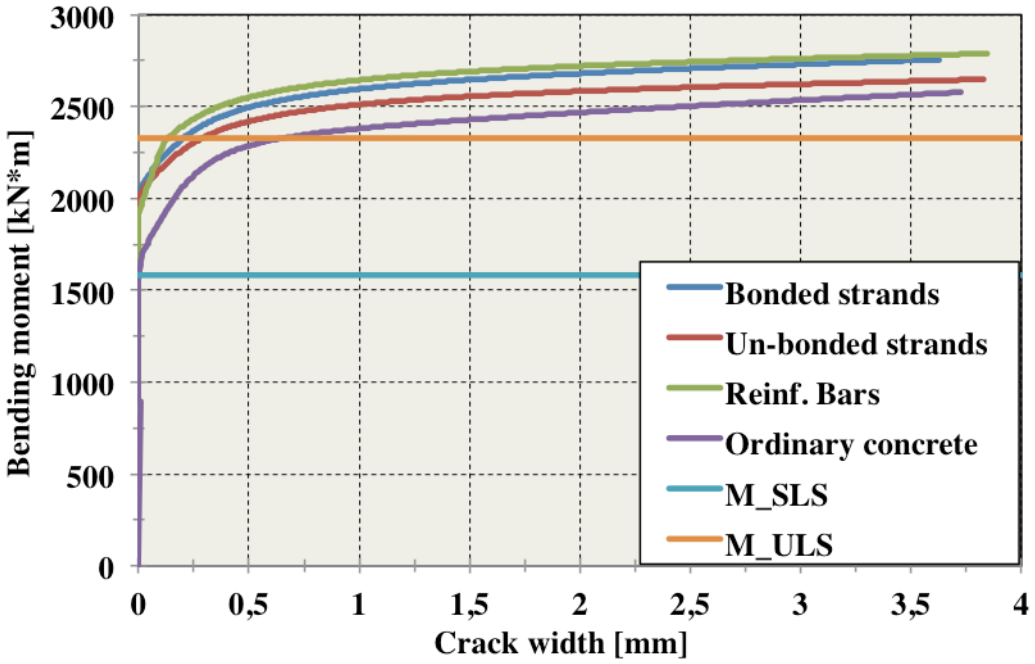

Figure 4–7: $M - w$ relations using different longitudinal reinforcements for a 20 m span

Table 4-4: Values of the cracking moment, resistant moment and stress range using different longitudinal reinforcements for the 20 m span

	Bonded strands	**Un-bonded strands**	**Reinf. bars**	**Ordinary concrete**
$\boldsymbol{M_{crack}}$[kN m]	2040	2016	1931	1582
$\boldsymbol{M_r}$[kN m]	2757	2649	2789	2579
$\boldsymbol{\Delta\sigma_{reinf}}$ [MPa]	65	0	74	54

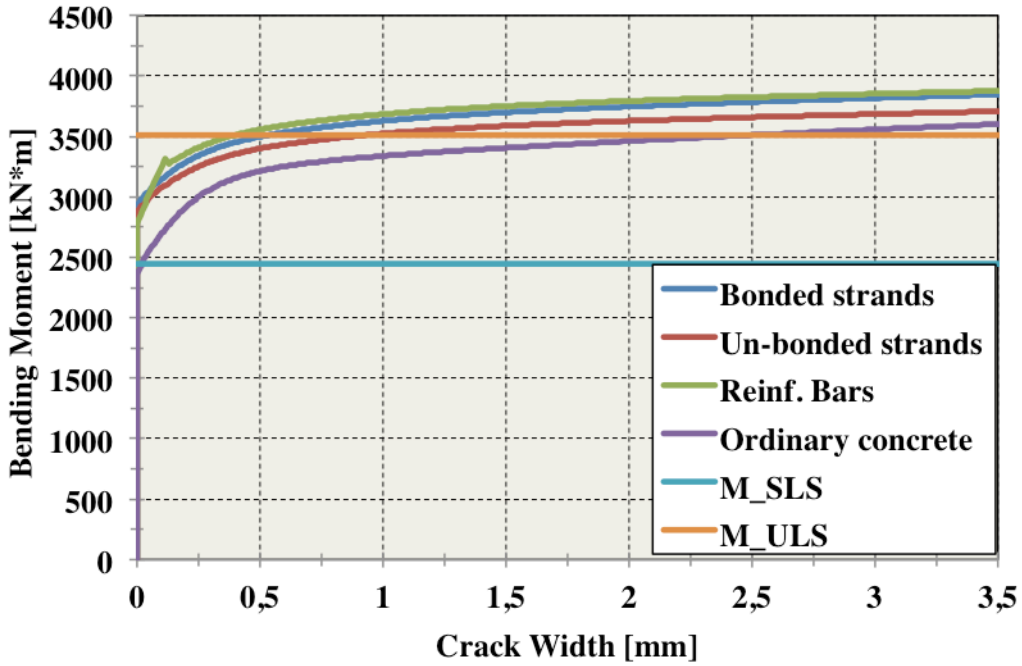

Figure 4–8: $M - w$ relations using different longitudinal reinforcements for a 25 m span

Table 4-5: Values of the cracking moment, resistant moment and stress range using different longitudinal reinforcements for the 25 m span

	Bonded strands	**Un-bonded strands**	**Reinf. bars**	**Ordinary concrete**
$\boldsymbol{M_{crack}}$[kN m]	2924	2874	2779	2384
$\boldsymbol{M_r}$[kN m]	3853	3721	3889	3615
$\boldsymbol{\Delta\sigma_{reinf}}$ [MPa]	57	0	94	98

4.4.2 Discussion of the results

The maximum capacity is attained for all reinforcement configurations. The use of reinforcing bars or bonded tendons provides, as expected, a larger ultimate bending capacity than using two un-bonded tendons. The stress range for the un-bonded tendons remains zero during the whole loading phases due to the possibility to slide with the surrounding concrete.

Looking at M_{crack}in the tables, each section has no cracks at serviceability state, respecting the criterion requested. Despite the metallic fibre absence, ordinary concrete sections respect the crack limitation imposed at SLS.

Stress ranges in the longitudinal reinforcement are calculated between the application of all dead loads and the application of the live load – load factors used correspond to the FLS combination. Even for the stress range criterion each section fulfills the limitation required.

This preliminary and simplified study tends to confirm the experimental results obtained in De Broucker (2013). There are no substantial advantages in terms of carrying capacity, cracking pattern and stress range in order to privilege one type of longitudinal reinforcement. The choice of un-bonded strands could be taken to limit the stress range or to assure an easier reparability of the cables. For the rest of the thesis only bonded strands will be considered for the design of the cross-section.

4.5 Flexural strength verification according to FIB

4.5.1 General

Many different equations are proposed in the literature to determine the resistant moment of a SFRC section. Basically the issue that governs the analytical evaluation of the resistant moment is the contribution given by the steel fibres. With respect to the plain concrete one more term is included the equilibrium force. Following the equilibrium equation for a rectangular concrete section:

$$\phi_c \cdot \alpha_1 \cdot f_c \cdot b = \phi_p \cdot A_{s,cables} \cdot f_{ps} + \phi_f F_{fibres} \tag{5.1}$$

where:

$\phi_c, \phi_{cf}, \phi_p$ are the material resistance factors;

$\alpha_1 f_c$ is the effective compressive strength of concrete at the ultimate limit state;

b is the width of the concrete section;

f_{ps} is the tensile strength in the prestressed strands at ultimate limit state.

The tensile contribution given by steel fibres to equilibrate the forces acting on the section depends on the post-cracking stress distribution. Some hypothesis on maximum crack openings must be made to determine the corresponding tensile stress distribution. Different kind of stress distribution over the cracked part of the section might be considered: a linear decreasing trend, a constant tensile value over the entire developed crack or the real stress distribution retrieved from experimental test.

The ultimate bending moment using the plastic approach of the FIB model code 2010 will be presented for the three sections studied. It is necessary to determine the flexural residual strength as explained in the guidelines.

Using the average values retrieved from the notched beam test – presented in Table 3-6 – the characteristic strengths are computed following the equation $\sigma_{ch} = \bar{\sigma} \cdot (1 - t \cdot V)$, already presented in the Section 4.2.2.

To consider a larger number of different SFRC mixes, the coefficient of variation V is taken equal to 18% - this value is the average coefficient computed for notched beam tests in Lambrechts (2003). Student's factor t is taken equal to 1.638.

$$f_{R3} = \overline{f_{R3}} \cdot (1 - t \cdot V) = 8.5 \cdot (1 - 1.638 \cdot 0.18) = 5.99\ MPa$$

The average value $\overline{f_{R3}}$ is taken from Table 3-8. It corresponds to the average equivalent flexural strength calculated for a CMOD equal to 2.5 mm.

The rigid-plastic stress distribution proposed by the Model code is illustrated in Figure 4–9. Equations for η and λ correspond to those of α_1 and β_1 adopted in the Canadian codes. Also, because FIB code adopted an equivalent tensile bending strength, the uniaxial tensile strength is obtained by dividing the value by 3. Therefore the 2 MPa, value from the $f_{R3}/_3$ must be compared with the 2,5 MPa adopted. The results in terms of resistant bending moment are slightly lower than the respective results calculated with AIS.

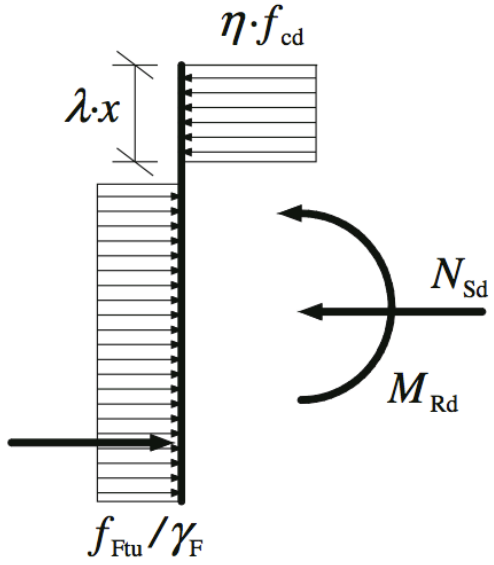

$$\eta = \alpha_1 = 0{,}85 - 0{,}0015 \cdot f_c' \geq 0{,}67$$

$$\lambda = \beta_1 = 0{,}97 - 0{,}0025 \cdot f_c' \geq 0{,}67$$

$$\gamma_F = {}^{1}/_{\phi_f} = {}^{1}/_{0.75} = 1.33$$

$$f_{Ftu} = {}^{f_{R3}}/_{3} = 2{,}0 \text{ MPa}$$

$$f_{cd} = 70\ MPa$$

Figure 4–9: Stress distribution (Model Code 2010)

4.5.2 Bending strength for the bounded strand condition

Considering the values presented in Figure 4–9, it is possible to compute the resisting bending moment of the SFRC section at the ultimate limit state for the three different sections (Table 4-9) for the bonded strand condition.

Table 4-6 to Table 4-8 summarise the condition at ultimate limit states. In all cases the depth of the compression zone is less than the slab thickness, which confirms the assumption of a rectangular beam at ultimate. Results are closed to those obtained with AIS.

Table 4-6: Strand properties, 15 m

A_p	1680	mm^2
d_p	605	mm
f_{py}	1640	MPa
f_{pu}	1860	MPa

Table 4-7: Strand properties, 20 m

A_p	1960	mm^2
d_p	780	mm
f_{py}	1640	MPa
f_{pu}	1860	MPa

Table 4-8 : Strand properties, 25 m

A_p	2240	mm^2
d_p	955	mm
f_{py}	1640	MPa
f_{pu}	1860	MPa

Table 4-9 : Bending capacity with FIB Model approach

	$M_{r\,-\,fib}$	
15 m	1766	kN·m
20 m	2667	kN·m
25 m	3745	kN·m

4.6 Deflection

With the simplified manual method the displacements at the center of the beam is calculated as a function of the total height chosen for the beam. The maximum displacement permitted for the simple-supported beam is taken equal to $L/800$, as the Quebec Ministry of Transportation recommends for bridge with sidewalks. The displacement due to live load can be calculated according to:

$$\Delta_{max} = \frac{5}{48}\frac{(M_{Live\ load})\ L^2}{EI} \tag{5.2}$$

The formula gives an approximate evaluation of the displacement at the middle section of the beam due to live load assuming it is uniformly loaded. Therefore that simplification is considered an easy and reliable indicator of the real displacement. Using this approach, all parameters are

known except for the total height of the cross-section. M_{FLS} is the actual value of the bending moment caused by live loads calculated for the fatigue limit state combination.

Figure 5–4 illustrates the evolution of the girders deflection under live load as a function of their depth. The values for the selected beam depth are given in Table 4-10.

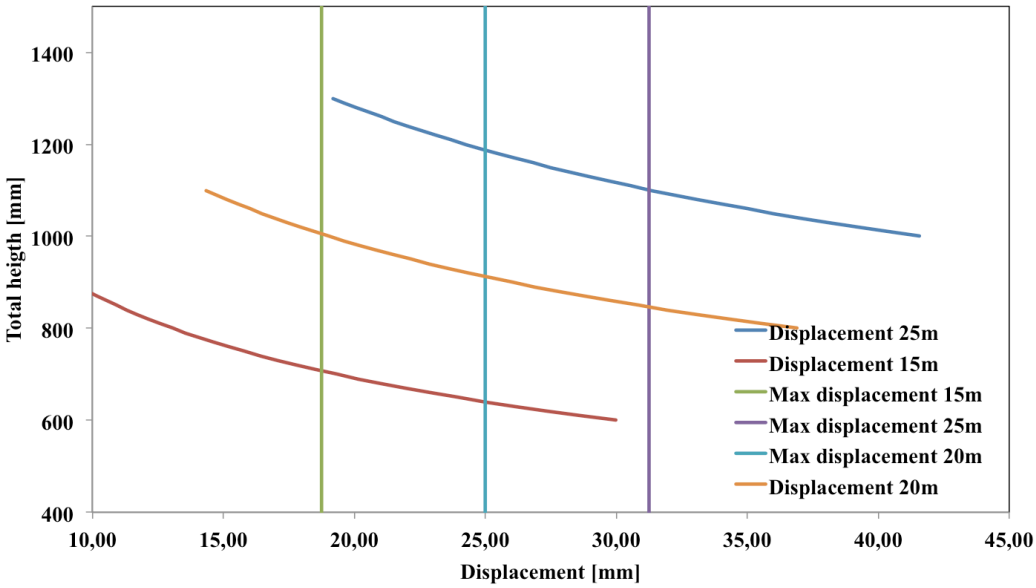

Figure 4–10: Mid-span deflection calculated with equation 5.2

Table 4-10: Maximum mid-span deflections permitted and displacements calculated for the designed height values

	15m	**20m**	**25m**
$\boldsymbol{\Delta_{max}}$ $(\boldsymbol{L/800})$	18,75	25	31,25
$\boldsymbol{h_{min}}$	710	920	1110
$\boldsymbol{h_{chosen}}$	800	1000	1200
$\boldsymbol{\Delta_{simpl}}$ **(5.2)**	13	19	24
$\boldsymbol{\Delta_{Abaqus}}$	13	19	25

Most of the times, the respect of the maximum displacement at SLS is the critical condition to be respected for prestressed concrete structure. Also for the structure studied in this chapter the

height of the sections must be chosen respecting this criterion. With respect to the previous research study, the total heights chosen for the cross-sections is increased. The selected girder depths are 800, 1000 and 1200 mm respectively for spans equal to 15, 20 and 25 m.

4.7 Determination of the live load effect

The calculation of the live load effects is done using two different methods: the simplified method proposed by the Canadian code (CSA-S6, 2006) and a bi-dimensional grillage model that takes into account the transverse contribution given by the connection between the beams. The loads are calculated for four different spans: 15, 20, 25 and 30 m. Simple supports are considered at each extremity. The number of beams used for a simply supported bridge may vary according to the deck width required. For each span a minimum of 5 to a maximum of 9 beams were considered. Taking a fixed beam width equal to 1.5 m, the corresponding total deck width range was between 6 m (one-lane bridges) and 13.5 m (three-lane bridges). The worst configuration for each span will be considered to determine the design loads. The design considers a single longitudinal beam. The UHPFRC joints will connect the beams transversally in order to fulfill all strength requirements.

4.7.1 Load factors

The load factors are directly taken from the Bridge Code. Three different factor combinations will be considered (Table 4-11): serviceability, fatigue and ultimate limit states. Factors for permanent loads are given in Table 4-12 whereas materials unit weights are presented in Table 4-13.

Table 4-11: Live load factors (CSA S6-06)

	Permanent loads			Transitory loads					Exceptional loads			
Loads	***D***	***E***	***P***	***L****	***K***	***W***	***V***	***S***	***EQ***	***F***	***A***	***H***
Fatigue limit state												
FLS Combination 1	1.00	1.00	1.00	1.00	0	0	0	0	0	0	0	0
Serviceability limit states												
SLS Combination 1	1.00	1.00	1.00	0.90	0.80	0	0	1.00	0	0	0	0
SLS Combination 2†	0	0	0	0.90	0	0	0	0	0	0	0	0
Ultimate limit states‡												
ULS Combination 1	α_D	α_E	α_P	1.70	0	0	0	0	0	0	0	0
ULS Combination 2	α_D	α_E	α_P	1.60	1.15	0	0	0	0	0	0	0
ULS Combination 3	α_D	α_E	α_P	1.40	1.00	0.50§	0.50	0	0	0	0	0
ULS Combination 4	α_D	α_E	α_P	0	1.25	1.65§	0	0	0	0	0	0
ULS Combination 5	α_D	α_E	α_P	0	0	0	0	0	1.00	0	0	0
ULS Combination 6**	α_D	α_E	α_P	0	0	0	0	0	0	1.30	0	0
ULS Combination 7	α_D	α_E	α_P	0	0	0.90§	0	0	0	0	1.30	0
ULS Combination 8	α_D	α_E	α_P	0	0	0	0	0	0	0	0	1.00
ULS Combination 9	1.35	α_E	α_P	0	0	0	0	0	0	0	0	0

Table 4-12: Permanent load factors

	SLS	ULS	FLS
Concrete	1.0	1.1	1.0
Roadside barrier	1.0	1.1	1.0
Asphalt	1.0	1.5	1.0
Live load	0.9	1.7	1.0

Table 4-13: Unit weights (a) and load factors (b) chosen for the concrete (CSA S6-06)

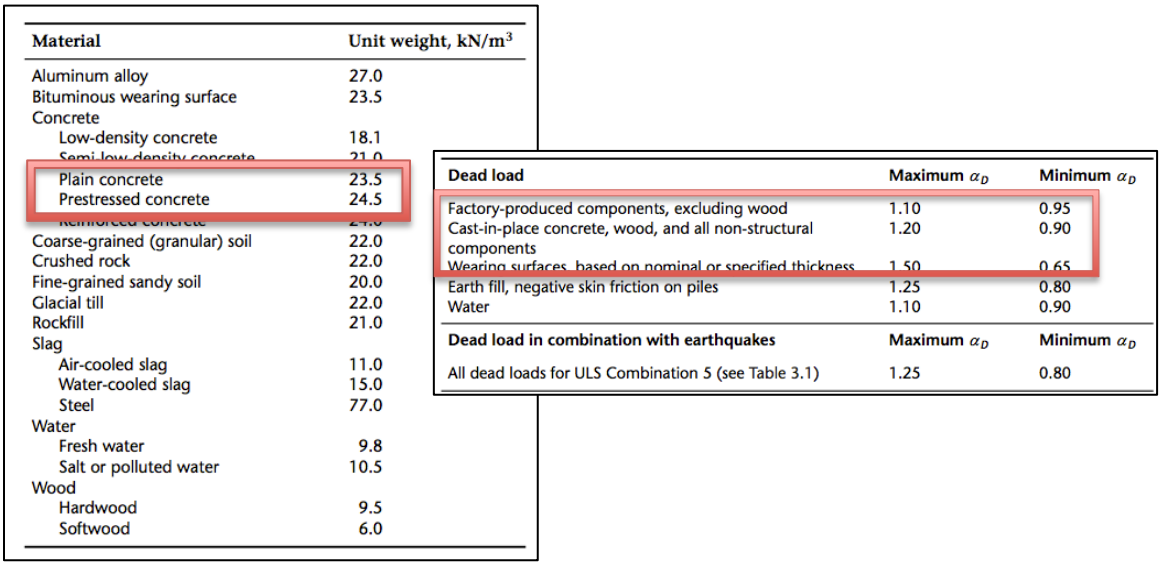

Material	Unit weight, kN/m³
Aluminum alloy	27.0
Bituminous wearing surface	23.5
Concrete	
Low-density concrete	18.1
Semi-low-density concrete	21.0
Plain concrete	23.5
Prestressed concrete	24.5
Reinforced concrete	24.0
Coarse-grained (granular) soil	22.0
Crushed rock	22.0
Fine-grained sandy soil	20.0
Glacial till	22.0
Rockfill	21.0
Slag	
Air-cooled slag	11.0
Water-cooled slag	15.0
Steel	77.0
Water	
Fresh water	9.8
Salt or polluted water	10.5
Wood	
Hardwood	9.5
Softwood	6.0

Dead load	Maximum α_D	Minimum α_D
Factory-produced components, excluding wood	1.10	0.95
Cast-in-place concrete, wood, and all non-structural components	1.20	0.90
Wearing surfaces, based on nominal or specified thickness	1.50	0.65
Earth fill, negative skin friction on piles	1.25	0.80
Water	1.10	0.90
Dead load in combination with earthquakes	**Maximum α_D**	**Minimum α_D**
All dead loads for ULS Combination 5 (see Table 3.1)	1.25	0.80

4.7.2 Permanent loads

The permanent loads considered are: the self-weight of the beam, the asphalt layer and the traffic barriers. The layer of asphalt is considered as a uniformly distributed load over the flanges of the beams. A linearly distributed load equal to 13.5 kN/m is taken to represent the barrier load at both sides of the bridge deck. To make it conform to the design, it is assumed that the load is uniformly redistributed between the minimum number of beams: $w_{barriers} = {}^{13.5}/_{5} = 2.7\ {}^{kN}/_{m}$. The unit weights considered for the asphalt and the concrete are indicated in Table 4-14.

Table 4-14: Unit weights

	Density	Unit weight
Asphalt	23.5	kN/m^3
Concrete	24.5	kN/m^3

The design bending moments and the shear forces the beam are calculated following a simple-supported beam scheme: the maximum bending moment is calculated at the middle cross-section

of the beam $M_f = {w \cdot l^2}/{8}$; and the shear force $V_f = w \cdot \left({l}/{2} - d_v\right)$. The bending moments and shear at various limit stages are presented in Table 4-15 and in Table 4-16.

Table 4-15: Dead load bending moments and shears

	15 m		20 m		25 m	
	M_f [kN-m]	V_f[kN]	M_f[kN-m]	V_f[kN]	M_f[kN-m]	V_f[kN]
Concrete	333	82	647	110	1096	138
Asphalt	64	16	115	21	179	27
Barriers	76	19	135	25	211	31

Table 4-16: Design bending moments and shears at different limit states

	$\mathbf{M_f}$ [kN-m]		$\mathbf{V_f}$ [kN]	
	FLS and SLS	ULS	FLS and SLS	ULS
15 m	473	546	117	135
20 m	896	1032	156	180
25 m	2264	2594	196	226

4.7.3 Live loads

The live loads are calculated according to the Appendix B. The simplified procedure proposed by the code CSA-S6-06 is followed. The truck load is illustrated in Figure 4–11. Two load configurations were considered to determine M_T. The factors presented in Table 4-17 and Table 4-18 are determined according to the length, the deck configuration (number of beams), the limit state investigated (ultimate and service or fatigue) and the position of the beam (external or internal). For each deck configuration the largest factors are highlighted in red to emphasise the deck configuration that should be taken into account for the design.

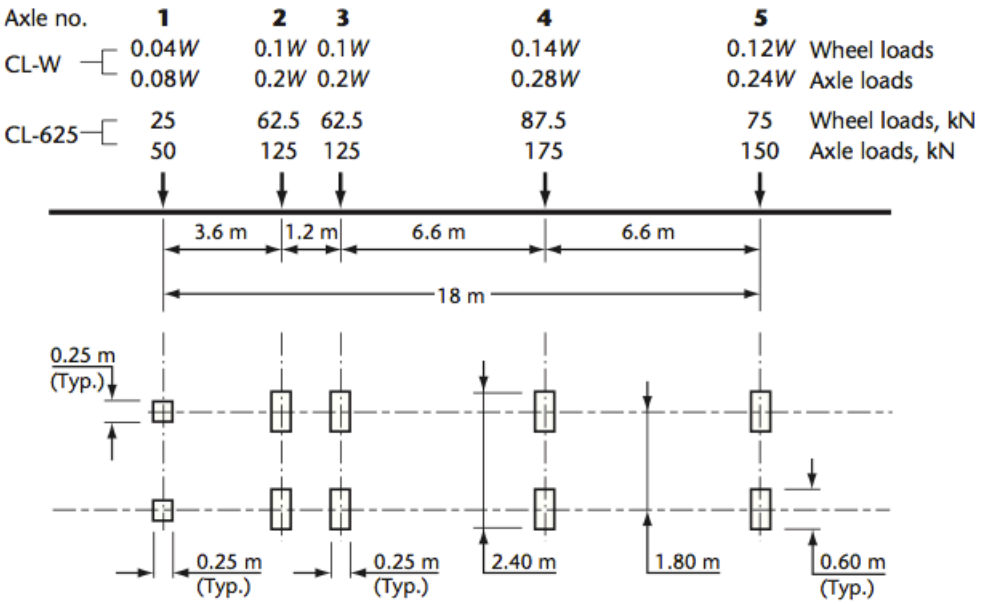

Figure 4–11: CSA-625 load (CSA S-06)

Software CSI Bridge allowed a more detailed study to determine design moments and shear forces produced by live loads. The Table 4-18 summarises the designing factors calculated with a 2D grillage analysis. This deck is modelled by longitudinal and transverse elements as represented in Figure 4-12.

Different sections are assigned to each element in order to represent the real geometrical properties of the real model. This approach allows also moving the live load transversally inside the predefined road width.

Table 4-17: Load factors calculated by the simplified method proposed by the CSA-S6

	$M_{ULS}(ext)$	$M_{ULS}(int)$	$M_{FLS}(ext)$	$M_{FLS}(int)$	V_{ULS}	V_{FLS}
15 – 5	0,41	0,43	0,41	0,35	0,48	0,45
15 – 6	0,38	0,40	0,35	0,34		
15 – 7	0,38	0,40	0,31	0,34		
15 – 8	0,40	0,42	0,39	0,35		
15 – 9	0,39	0,41	0,37	0,35		
20 – 5	0,41	0,42	0,40	0,34	0,48	0,45
20 – 6	0,37	0,38	0,34	0,33		
20 – 7	0,37	0,38	0,30	0,33		
20 – 8	0,40	0,40	0,39	0,33		
20 – 9	0,39	0,39	0,37	0,33		
25 – 5	0,40	0,41	0,39	0,33	0,48	0,45
25 – 6	0,37	0,37	0,34	0,32		
25 – 7	0,37	0,37	0,30	0,32		
25 – 8	0,40	0,39	0,39	0,32		
25 – 9	0,39	0,38	0,37	0,32		
30 – 5	0,40	0,40	0,39	0,33	0,48	0,45
30 – 6	0,37	0,37	0,33	0,31		
30 – 7	0,37	0,37	0,30	0,31		
30 – 8	0,40	0,38	0,39	0,32		
30 – 9	0,38	0,37	0,37	0,32		

Note: Governing values are highlighted in red

Table 4-18: Load factors calculated with CSI Bridge

	$M_{ULS}(ext)$	$M_{ULS}(int)$	$M_{FLS}(ext)$	$M_{FLS}(int)$	V_{ULS}	V_{FLS}
15 – 5	0,37	0,38	0,29	0,25	0,48	0,36
15 – 6	0,34	0,33	0,30	0,26	0,42	0,40
15 – 7	0,32	0,32	0,30	0,25	0,51	0,35
15 – 8	0,34	0,33	0,30	0,26	0,43	0,39
15 – 9	0,33	0,32	0,30	0,26	0,42	0,39
20 – 5	0,37	0,37	0,30	0,27	0,47	0,34
20 – 6	0,34	0,33	0,30	0,25	0,41	0,38
20 – 7	0,31	0,31	0,29	0,25	0,48	0,35
20 – 8	0,34	0,33	0,29	0,25	0,41	0,37
20 – 9	0,33	0,31	0,29	0,25	0,40	0,37
25 – 5	0,38	0,38	0,30	0,27	0,46	0,34
25 – 6	0,34	0,34	0,30	0,25	0,41	0,37
25 – 7	0,32	0,31	0,30	0,25	0,47	0,35
25 – 8	0,35	0,34	0,30	0,25	0,41	0,36
25 – 9	0,34	0,32	0,30	0,25	0,41	0,36
30 – 5	0,38	0,37	0,30	0,26	0,46	0,34
30 – 6	0,35	0,33	0,30	0,25	0,41	0,37
30 – 7	0,32	0,31	0,29	0,25	0,46	0,35
30 – 8	0,36	0,33	0,29	0,25	0,41	0,36
30 – 9	0,34	0,32	0,29	0,24	0,41	0,36

Note: Governing values are highlighted in red

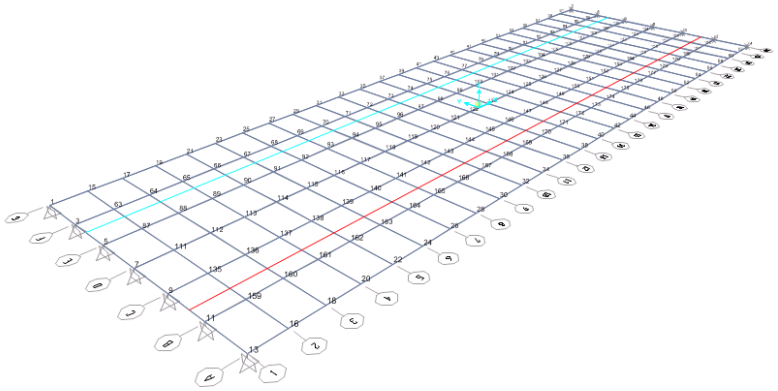

Figure 4–12: Details of the 2D-representation of the bridge in CSI Bridge

The designing factors obtained with the 2D refined model result to be smaller than the ones calculated with the simplified method proposed by the Code. An overall accordance between the two methods is clear. Although the code proposes more conservative values, it was decided to consider the factors coming from the more sophisticated analysis for the calculation of load effects.

Table 4-19: Bending moments at different limit states [kN-m]

	M_{ULS}	M_{SLS}	M_{FLS}
15m	1379	914	859
20m	2328	1583	1510
25m	3511	2442	2344
30m	5012	3545	3413

Table 4-20: Shear forces at different limit states [kN]

	V_{ULS}	V_{SLS}	V_{FLS}
15m	491	305	280
20m	590	377	350
25m	680	447	419
30m	768	518	489

CHAPTER 5 NLFEA WITH ABAQUS AND EPM3D

5.1 Introduction

The validation of the constitutive model EPM3D showed the capabilities of this model in reproducing the behaviour of prestressed SFRC simple-supported beams. The nonlinear behaviour of the three beams presented above is presented in detail in this section for bending and shear.

Even if the model EPM3D demonstrated to be able to reproduce the behaviour – in terms of cracking pattern and ultimate resistance – for any type of longitudinal reinforcement, the FE analyses will investigate the behaviour of the structure using only bonded tendons. The 15 m girder geometry is illustrated in Figure 5–1 and the loading is presented in Figure 5–2.

Four models are created for each beam.

- A first model aims to investigate the bending behaviour of the structure. The beams are uniformly loaded along their length. Transversally, the load is spread over a width equal to 200 mm – equal to the thickness of the bottom edge of the beam web.
- Three other models investigate the shear behaviour. A concentrated load is uniformly distributed over a 600 mm long and 200 mm wide steel plate. The shear span ratio corresponding to the load position changes according to the model investigated. Different shear span ratios are used to investigate the different failures occurred.

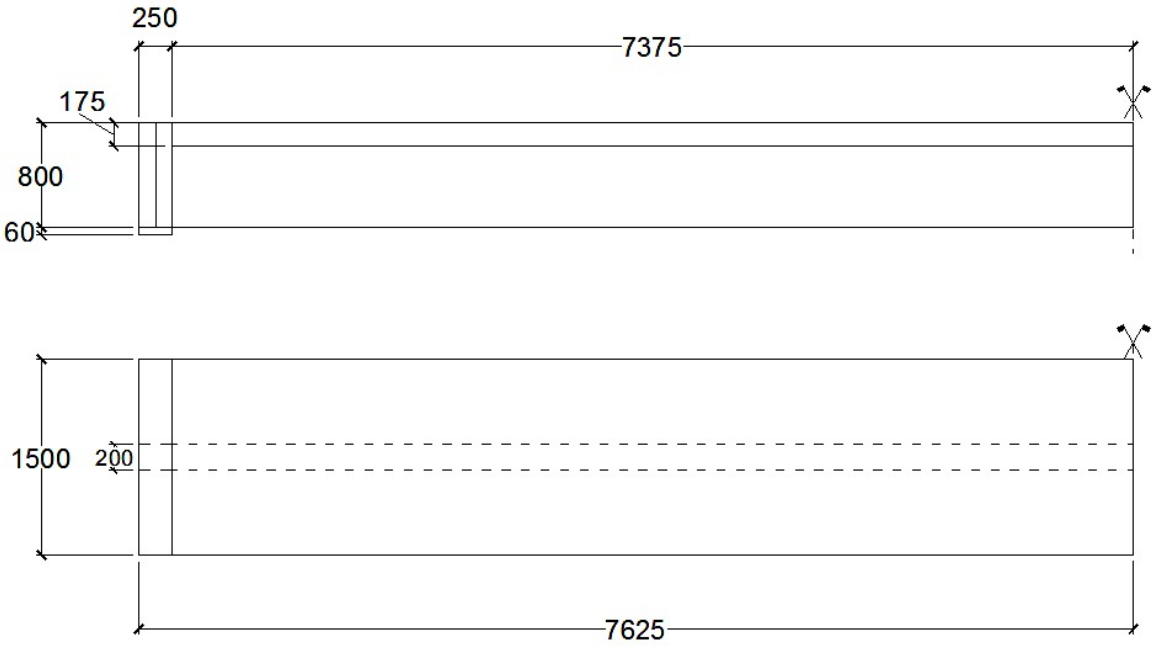

Figure 5–1: Side and top views for the 15m beam modeled

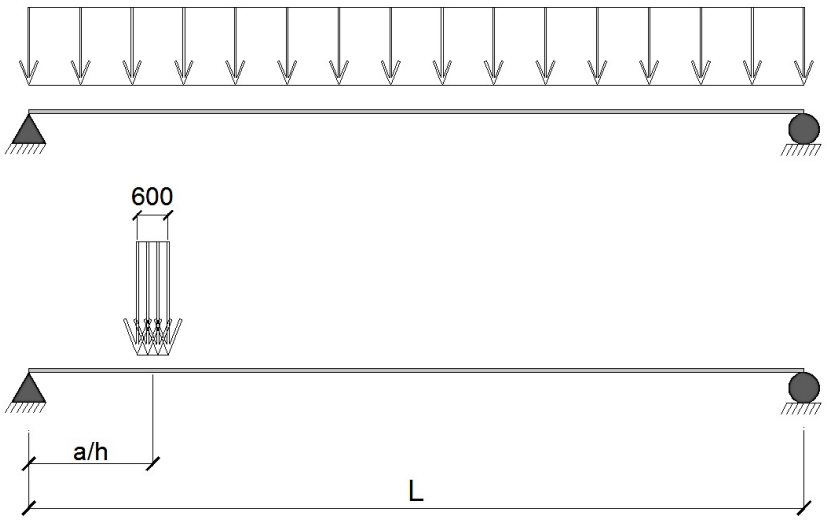

Figure 5–2: Simplified bending and shear load configurations

Concerning the characterisation of the SFRC, the type of the finite elements used for each model is chosen within the explicit element library – hexagonal shape, reduced integration and the "relax stiffness" hourglass control activated characterise the finite element taken, as previous studies suggest in accordance with the implementation of the subroutine EPM3D. The dimension chosen for the single finite element is equal to 75 mm. Different models using bigger and smaller elements were done; the size chosen guaranteed a good convergence level of the solution, a good stability of the results throughout the numerical analyses and a computational time not too elevated. Truss elements chosen within the explicit library with a size of 25 mm were adopted for both transverse and longitudinal reinforcements.

As done for the validation of the model, the enlarged extremities are modelled with an elastic concrete ($E = 35000\ MPa$ and $\upsilon = 0.2$) to avoid the cracks due to the concentration of the stresses in the anchorage zone. Moreover, the supports $(250{\times}10\times60\ mm)$ are modelled with elastic steel material ($E = 200000\ MPa$ and $\upsilon = 0.3$).

The numerical analyses are divided into three different steps to simulate the phases from the construction to the final utilisation of the beam:

- STEP 1: self-weight and the first level of prestressing force;
- STEP 2: second level of prestressing force;
- STEP 3: external load – applied according to the load configuration studied (Figure 5–2) up to the failure of the structure.

A realistic stress value equal to $0.7f_{pu}$ is applied to each bonded T15 tendons.

The time of each step are chosen to not exceed a predefined limit value of the energy of the model – a quasi-static analysis must be guaranteed up to the failure of the beam.

5.2 Bending

5.2.1 General

The primary goal of the nonlinear analyses is to validate the results obtained by the simplified approaches and to investigate more in detail the behaviour of the structure according to the load evolution up to the failure.

The first FE model of each beam aims to analyse the flexural behaviour of the sections conceived. The entire section is modelled and uniformly loaded as illustrated in Figure 5–2.

The load configuration, boundary condition and section geometry exhibit a double symmetry with respect to the centre of the structure and the numerical models therefore considered only a quarter of the entire beam. No stirrups were used in the model

The results presented herein focus on:

- calculation of the stress range in the prestressed tendon;
- distribution of the stresses through the SFRC sections;
- identification of the rupture mode;
- calculation of displacements at any limit states.

The number of horizontal strands was previously determined using the software AIS. Several nonlinear analyses were carried out to confirm and validate the results obtained. FE analyses offer a more detailed study of the structure behaviour according to the increasing loads up to the failure. EPM3D allows detecting the evolution of the cracking pattern on the sections studied. The effective integration between the software ABAQUS and the quality of the constitutive model EPM3D will permit a perfect visualisation of the results. The State Dependent Variable implemented in the model allows the identification of the post-cracking tensile stresses directly on the structure. This represents an easy and quick way to detect the evolution of the crack pattern and the failure mode.

5.2.2 Flexural behaviour of the 3 girder types

5.2.2.1 15m

Figure 5–4 shows the crack pattern identified by the remaining tensile strength (grey for uncracked and blue for opened crack) whereas Figure 5–3 presents the moment deflection response (the applied bending moment is calculated at the mid-span section). Table 5-1 gives the main results for the three different spans analysed. The three red points in Figure 5–3 highlight the points corresponding to the three crack patterns presented in Figure 5–4. Teh Figure 5-4c aims to illustrate the governing crack that leads to the beam failure.

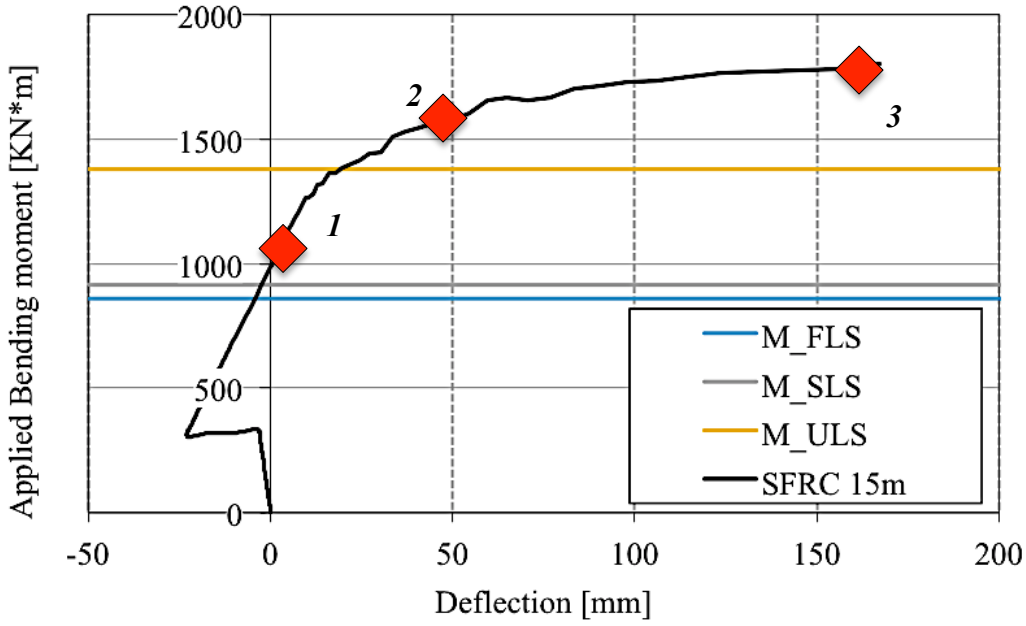

Figure 5–3: Moment-deflection relation of the 15 m beam

Table 5-1 : Main results for the 15m-girder

$\boldsymbol{M_r}$	1832,90	$kN \cdot m$
$\boldsymbol{\Delta_{ULS}}$	209,47	mm
$\boldsymbol{M_{1^{st}crack}}$	1154,72	$kN \cdot m$
$\boldsymbol{\Delta\sigma_{FLS}}$	61,57	MPa
$\boldsymbol{\Delta_{SLS}}$	13,36	mm

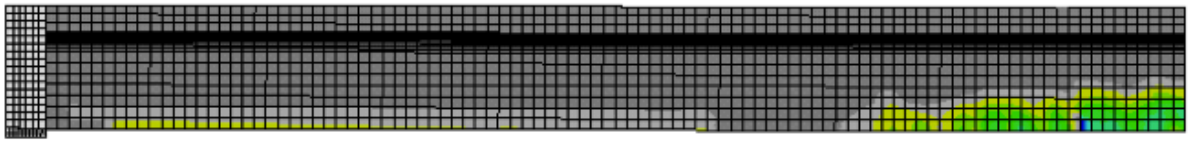

(a) Cracking load. M_{crack} = 1155 kN·m

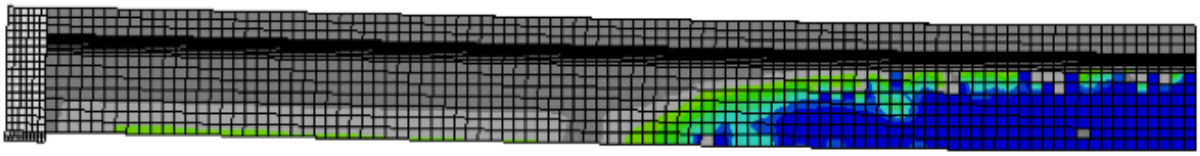

(b) The concrete web is completely cracked. M ≅ 1500 kN·m

Colour legend: blue stands for cracked concrete and green for the beginning of cracking.

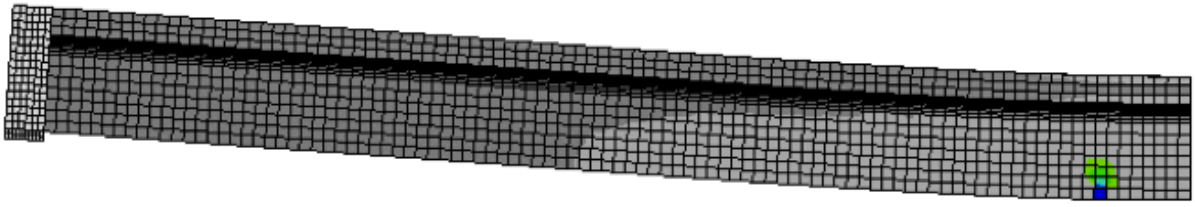

(c) Bending failure. M_r = 1833 kN·m. Controlling crack

Figure 5–4: Cracking pattern of the 15 m beam for different bending moment

5.2.2.2 20m

As presented for the 15m-girder, Figure 5-5 illustrates the applied-moment deflection relationship for the 20m-girder. The applied moment presented refers to the mid-span section, which is the critic one facing to bending loads. Table 5-2 summarizes the most important results from the numerical study. In the Figure 5-6 the cracking pattern at three different load levels is presented. As for the 15m-girder, the Figure 5-6c shows the failure crack that causes the bending failure.

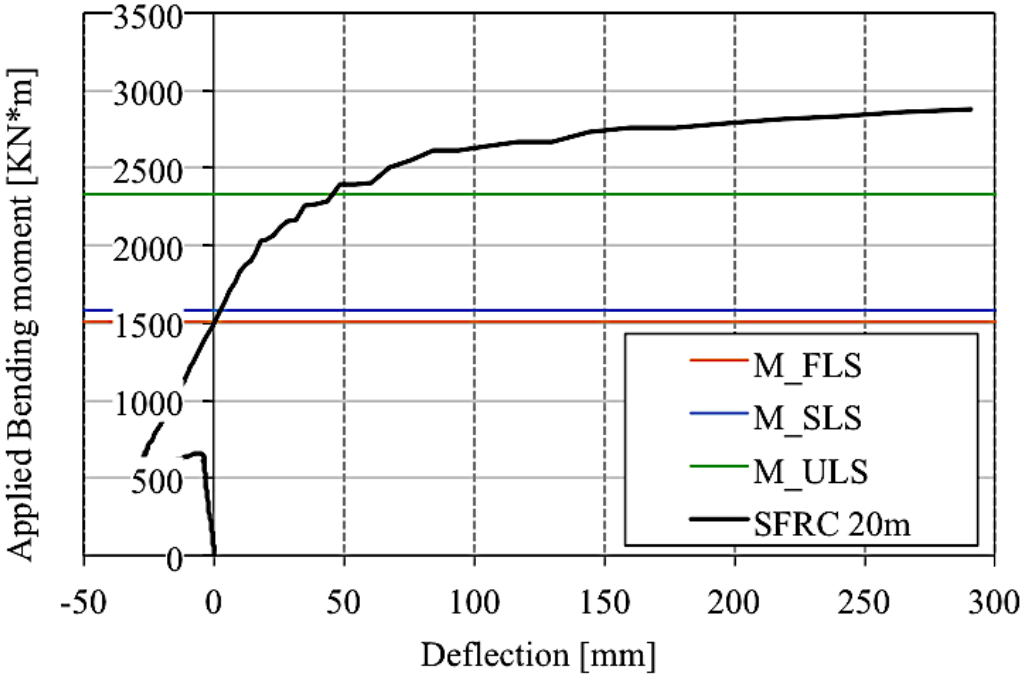

Figure 5–5: Moment-deflection relation of the 20 m beam

Table 5-2 : Main results for the 20m-girder

M_r	2879,67	kN·m
Δ_{ULS}	290,86	mm
$M_{1^{st}crack}$	1830,64	kN·m
$\Delta\sigma_{FLS}$	62,11	MPa
Δ_{SLS}	19,06	mm

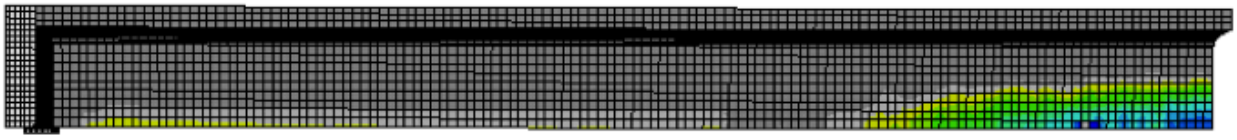

(a) First crack appearing. M_{crack} = 1830 kN·m

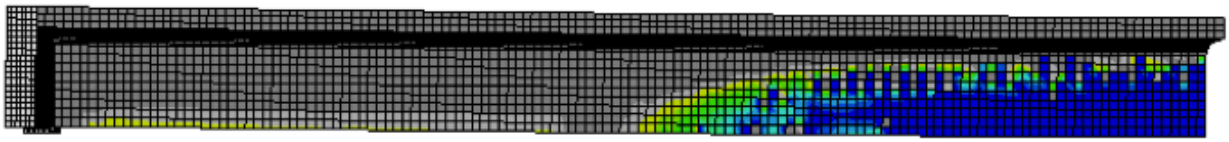

(b) Concrete web cracked. M ≅ 2500 kN·m

Colour legend: blue stands for cracked concrete and green for the beginning of cracking.

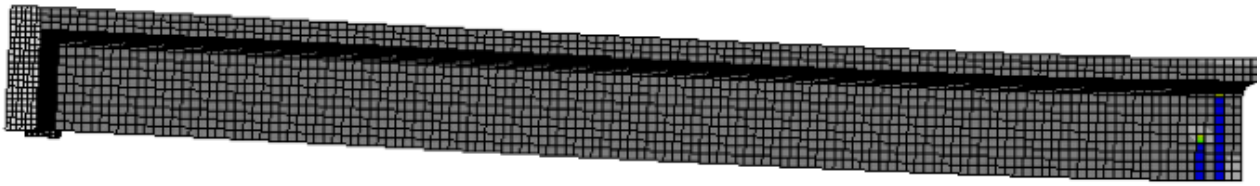

(c) Bending failure. M_r = 2880 kN·m. Controlling cracks.

Figure 5–6: Cracking pattern of the 20m beam

5.2.2.3 25m

For the 25m-girder, the Figure 5-7 shows the applied-moment deflection relationship. The main results from the numerical analysis are summarized in Table 5-3 and Figure 5-8 illustrates the cracking pattern at three different loading phases.

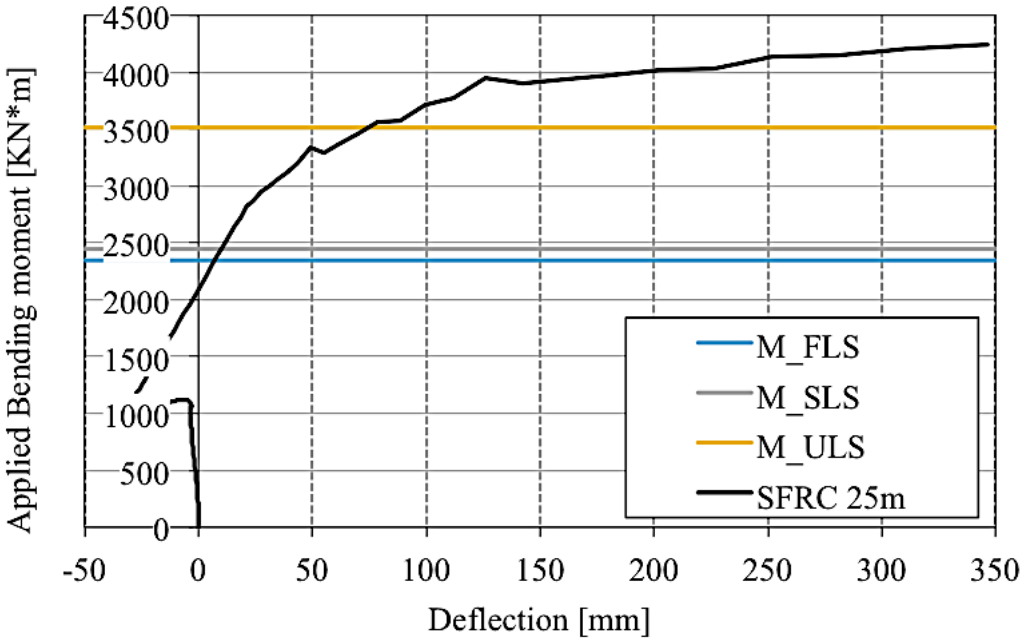

Figure 5–7: Moment-deflection relation of the 25 m beam.

Table 5-3 : Main results for the 25m-girder

M_r	4241,53	kN·m
Δ_{ULS}	346,66	mm
$M_{1^{st}crack}$	2558,75	kN·m
$\Delta\sigma_{FLS}$	64,27	MPa
Δ_{SLS}	25,18	mm

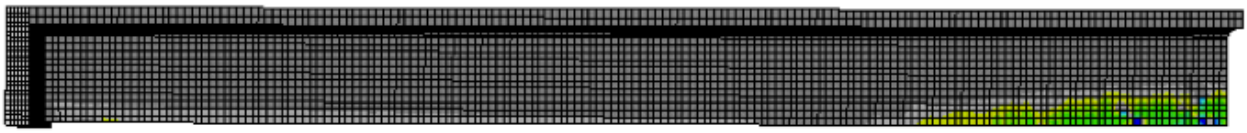

(a) First crack appearing. M_{crack} = 2559 kN·m

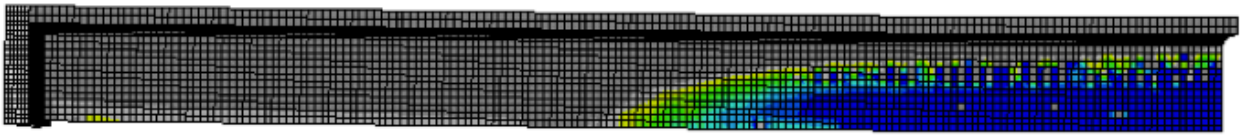

(b) Concrete web cracked. M ≅ 3500 kN·m

Colour legend: blue stands for cracked concrete and green for the beginning of cracking.

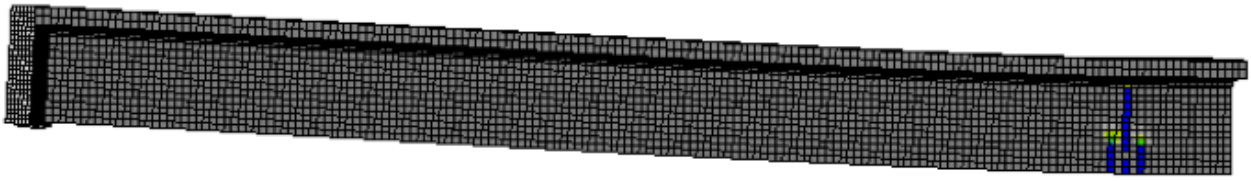

(c) Bending failure. M_r = 4242 kN·m. Controlling cracks.

Figure 5–8: Cracking pattern of the 25 m beam.

5.2.3 Discussion of the results

Results presented above showed the respect of all the design criteria at each limit states. The agreement between results calculated with AIS and the values retrieved by the nonlinear analysis confirms the reliability of the study. Even the simplified method used to calculate the displacement at SLS demonstrated to provide an accurate prediction according to the value calculated with ABAQUS. The structure collapsed for bending stresses at the middle of the span. Differently from the beam tested experimentally, for all the analyses the mostly stressed tendons broke before the concrete reached the maximum compressive strength. This shows that a very high ductility can be reached.

As specified, cracks started developing for a load larger than the ones calculated for the serviceability limit state. The bending behaviour of the beam showed a good ductility as demonstrated by the elevated values of displacements at ultimate limit state. The cracking pattern analysed step by step showed to be dependent on the height of the section. In analysing the tensile stresses reached by the beams, it is possible to determine an approximate value for the crack spacing: 75, 100 and 100 mm respectively for the 15, 20 and 25 m span girders. It is also necessary to highlight the importance of the post-cracking tensile relationship used for the numerical analysis. In this numerical study the simplified σ-w relation presented in the Figure 4-3 has been used. A more detailed relationship must be used – related to experimental results on the actual SFRC mix – to get a more precise description of the crack development at serviceability limit states. Fibre contribution at ultimate limit state – for bending failure – could be considered irrelevant. The prestressed tendons contribute basically the whole bending capacity of the section.

Although the section is un-cracked at SLS, the use of steel fibres allows using straight strands rather than deviated ones, which imply increasing fabrication costs and difficulties.

The application of the prestressing force through two phases demonstrated to provide displacement at the mid-span relatively low after the first phase. The anchorage of the tendons was not modelled in detail, as it was not the primary goal of this study. To avoid concentrations of stresses in the zones close to the supports, a more detailed investigation would be needed. The presence of tendons in the bottom part of the section could require the use ducts or other systems to limit the stresses close to the supports.

5.2.4 Ordinary concrete vs. SFRC

For the beam with a span equal to 15 m, it was decided to compare the numerical results obtained with the ones obtained using a concrete without steel fibres. The material introduced in the model is exactly the same as for the SFRC used for all others; the only difference is the post-cracking behaviour. Results from $M - \Delta$ relation (Figure 5–9) demonstrate that the absence of fibres do not avoid the respect of all design criteria.

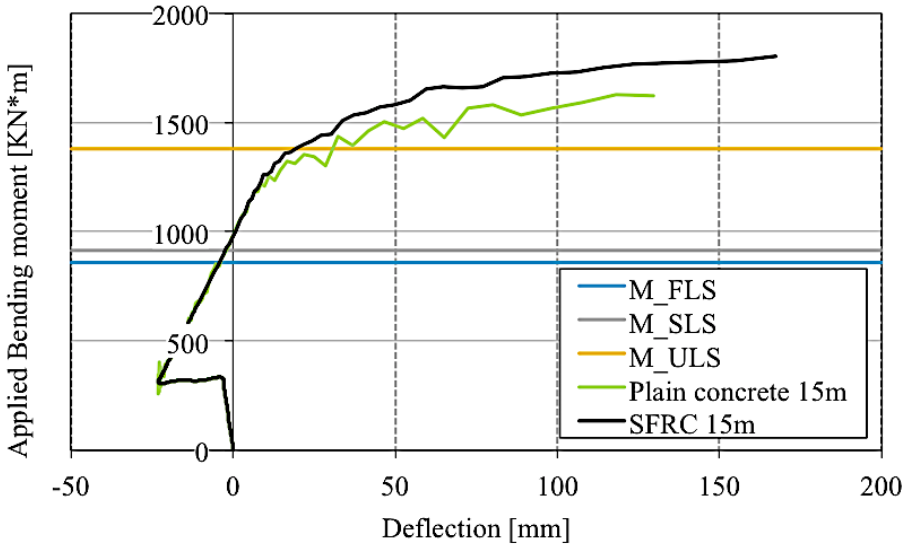

Figure 5–9 : Moment – deflection relation at the mid-span section

An increased ductility and a bigger ultimate bending moment (Figure 5–9) and a more distributed crack pattern (Figure 5–6 and Figure 5–10) are the main characteristics determined by using steel fibres for such structure. As seen in the Figure 5–10, the section made without fibres has a shear failure with plasticisation of the shear reinforcement. The colour red highlights the attainment of the plastic stress for the shear reinforcement.

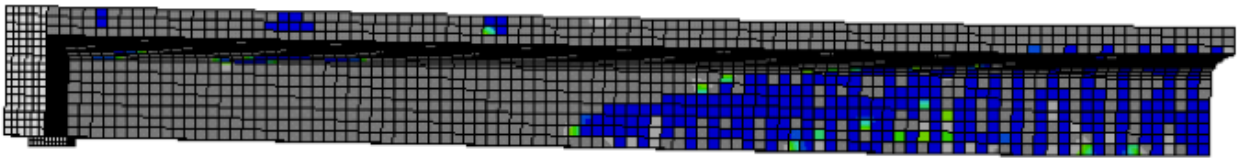

(a) 15m beam failure without steel fibres

(b) Shear reinforcement strains

Figure 5–10: Cracking pattern for the 15 m beam without steel fibres

It is preferable to avoid the fragility property of a shear failure. The addition of steel fibres can give the necessary shear contribution to prevent that kind of failure. Moreover fibres allow simplifying the design of the shear reinforcement. A minimum amount is still required, as highlighted from the experimental campaign described in Chapter 3.

5.2.4.1 Discussion of the results

The $M - \Delta$ relation is a slightly unstable due to the brittleness caused by the quick propagation of cracks. A lower loading rate would probably stabilize the response, even if the relation obtained is considered acceptable. Despite the fulfilment of all the conditions required, fibres showed an increase of the ductility of the beam.

- *OVERALL RELATION*: the response up to the development of the first crack is identical for both analyses. Both materials have the same pre-pic tensile behaviour and they both develop the first crack for an identical bending moment. The post-cracking behaviour is extremely different. The brittleness in crack propagation showed by the ordinary concrete causes a more premature failure of the structure than the SFRC beam.

- *CRACK IN ANCHORAGE PART*: The ordinary concrete beam presented few cracks along the integrated slab in the zones close to the supports. The appearance of this crack is due to the excessive tensile stresses after the application of the entire prestressing force. Probably, for the SFRC beam, steel fibres act avoiding the development of a macro-crack. Fibres promote a better redistribution of the tensile stresses on a larger area; SFRC structure develops more micro-cracks instead of wider cracks.
- *DUCTILITY*: Globally the steel fibres contributed positively once the structure starts cracking up to the failure. The displacement of the mid-span section at failure and the ultimate resistant moment of the ordinary concrete beam are respectively 22% and 10% lower than the value calculated for SFRC beam.
- *FAILURE CRACKS*: the cracks at failure of the plain concrete beam show a decreasing angle of propagation with respect the main axe of the structure. The vertical cracks close to the mid-span section can be explicated with the concept of "concrete teeth" proposed by Kani (1967). Once these teeth offer the maximum bending resistance, an arch mechanism is developed around the teeth and the flexural failure takes place.
- *CRACK SPACING*: Comparing the images of the crack pattern at failure, it is clear that the presence of fibres create a widespread micro-crack pattern close to the mid-span section. Crack opening and crack spacing are lower for the SFRC beam.
- *SHEAR FAILURE:* It is preferable to avoid the fragility of the shear failure of the beam without steel fibres. The addition of fibres permits to simplify the design of the shear reinforcement. This simplification would mean less cost and difficulties linked to the fabrication process.

5.3 SHEAR

5.3.1 Calculation of transverse reinforcement

The transverse reinforcement adopted is a classic 15M stirrup. It was decided to adopt a stirrup spacing equal to 400 mm for the 15 m span girder and 500 mm for the other two larger size sections. Shear resistance is calculated following the Canadian Bridge Code concerning concrete

and reinforcement contributions. Between the several formulas to determine the fibre shear contribution it was chosen to take the simplest one proposed by Casanova (1995):

$$V_r = V_c + V_s + V_{fib} \tag{5.3}$$

$$V_c = 2.5 \cdot \beta \cdot \phi_c \cdot f_{cr} \cdot (b_v \cdot d_v) \tag{5.4}$$

$$V_s = \phi_s \cdot \frac{f_y \cdot A_v}{s \cdot \tan\theta} \tag{5.5}$$

$$V_{fib} = \phi_f \sigma_{fib}(w_m) \cdot b_v \cdot d_v \tag{5.6}$$

For prestressed concrete girder, the contribution of the horizontal prestressing force is included in Vc. The values of β are calculated according to the general method proposed in the Canadian Highway Bridge Design Code CSA-S6.

Table 5-4 summarises the results for the three girder sizes using the equation from 5.3 to 5.6. The sum of the concrete and reinforcement contributions gives an acceptable shear resistance. The fibre contribution is calculated using a safely value for the average crack. The equation (5.6) is very similar to the one proposed by Casanova (1995). The $\sigma_{fib}(w_m) = 1.5\,MPa$ corresponds to an average opening crack $w_m = 1.5\,mm$ (taken as suggested from the Australian draft code), calculated from the $\sigma - w$ relation used throughout the design process.

Table 5-4 : Shear capacity

	$\boldsymbol{V_c}$ [kN]	$\boldsymbol{V_s}$ [kN]	$\boldsymbol{V_{fib}}$ [kN]	$\boldsymbol{V_c + V_s}$ [kN]	$\boldsymbol{V_r}$ [kN]
15m	294	354	184	648	832
20m	379	365	237	744	981
25m	464	447	290	911	1201

5.3.2 Nonlinear analysis

15 m girders

To fully characterize the shear behaviour of the different sections three model were done. For each model only a quarter of the beam was analysed. The difference between the three models

done for each section was the position of the load, which was placed at a distance of 1.5 h, 2 h and 3 h from the support of a beam. Results are treated with a particular focus on the ultimate shear resistance and the failure mode, illustrated from Figure 5–11 to Figure 5–13 for the three girder spans. The plasticisation of the shear reinforcement allowed to detect a shear failure instead of the failure of the strands or the compressive concrete.

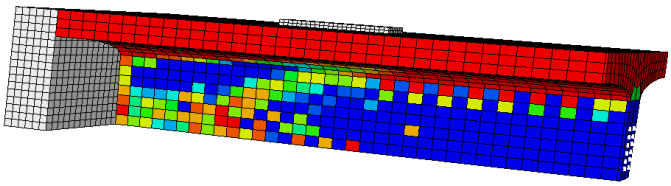

a) shear span to depth ratio $^{a}/_{h} = 1.5$ -: Shear failure

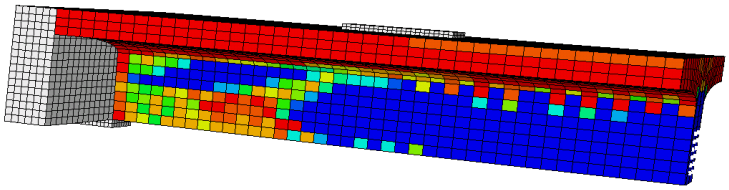

b) shear span to depth ratio $^{a}/_{h} = 2.0$ – Shear/bending failure

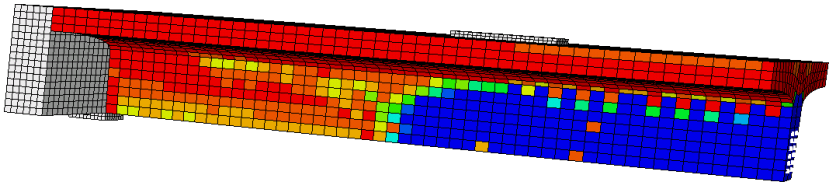

c) shear span to depth ratio $^{a}/_{h} = 3.0$ -Bending failure

Figure 5–11: Failure modes for the 15 m girders

Colour legend: blue represents cracked concrete, green stands for the beginning of the cracking, and red colour is for uncracked concrete

20m girders

As done for the 15m-girder Figure 5–12 illustrates the cracking pattern for three different shear span to depth ratios. The shear failure is individuated by the plasticisation of the shear reinforcement.

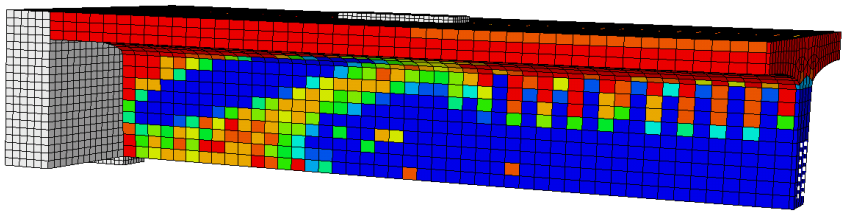

a) shear span to depth ratio $^{a}/_{h} = 1.5$. Shear failure

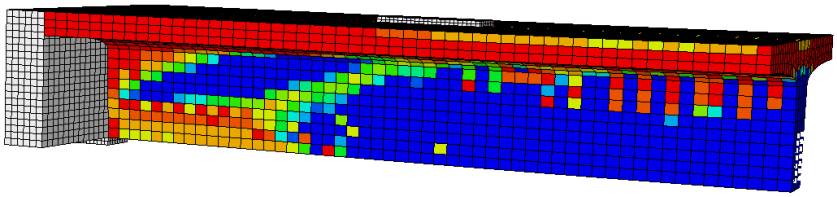

b) shear span to depth ratio $^{a}/_{h} = 2.0$ – Shear/bending failure

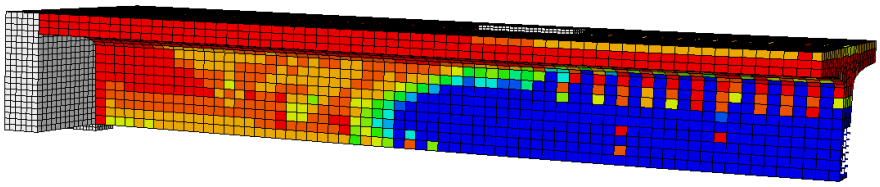

c) shear span to depth ratio $^{a}/_{h} = 3.0$ -Bending failure

Figure 5–12 : Failure modes for the 20m girders

Colour legend: blue represents cracked concrete, green stands for the beginning of the cracking, and red colour is for uncracked concrete

25m girders

The Figure 5–13 shows the cracking pattern at failure for three different shear span to depth ratios retrieved from the numerical analyses of the 25m-girder.

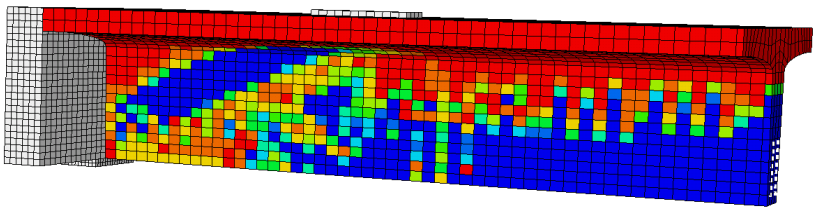

a) shear span to depth ratio $^{a}/_{h} = 1.5$ – Shear failure

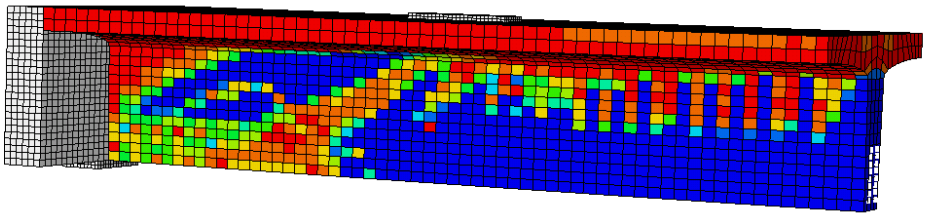

b) shear span to depth ratio $^{a}/_{h} = 2.0$ – Shear failure

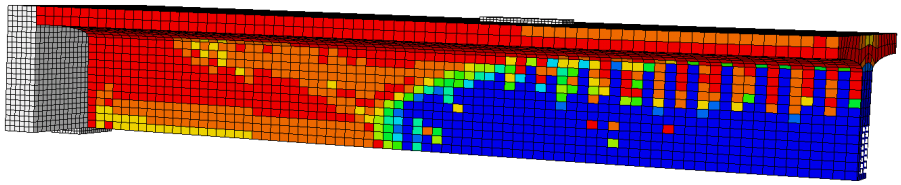

c) shear span to depth ratio $^{a}/_{h} = 3.0$ -Bending failure

Figure 5–13 : Failure modes for the 25m girders

Colour legend: blue represents cracked concrete, green stands for the beginning of the cracking, and red colour is for uncracked concrete

From the figures presented above three different kind of rupture came up according to the shear distance used:

- $a/h = 1.5$; shear failure with the plasticisation of the shear reinforcement;
- $a/h = 2$; shear/bending rupture;
- $a/h = 3$; bending rupture.

The numerical analysis can easily detect the different failure modes. As a function of the shear ratio the resistant mechanism changes. The two well-known mechanisms might be associated to the concepts of slender and deep beam. When shear and flexion resistances act at the same time the bending bearing resistance can be seen as the sum of arch and beam actions.

5.3.3 Without shear reinforcement

A further study is so conducted on the 15m girders. Two different numerical models of the same beam are done using respectively SFRC and reinforced concrete. No stirrups are used in any of the numerical model investigated.

A similar experimental study has been carried out by Kani (1967) for reinforced concrete. The use of numerical tools could give a reliable prevision of the variation of either the bending or the shear resistance according to the shear ratio. Therefore the beam with a 800 mm height was modelled using ordinary concrete trying to reproduce the results obtained by Kani's study with the so-called Kani's valley. Four different shear spans were studied and the results compared in Figure 5–14 with the corresponding ones of SFRC models.

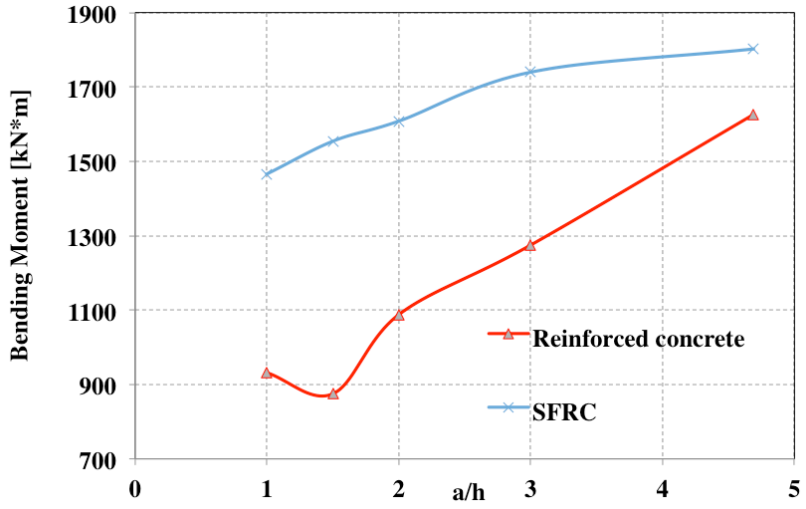

Figure 5–14: Bending resistance according to the shear span to depth ratio $^{a}/_{h}$ with and without steel fibres in the concrete mix.

The resistance values in the Figure 5–15 refer to ultimate resistance at failure of the structure. For shear span to depth ratio larger than 2 the fibre contribute with a low percentage on the beam bending resistance. For shear failures, the bending resistance gained with the addition of steel fibres become relevant.

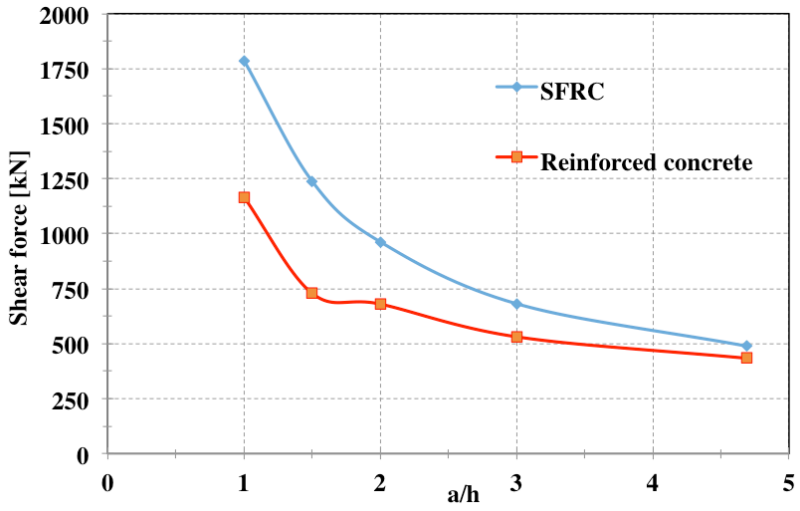

Figure 5–15: Shear resistance according to the shear span ratio a/h with and without steel fibres in the concrete mix.

As showed in Figure 5-15 and 5-16 the numerical analyses are able to reproduce the Kani's valley for the reinforced concrete. The bearing capacity of the beam is reduced with the decreasing of the shear span. The percentage reductions of bearing capacity are in accordance with the values found by Kani for his experimental study. What is new is the comparison with the SFRC behaviour. The slope is sensibly reduced and the valley is not perceptible. The fibres increases considerably the shear capacity at failure for shear span < 2.5. Comparing the failures obtained using the two different materials an increasing in ductility is noted in the shear failure of SFRC beams.

To be highlighted is also the increase in shear gain using fibres with respect to reinforced concrete results. Assuming that the fibre shear contribution may be taken into account following a simple formula similar to what proposed by Casanova (1995) for a generic T section:

$$V_{fib} = 0.9 \cdot b \cdot d \cdot \sigma_{fib}(w_m) \tag{5.7}$$

where $V_{fib} = V_r^{SFRC} - V_r^{Reinf\ concrete}$.

For a the shear span to depth ratio equal to 2 the difference between the shear resistances of the 15m-girder with and without steel fibres is equal to 264 kN. If the equation 5.7 is used to evaluate the fibre contribution to shear resistance, the shear strength offered by steel fibres can be calculated:

$$\sigma_{fib}(w_m) = 2.07\ MPa$$

The equations used to compute the fibre contribution to the shear capacity demonstrated to be reliable. Further applications must be investigated to get a clear vision of all the different variables involved in shear resistance for SFRC prestressed girders. Different geometrical sections, fibre contents and geometry, presence of prestressed tendons, presence of shear reinforcement should be taken into account. For design purposes a conservative value of crack width should be taken into account to calculate a conservative shear contribution offered by fibres. The different orientation of the fibres along the diagonal shear crack have not to be ignored.

CHAPTER 6 CONCLUSIONS

6.1 Validation of the constitutive model EPM3D

6.1.1 Review of the objectives

The goal of the first part of the thesis was to validate the constitutive model implemented in the subroutine EPM3D for SFRC. This numerical tool had to demonstrate its ability to reproduce the bending and shear behaviours of the large-scale beams tested by De Broucker (2013). For each beam tested the numerical analysis should reproduce a reliable load-displacement relation, predict the failure modes obtained experimentally, and estimate the values of the measured crack openings. The validation of the constitutive model is a required step to support its later use for the design of similar structures where steel fibres and prestressed strands act together.

It has been confirmed the small bending contribution at the ultimate limit state offered by fibres due to the predominance of the prestressing tendons and conventional reinforcement (Figure 5–9) whereas design criteria were such that sections remained uncracked under service conditions. However steel fibres still have a strategic importance for such application. The use of steel fibres lead to:

- an increased ductility of the structure, as seen for the 15m-girder (Figure 5–9);
- a simplification of the steel reinforcement design of the girders;
- the use of only one transverse reinforcement layer in the slab, compared to two transverse and two longitudinal reinforcement layers for the slab without fibres as determined by Faggio (2014);
- a reduction of the crack width in negative bending moment in the slab caused by transverse loads due to the contribution of the fibres at SLS (Faggio, 2014), contribution to an increase of the structure durability;
- an important contribution to shear ultimate strength (Figure 5–15).

6.1.2 SFRC

The increasingly use of steel fibres in concrete structures requires reliable nonlinear constitutive models able to reproduce their performances. The constitutive model implemented in subroutine EPM3D permits to study the SFRC by introducing directly the $\sigma - w$ relation. This approach allows to manage directly the post-cracking behaviour by the user. Basically the $\sigma - w$ may be determined either by applying the inverse analysis on a bending test results, by carrying out direct tensile tests, or by using prescribed values. In this projects, it was decided not to carry out direct tensile tests because of the difficulties in their realisation but also to remain close to practical practices. Previous studies (de Montaignac, 2012) showed that the inverse analysis applied on notched beam bending test results lead to non-conservative post-cracking relations. Thus for all numerical analyses of this thesis, the inverse analysis was applied to the average load-displacement curve retrieved from round panel bending tests. The reliable results obtained from the numerical analyses demonstrated the validity of the procedure used. Two different post-cracking relationships have been used in this project (Figure 6-1): the real properties in the validation phase, and characteristic proprieties for design.

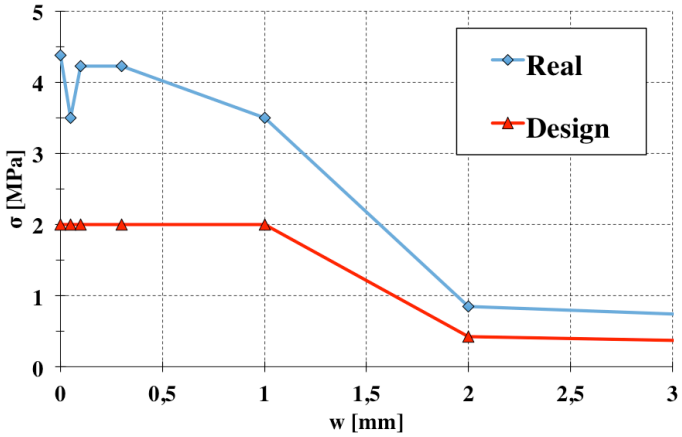

Figure 6–1 : σ-w relationships used for two different studies

A detailed and more accurate description of the behaviour of structures would be obtained with σ-w relationship experimentally retrieved using inverse analysis applied on round panel test results. Using the exact post-cracking tensile relationship allows to describe completely the

cracking phase of the structure – crack spacing, crack opening. It is also suggested to introduce a reduction of the tensile properties for very small crack width as illustrated in Figure 6-1. A simplified post-cracking tensile curve could be used to design a new structure as applied in this project. This relationship is able to predict the overall behaviour of the structure.

6.1.3 Flexural reinforcement

Three types of longitudinal reinforcement were used for the first three beams tested by De Broucker (2013). The last row of the reinforcement was respectively constituted by: bonded strands, un-bonded strands and 30M reinforcing bars.

The numerical analyses permitted to reproduce accurately the results obtained experimentally. Numerical analyses reproduced $P - \Delta$ relations in agreement with experimental evidences for both bonded and un-bonded strands. Up to the failure, the numerical analyses demonstrated to well predict the bending behaviour. Little discrepancy was obtained in predicting the displacement, the load at failure, and the crack width and spacing. The variability of the concrete mechanical properties may explain the order of magnitude of the errors of the results prediction (Table 3-12).

Numerical results of the third beam – with the reinforcing bars 30M – showed an imperfect relation for load values close to the failure. The surface of the reinforcement is not completely represented in the numerical analysis. However, the behaviour obtained experimentally is acceptably reproduced up to the failure.

6.1.4 Shear and bending failures

To investigate both bending and shear behaviours, two different load configurations were used in the experimental campaign as explicated in chapter three. The numerical studies demonstrated to be able to reproduce with accuracy the different cracking patterns and failure modes obtained experimentally. The attainment of the concrete compressive strength was observed for specimens R01 and R02. A shear/flexural failure for the R03 was well predicted even if a bending failure was expected. The shear diagonal cracks of the shear tests were also reproduced correctly.

Moreover, the prediction of shear failure for the beam R08 indicates the capability of the model to adapt to different material properties.

6.1.5 Calculation of crack openings

EPM3D demonstrates a great capacity for prediction crack opening. The measurements of both the linear LVDTs and the X-system of LVDTs are well reproduced by the numerical studies. In the case of prestressed structures the control of the crack openings is an important issue that it is not easily predicted. The results obtained by numerical analyses demonstrated to offer a good prevision of the crack evolution width the applied load.

6.2 Pre-design

The pre-design of three different T-cross-sections was articulated into different phases as follows: calculation of the required carrying capacity, preliminary study using different kind of longitudinal reinforcements, and a nonlinear FE study to investigate both flexural and shear behaviours of the sections. The design of three sections covering a span range between 15 and 25 m was done.

The final sections designed respect the design criteria chosen for SLS, FLS and ULS. The most restrictive design criterion was the deflection calculated at the serviceability limit state. This criterion forced to increase the height of the sections with respect to the initial idea in the previous research project (Massicotte et al., 2012). In doing so, no cracking was obtained in service conditions in the girders.

The validation of the constitutive model EPM3D authorized the use of FE analyses to investigate the behaviour of the beams analysed. The FE analyses permitted to detect the following information according to the load level up to the failure: compressive and tensile stresses for each section of the beam, deflection at girder mid-span, the development of cracks, the failure mode and the carrying capacity. The study highlighted:

- the respect of all the design criteria enumerated in section 4.2.7;
- a pronounced ductility offered by the addition of the fibres both for bending failure and shear failures;

- formation of closer and thinner cracks, correct widths and spacing being obtained using the post-cracking tensile relationship retrieved from the experimental characterisation of the SFRC used.

The study of the shear behaviour using different shear span ratios highlighted:

- shear failure start being predominant for a/h ratio approximately equal to 2;
- each section respect the required ultimate shear resistance.

Globally three sections were designed. The geometry of each section is shown in Figure 4–4.

6.3 Normal concrete vs. SFRC behaviour

The behaviour of the 15 m beam was studied using normal concrete without fibres. The study of the bending capacity of the section varying the shear ratio reproduced the typical Kani's valley presented in the literature. The same section analysed using the addition of steel fibres highlighted a different behaviour. Decreasing the shear ratio a/h form 5 down to 1, thereby forcing a shear failure, reduces the girder capacity by 20%, significantly less than the corresponding reduction of 45% for normal concrete. This gain in carrying capacity is due to the shear contribution offered by the fibres. The fibres can bridge and control the development of the diagonal shear crack in the first stages of its appearance. In doing so, fibres reduce the brittleness of the shear failure increasing the shear strength of the section.

For elevated shear span ratios the gain in bending resistance offered by the fibres is not so elevated. At ultimate state fibres are therefore more efficient to prevent a shear brittle failure whereas the maximum flexural moment is only marginally influenced by adding steel fibres. Briefly the numerical studies highlighted the following points for the girder design:

- fibres can reduce the brittleness of a shear failure;
- the addition of fibres can increase considerably the shear capacity of the beam;
- at ultimate the additional bending resistance provided by the fibres can be neglected;
- fibres reduce crack openings and their spacing.

6.4 Recommendations

EPM3D is a useful and reliable numerical tool. Its development should lead to define crack openings according to the loading level on the structure. Adopting a $\sigma - w$ design approach, the crack width represent necessary information to determine the contribution to the bearing resistance offered by fibres.

Results obtained with nonlinear analyses in bending were the same results obtained by simplified methods. Moreover the FE analyses offer a complete description of the behaviour of the structure throughout the loading phases.

The literature lacks of a worldwide-recognised formula to take into account the contribution of the fibres in shear at ultimate limit state. Because of the elevated costs of experimental tests on large-scale beams the constitutive model EPM3D should be used to replace them. A preliminary numerical study would give the necessary information to improve the quality of the experimental tests.

For the design of the double-T-beams, the respect of the mid-span displacement at SLS oblige to increase the height of the section to increase the inertia. An excessive height of the section would cause problems for the casting of the SFRC. Two different possibilities may be investigated:

- to enlarge the web of the beam allowing to place three or more rows of tendons;
- to enlarge the bottom of web in order to increase the inertia and concentrate the tendons at the bottom of the beam considering however that this solution would probably cause difficulties for the orientation of the fibres at the bottom of the beam which would require further feasibility studies.

The orientation of the fibres during the casting of the SFRC is particularly relevant. The constitutive model could be improved to take into account the variability linked to the different orientation.

At the ULS, even if the fibre contribution to bending capacity is marginal, steel fibres offer an important gain in terms of shear capacity. A simple formula – which considers an average tensile strength offered by fibres along the diagonal shear crack – seems to be an efficient and quick way to determine the fibre contribution to shear resistance. A similar approach is considered in the draft Australian Bridge Code (Foster, 2014). The tensile strength to be taken into account could

be retrieved from the post-cracking tensile relation – direct tensile test or inverse analysis method on bending tests are both valid solutions – in correspondence of a crack width of 1.5 mm. This method still remains a proposal; the influences of the geometrical section, the prestressing tension applied and the fibre characteristics are still to be investigated.

BIBLIOGRAPHY

ACI 544, (1996). State of the Art Report on Fiber Reinforced Concrete. ACI Committee 544, Report 544.1R-96, American Concrete Institute, Detroit, USA.

AFGC-SETRA (2002). Ultra high performance fibre-reinforced concretes, interim recommendations. AFGC Publication, France.

Ashour, S. A., Hasanain, G. S., and Wafa, F. F. (1992). Shear behavior of high-strength fiber reinforced concrete beams. *ACI Structural Journal*, Vol. 89, No. 2, pp. 176-184.

ASTM - American Society for Testing and Materials (2012). Standard Test Method for Flexural Toughness of Fiber Reinforced Concrete (Using Centrally Loaded Round Panel). ASTM, West Conshohocken, Pa.

Bastien, D. (2004). Structural use of fibre reinforced concrete for designing bridge decks. M.A.Sc. Thesis, Ecole Polytechnique of Montreal. (In French), 179.

Bélanger, A. (2000). Design of bridge decks using reduced reinforcement and steel fibre reinforced concrete. M.A.Sc. Thesis, Ecole Polytechnique of Montreal.

Bentur, A., Wu, S.T, Banthia, N., Baggott, R., Hansen, W., Katz, A., Leung, C.K.Y., Li, V.C., Mobasher, B., Naaman, A.E., Robertson, R., Soroushian, P., Stang, H., and Taerwe, L.R. (1995). Fibre-matrix interfaces. In *High Performance Fibre Reinforced Cementitious Composites*, eds. Naaman and Reinhardt. Chapman and Hall, London, pp. 149-191.

Braike, S., (2007). Conception d'éléments préfabriqués de ponts avec des bétons à haute et ultra haute performance. M.A.Sc. Thesis, École Polytechnique de Montréal. (In French).

CAN/CSA-S6-06 (2006). A National Standard of Canada. Canadian highway Bridge Design Code. MISSISSAUGA ON, Canada.

Casanova, P. (1995). Bétons rénforcés de fibres métalliques du matériau à la structure. Ph.D. thesis, Ecole nationale de Ponts et Chaussées, Paris.

Charron, J.-P. (2007). Techniques du béton, École Polytechnique de Montréal. Notes de cours.

CNR-DT 204 (2006). Guidelines for design, construction and production control of fiber reinforced concrete structures. National Research Council of Italy, Rome.

De Broucker, W. (2013). Étude du comportement en flexion et à l'éffort tranchant de poutres en BRF précontraintes. M.A.Sc. Thesis, École Polytechnique de Montréal. (In French).

De Montaignac, R., Massicotte, B., Charron, J.-P., Nour, A. (2012). Design of SFRC structural elements: post-cracking tensile strength measurement. Mater Struct, Vol 45, pp. 609-622. doi:10.1617/ s11527-011-9784-z

De Montaignac, R., Massicotte, B., Charron, J.-P. (2012). Design of SFRC structural elements: flexural behavior prediction. Magazine of concrete research. Vol 45 (19), v. 45, pp. 623-636.

De Montaignac, R., Massicotte, B., Charron, J.-P. (2013). Finite-element modeling of SFRC members in bending Mater Struct. Pp. 1133-1146. doi:10.1617/ s11527-011-9784-z

De Montaignac, R. (2011). Analyse du comportement d'éléments fléchis en béton renforcé de fibres métalliques : du matériau à la structure. PhD thesis, École Polytechnique de Montréal.

Design and Construction of Field-Cast UHPC Connections. Graybeal, Ben (2014). Turner-Fairbank Highway Research Center.

Di Prisco, M., Plizzari, G. and Vandevalle, L. (2009). Fibre reinforced concrete: new design perspectives. *Materials and Structures*, Vol. 42, pp. 1261-1281.

Di Prisco, M., Plizzari, G., Vanderwalle, L., (2012). Fibre reinforced concrete: new design perspectives. Materials and Structures (2009) 42, pp.1261–1281.

Ding, Y., Zhiguo, Y., Said, J. (2011). The composite effect of steel fibres and stirrups on the shear behaviour of beams using self-consolidating concrete. Engineering Structures 33 - 107–117.

EN 14651 (2005). Test method for metallic fibered concrete - Measuring the flexural tensile strength (limit of proportionality (LOP), residual). European Committee for Standardization, Brussels.

Faggio, L. (2014). Conception des semelles de poutres précontraintes en T en BRF avec joints en BFUP. École Polytechnique de Montréal. (In French).

FIB (2010). Model code 2010. First complete draft. International Federation for Structural Concrete, Lausanne.

Ftima, B., (2013). Utilisation de la method des elements finis non-linéaires pour la conception des structures en béton armé: application aux structures massives. PhD thesis, Phd Thesis, École Polytechnique of Montréal.

Habel, K., Charron, J-P. et al. (2008). Ultra-high performance fibre reinforced concrete mix design in central Canada. *Can. J. Civ. Eng.* Vol. 35 217-224.

Hibbitt, H. D., Karlson, B. I. and Sorensen, E. P, (2010). ABAQUS version 6.10, finite element program. Hibbitt, Karlson and Sorensen, Providence, USA.

Kani, G.N.J. (1967). How safe are our large reinforced concrete beams?. *ACI Journal*, Volume 64, No. 12, pp. 128-141.

Khuntia, M., Stojadinovic, B., and Goel, S. C. (1999). Shear strength of normal and high strength fiber reinforced concrete beams without stirrups. *ACI Structural Journal*, Vol. 96, No. 2, pp. 282-289.

Kim, J-K. and Mai, Y-W. (1998). Engineered interfaces in fiber reinforced composites. Elsevier, Oxford.

Kooiman, A.G., (2000) Modelling SFRC for structural design, PhD. Thesis, university of Delft, Delft, Netherlands, ISBN: 90-70235-60-X.

Kwak, Y. K., Eberhard, M. O., Kim, W. S., and Kim, J. (2002). Shear strength of steel fiber-reinforced concrete beams without stirrups. *ACI Structural Journal*, Vol. 99, No. 4, pp. 530-538.

Lambrechts, A.N. (2004). The variation of steel fibre characteristics – Study on toughness results 2002- 2003. In *Fibre Reinforced Concrete from Theory to Practice*, eds. S. Ahmad, M. di Prisco, C. Meyer, G.A. Plizzari, S. Shah, International Workshop on Advances in Fiber Reinforced Concrete, Bergamo, Italy, pp. 135-148.

Li, V.C. and Stang, H. (1997): Interface Property Characterization and Strengthening Mechanisms in Fibre Reinforced Cement Based Composites. *Journal of Advanced Cement Based Materials*, pp. 1-20.

Lim, D. H. and Oh, B. H. (1999). Experimental and Theoretical investigation on the shear of steel fiber reinforced concrete beams. *Engineering Structures*, Vol. 21, No. 10, pp. 937-944.

Löfgren I., Stang H. and Olesen J. F. (2008). The WST method, a fracture mechanics test method for FRC. *Materials and Structures*, Vol. 41, pp. 197-211.

Löfgren, I. (2008). Fibre-Reinforced Concrete for Industrial Construction - A Fracture Mechanics Approach to Material Testing and Structural Analysis. Doctoral Thesis, Chalmers University of Technology, Department of Civil and Environmental Engineering, Structural Engineering, Göteborg, Sweden.

Mansur MA, Chin MS, Wee TH. (1999). Stress–strain relationship of high strength fiber concrete in compression. *J Mater. Civ. Eng.*; 11 (1) : 21–9.

Mansur, M.A., ASCE, M., Ong, K. C. G., Paramasivam, P., (1989). Shear strength of fibrous concrete beams without stirrups. *J. Struct. Eng.* 112 pp. 2066-2079.

Massicotte, B. (2004). Implementing SFRC design into North American codes: application to a building floor. Invited paper to the International workshop on the advanced in fibre reinforced concrete, Bergamo, Italia, September 24–25, pp 73–80

Massicotte, B., Forget, M., Conciatori, D. 2012. Développement de ponts en béton entièrement préfabriqués – Conception d'un nouveau type de poutres. Rapport de recherche. École Polytechnique de Montréal. (In French).

Massicotte, B., Rochon-Massicotte, B. et Conciatori, D. 2010. État des connaissances sur la préfabrication des ponts en béton. Rapport SR10-09, École Polytechnique de Montréal. (In French).

Massicotte, B., Faggio, L., Cordoni, N., Nour, A. and Conciatori, D. (2014). Design and construction of SFRC bridge decks – Building on past experiences and recent developments. FRC 2014 Joint ACI-fib International Workshop - Fibre Reinforced Concrete: from Design to Structural Applications, Montréal, Canada, 134-153.

Meda, A., Minelli F., Plizzari, G.A., Riva, P., (2005). Shear behaviour of steel fibre reinforced concrete beams. *Materials and structures* 38, pp 343-351.

Ministry of transport Quebec, 2011. Le réseau routier québecois. (In French)

Moffatt, K. and Massicotte, B. (2004). Design of continuous SFRC bridge decks for serviceability criteria. *Proceeding of the Sixth RILEM Symposium of Fibre-Reinforced Concrete*, Varrena, Italia, September 20-22, pp. 1173-1182.

Naaman, A. and Reinhardt, H. (1996). High performance fibre reinforced cement composites 2. Second International RILEM Workshop pp. 292-329.

Naaman, A.E. and Shah, S.P. (1976). Pull-Out Mechanism in Steel Fibre-Reinforced Concrete. *Journal of the Structural Division*, ASCE, 102(ST8), pp. 1537-1548

Nour, A., Massicotte, B., De Montaignac, R., Charron, J.-P. (2011) Derivation of a crack opening deflection relationship for fibre reinforced concrete panels using a stochastic model: application for predicting the flexural behaviour of round panels using stress crack opening diagrams. J Cem Concr Res 41(9):964–974

Oh, B. H. Flexural analysis of reinforced concrete beams containing steel fibres. *J. Struct. Eng.*, 118-10, pp. 2821-2838.

PCI NORTHEAST (2010). Northeast Extreme Tee (NEXT) Beams.

RILEM (2001) RILEM TC 162-TDF. Test and design methods for steel fiber reinforced concrete: uni-axial tension test for steel fiber reinforced concrete. *Mater Struct* 34:3–6

Romualdi, J. P. and Batson, G. B. (1963). Mechanics of crack arrest in concrete. ***Proc. ASCE, 89*** EM3 147-168.

Romualdi, J. P. & Mandel, J. A. (1964). Tensile strength of concrete affected by uniformly distributed closely spaced short lengths of wire reinforcement. AC1 J. ***Proc.,*** 61(6) 657-671.

Rossi, P. (1988). Les bétons de fibres métalliques. Presses de l'ENPC, Paris, France. (In French)

Serna, P., Arango, S., Ribeiro, T., Nunez, A.M. and Garcia-Taengua, E. (2009). Structural cast-in- place SFRC: technology, control criteria and recent applications in Spain. *Materials and Structures*, Vol. 42, pp. 1233-1246.

Shah S.P, Ouyang C. and Swartz S.E. (1995). Fracture mechanics of concrete: Applications of fracture mechanics to concrete, rock, and other brittle materials. John Wiley and Sons, New York.

Sharma, A. K. (1986). Shear strength of steel fiber reinforced concrete beams. *ACI Journal Proceed*., Vol. 83, No. 4, pp. 624-628.

Slater, E., Moni, M., Shahria Alam, M. (2012). Predicting the shear strength of steel fiber reinforced concrete beams. *Construction and Building Materials* 26, pp. 423–436.

Swamy, R. N., Jones R., and Chiam, A. T. P. (1993). Influence of steel fibres on the shear resistance of lightweight concrete I-beams. *ACI Structural Journal*, Vol. 90, No. 1, pp. 103-114.

Tordjman, F., 2012. Caractérisation mécanique en traction des BRF. M.Sc. Thesis, École Polytechnique de Montréal.

Voisin, O., Androuët, C., Charron, J.-P., Massicotte, B., 2011. Développement de deux bétons renforcés de fibres métalliques. École Polytechnique de Montréal.

UNI 11039 (2003). Steel Fibre Reinforced Concrete - Definitions, Classification and Designation. UNICEMENTO - Ente di Normazione dei Leganti Idraulici, Malte, Calcestruzzi e Cemento Armato, Febbraio 2003, pp. 13. (In Italian)

Zhang, J., Stang, H. (1998). Application of stress crack width relationship in predicting the flexural behavior of fiber- reinforced concrete. *J Cem Concr Res* 28(3):439–452.

Zollo, R.F. (1996). Fiber Reinforced concrete: an overview after 30 years of development. University of Miami, Florida.

APPENDIX A – EXPERIMENTAL STUDY OF DRAMIX 5D FIBRES

In the last few years the variety of fibres designed allows choosing between different shapes, lengths and diameters. This variety of kind of steel fibres allows engineers to find the correct fibre to reach the specific performances desired. Bekaert is the world largest steel fibre producer for concrete mix. They recently introduced a new type of fibres called 5D, which was characterised in this research project. Although this type of fibre was not considered for the application developed in this thesis, its characterisation for eventual structural applications is important and the process involved in determining the tensile properties is a important step for understanding the behaviour on SFRC members in tension.

Tensile strength, wire ductility and anchorage strength of this fibre are the largest that could be find between the Dramix ranges. The fibre Dramix 5D 6560 used in this experimental program, has the following characteristics (Figure A. 1):

- length: 60 mm;
- diameter: 0.90mm;
- length/diameter ratio: 65;
- Tensile strength: 1300 N/mm^2.

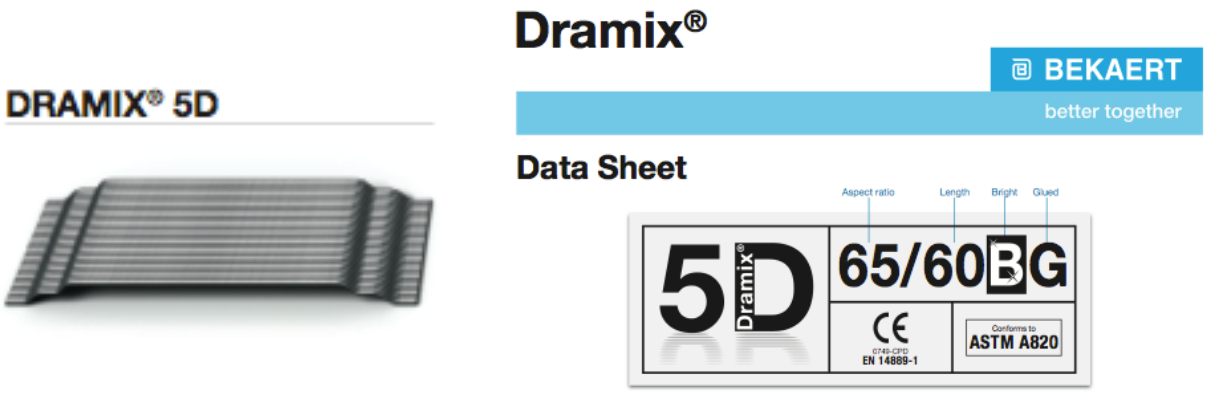

Figure A. 1: DRAMIX 5D fibre

There are no theoretical approach that would allow describing the post-cracking behaviour of a SFRC knowing separately the mechanical characteristics of steel fibres and concrete matrix. Therefore, the tensile behaviour of a SFRC mix can only be determined by experimental tests.

The curve σ-w is the one chosen to describe the behaviour of the concrete mix because it provides directly information for serviceability limit states. Moreover, it provides information that is not dependent on the size of the structure and on the orientation or the nature of the action applied on the structure. This allows using the relation retrieved without any more adjustments or modifications except to account for fibre orientation and density.

Three types of tests were available to characterise the tensile behaviour: the two standard bending tests, following the EN14651 and ASTM C1550, and the RILEM uniaxial test. Although the uniaxial test permits a direct measurement of the post-crack properties, it needs adequate equipment and cannot be easily performed due to the anchoring conditions and the weak stability during the loading process. Previous experimental campaign demonstrated the inverse analysis to be a reliable procedure to retrieve the σ-w relations. Therefore, each bending test represents an easy and good alternative to the difficulties related to the direct traction test. For the lack a large quantity of fibres and the difficulties linked to the direct traction test, is was decided to carry out only the two bending tests to investigate the tensile behaviour.

Between July 15th and July 22th 2013, three different concrete mix were manufactured at the Polytechnique Montréal structure laboratory. The three concrete-mixes with fibre content of respectively 60 kg/m^3, 80 kg/m^3 and 100 kg/m^3 (0.75%, 1.0% and 1.25%) were designed using the Baron-Lasage method. The cement by the producer HOLCIM was used for all batches. Four notched beams, 4 round panels, and about 20 cylindrical specimens were produced for each of the three SFRC mixes. The volume capacity of the mix-plant of the laboratory did not allow fabricating such an elevated quantity of concrete and the entire experimental campaign was split into six different batches. The specimens have been cured in the humid room for 7 days and tested about 60-70 days after being manufactured. Bending and compression tests were realized in September 2013. Graduate students Léa Faggio and Nicola Cordoni, under the supervision of the technician Cédric Androuet, fulfilled the whole program from the production of the specimens through the realisation of the tests up to the treatment of data.

In this report only the average relation will be presented – P-Δ, load–CMOD or σ-w relations – to privilege the comparison among the three mixes and with other SFRC in previous studies.

Few similar tests on SFRC mixes have already been done and some considerations shall be highlighted before reporting the results.

- EN bending test requires the specimens to be sawn, the notch on the specimens being introduced to initiate the development of the crack at the mid-span section. The middle section is not necessarily the weakest one along the specimen. For that reason the tensile strength retrieved from the test may overestimate the real value for small crack openings.
- EN guidelines explain to fill the formwork from the centre first, then at both extremities. This was defined for SFRC without self-compacting characteristics. Specimen fabrication was adapted at Polytechnique Montreal by specifying to move the bucket full of concrete along the length of the specimen. Doing so the orientation of the fibres mostly follows the direction along the length of the specimen. Therefore the results from the EN test do not reproduce accurately the post-cracking properties of real-scale structure where the distribution and the direction of the fibres follow a more random distribution, such as slabs or pavements. EN bending test is appropriate to retrieve the characteristics of structure where one dimension is really prevalent over the other two, for example a slender beam, even if the casting phase has to be planned and coordinated carefully.
- Round panels show a random distribution of the fibres in the main plane of the specimens. This fibre distribution allows a good prevision of post-cracking behaviour of structures as slabs, pavements or roof concrete sheets but it underestimates the real values in the centre of long beams, where the orientations of the fibres is mostly perpendicular to the crack pattern;

Lambrechts (2003) studied the variability in test results. She found a dispersion of about 10% for circular specimen results, and of about 18% for the EN results. This is due mainly to the larger concrete volume involved in round panel tests. Bastien (2004) and Bélanger (2000) found the same results in terms of variability for their experimental campaigns.

Both inverse analysis approaches implemented in software CalInv (Nour et al, 2011) demonstrated a good reliability in all the previous experimental studies (de Montaignac et al,

2012); the software is considered reliable and so used also for the characterisation of the SFRC at issue.

A.1.1 Compression tests

The compressions on the 4450-kN AMSLER universal press (Figure A-2) were carried out to evaluate the principal mechanical characteristics: the compressive strength f_c', the Young's module E, and the Poisson ratio ν for each batch manufactured of the three different mixes (60 kg/m^3, 80 kg/m^3 and 100 kg/m^3 of fibre contents). The minimum compressive strength to be reached was 70 MPa and, as reported in Table A. 1, each concrete mix has achieved the objective. The addition of the fibres does not increase the compressive strength of the material but rather slightly decreases it as pointed out by Rossi (1998). However from the results obtained in this experimental campaign, this tendency is not strong. Although that was not an objective of the investigation due to the limitation of the number of specimens and SFRC mixes, one can observe that fibre content does not influence the elastic modulus E and the Poisson's ratio and the results obtained.

Figure A. 2: Specimen under AMSLER Press Polytechnique Montréal structures Laboratory

The procedure followed during the compressive tests is described in the documents written by Androuët (2014). For each batch of concrete, three cylinders were tested to determine f_c' and one other cylinder per batch was tested to compute the modules E_c and ν. The characteristic $f_c^{'}$ values presented in the table 1 are the average values between three test results obtained for each batch whereas E_c and ν are the values retrieved from only one cylinder. Figure A. 3 presents the composition of a typical mix.

Table A. 1: f_c', E_c and ν for the three concrete mix

	BRF70 60kg batch 1	BRF70 60kg batch 2	BRF70 80kg batch 1	BRF70 80kg batch 2	BRF70 100kg batch 1	BRF70 100kg batch 2
fc' [Mpa]	89.4 (65days)	87.4 (58days)	81.4 (69days)	84.7 (67days)	91.2 (71days)	84.4 (69days)
E [Mpa]	38580 (65days)	36111 (58days)	38271 (69days)	36851 (67days)	37766 (71days)	36754 (69days)
ν	0.264 (65days)	0.25 (58days)	0.272 (69days)	0.278 (67days)	0.246 (71days)	0.275 (69days)

FORMULAIRE DE MELANGE POUR PÂTE, MORTIER ET BETON

Paramètres

Nom du mélange : BRF70-HOLn07fib60kg5D6560 batch1 — Préparé par : Cédric

Critères	Valeur
AC/C	0.00
E/C	0.30
E/L = E/(C+FS)	
S/C	1.30
S/G	1.34

Critères	Valeur
Sup. (ml/kg L)	54.9
(% sec L)	2.30
AEA (ml/kg L)	0.00
Visc. (ml/Leau)	0.00
Autre (ml/kg L)	0.0

Critères	Valeur
Fibre (%)	0.8
Air (%)	2.5
Pâte (%)	44.7
Vgâchée (l)	140.0

Recette de béton fibré à haute performance

Composante	Identification composante	ρ (kg/l)	Masse recette (kg/m3)	Volume recette (l/m3)	Masse gâchée (kg) *	Volume gâchée (l)
Ciment	HSF (CSL)	3.03	650.00	214.52	91.00	30.03
Ajout cimentaire	Pas d'ajout	0.00				
Eau	0	1.00	171.60	171.60	24.02	24.02
Superplastifiant	Plastol6200EXT	1.08	38.36	35.69	5.37	5.00
Extrait liquide (%)	61	1.00	23.40	23.40	3.28	3.28
Entraîneur d'air	Pas de AEA	0.00	0.00	0.00	0.00	0.00
Extrait liquide (%)	100	1.00	0.00	0.00	0.00	0.00
Agent viscosant	Pas de VISC	0.00	0.00	0.00	0.00	0.000
Extrait liquide (%)	1	1.00	0.00	0.00	0.00	0.00
Autre adjuvant	Pas d'autre adj	0.00	0.00	0.00	0.00	0.00
Extrait liquide (%)	100	1.00	0.00	0.00	0.00	0.00
Eau total (adj. inclus)	0	1.00	195.00	195.00	27.30	27.30
Sable	Joliette	2.694	844.51	313.48	118.23	43.89
Pierre	2.5-10 Gr. St F	2.71	628.78	232.02	88.03	32.48
Fibres	Dramix5D65-60	7.80	60.00	7.69	8.40	1.08
Air	0	0.00	0.00	25.00	0.00	3.50
Total	0	0	2393.25	1000.00	335.06	140.00

** : Masse granulats en Msss*

Teneur en eau et correction des masses de granulats

Caractéristiques		Sable	Pierre	
Poids tare : PT		54.60 g	54.00 g	
Poids tare + granulats humides : PH		653.70 g	1054.70 g	
Poids tare + granulats séchés : PS		641.50 g	1050.80 g	*Total eau*
Absorption : A		0.0062 (-)	0.0068 (-)	apportée
Teneur en eau	TE = (PH - PS) / (PS - PT)	0.0208 (-)	0.0039 (-)	*par granulats :*
Eau apportée par granulats	Eau = [(TE - A) x Msss] / (1 + A)	1.71 kg	-0.25 kg	1.46 kg
Masse corrigée des granulats	Mhumide = [(1 + TE) x Msss] / (1 + A)	119.95 kg	87.78 kg	

Matériaux à préparer pour une gâchée de 140 litres

Composante	Masse théorique (kg) Masse	Msss	Masse au laboratoire (kg) Mcorrigée	Mpesée
Ciment	91.00 kg	------	------	91.00 kg
Ajout cimentaire	kg	------	------	kg
Eau	24.02 kg	------	22.56 kg	22.562 kg
Superplastifiant	5370.6 g	------	------	5370.593 g
Autre adjuvant	0.0 g	------	------	0.000 g
Entraîneur d'air	0.0 g	------	------	0.000 g
Agent viscosant	0.0 g	------	------	0.000 g
Sable	------	118.23 kg	119.95 kg	119.95 kg
Pierre	------	88.03 kg	87.78 kg	87.78 kg
Fibres	------	8.40 kg	------	8.40 kg

Mcorrigée d'eau correspond à la masse théorique + Total eau apportée granulats

Caractéristiques de la gâchée

Contact E/C (date, heure) :	2013/07/15 @ 14h		fc 7j/28j (MPa) :	
Température (°C) :	26.4		Masse béton airmètre (kg) :	17.0808
Affaissement / Etalement (mm) :	235	570	Volume airmètre (l) :	7
Temps d'écoulement (s) :			Masse vol. béton exp. (kg/m3) :	2440.114286
			Teneur en air (%) :	1.1

Remarques : Abrams=235/540-600;T50=13;L-Box=82/84;T20=1;T40=2.

Groupe de recherche en GÉNIE DES STRUCTURES

V.1.5.3 - JPC/CA, 24 août 2012

Figure A. 3: Example for the concrete mix design of the BRF 60kg/m^3 Dramix 5D 6560

A.1.2 RILEM notched beams

A.1.2.1 General

The European standard EN14651 (2005) notched beam test allows an indirect evaluation of the post-cracking tensile behaviour of SFRC in terms of residual flexural tensile strength.

The standard proposes to determine the residual flexural tensile strength as a function of the fictitious stress at the tip of the notch which is assumed to act in an uncracked mid-span section, with linear stress distribution, of a prism subjected to the centre-point load Fj corresponding to $CMOD_j$ where $CMOD_j > CMOD_{FL}$ (F_L indicated the load corresponding to the limit of proportionality) or to δ_j where $\delta_j > \delta_{FL}$ (j = 1,2,3,4)" (EN 14651:2005). The test can also be used to determine the direct post-cracking tensile using an inverse analysis procedure such as proposed by Nour et al. (2012).

The apparatus, the dimensions of the specimen, the accuracy to be reached in the results and the procedure to be followed are explained in the standards guideline document. Following accurately the standard test procedure is essential to obtain reliable post-cracking properties. A brief explanation of the main issues to be respected are presented in the following.

A.1.2.2 The Apparatus

The testing apparatus (Figure A. 4) consists in three steel rollers, a load-measuring device, a machine operating in a controlled manner and linear displacement transducers measuring vertical displacements and CMODs (crack mouth opening displacement).

Two of the three rollers are used to support the specimens and the last one is needed to transmit and distribute the linear load at the mid-span section. The steel circular cross-section shall measure a diameter of 30 ± 1mm and a length 10 mm bigger than the test specimen. At the École Polytechnique de Montréal the rollers utilised during the tests have different diameter (25mm) and length (152mm).

Differently from the EN guidelines, the tests were done controlling the vertical displacement of the specimen increased at a constant rate of 0.2 mm/min. To avoid the instability of the specimen, when a vertical displacement of 4.5 mm was reached the test continued controlling the vertical

displacement of the load machine. In this case the European standard accepts this procedure and provides the approximated formula for the calculation of the CMOD from displacement values:

$$CMOD = (\delta - 0.04)/0.85 \text{ [mm]} \quad (A.1)$$

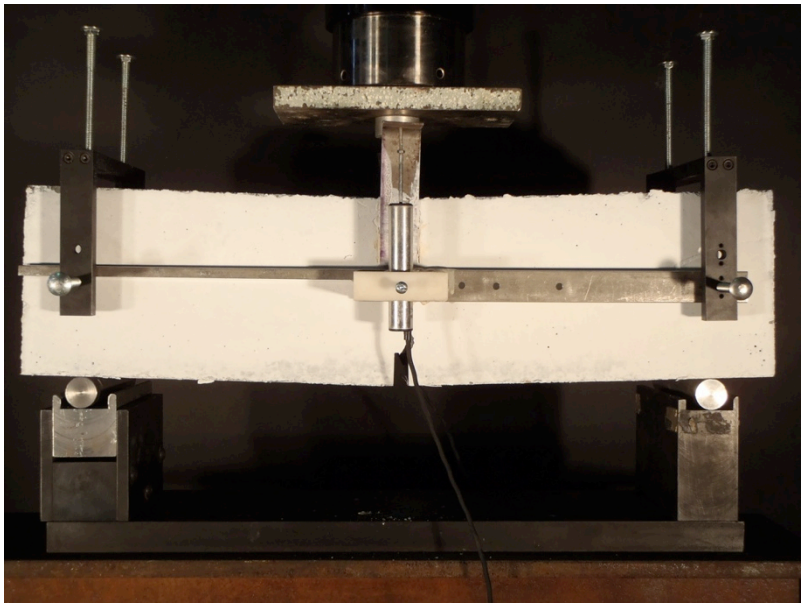

Figure A. 4: The apparatus

A.1.2.3 The Specimen

European standard considers the bending test to provide an acceptable result representation only for fibre length up to 60 mm, which is respected for the fibres considered.

As Figure A. 5 illustrates, specimen dimensions are fixed and they have to be respected with an accuracy of 1 mm. The same accuracy is needed for the notch width that shall measure 5 mm ± 1 mm. For this specific experimental program, all dimensions were measured before every single test.

The notch of every specimen was sawn following the procedure suggested in the EN document, similarly for the positioning of the apparatus, the specimen and the displacement transducers.

For this kind of bending test the casting phase assumes a relevant importance – the fibres shall be placed perpendicular to the bending cracks to be able to offer the maximum bridging properties to

the concrete specimen. The formworks shall be filled by moving the bucket full of concrete along the length of the mould. Hitting the formwork with a rubber hammer helped the concrete specimen to eject the air bubbles trapped within the material.

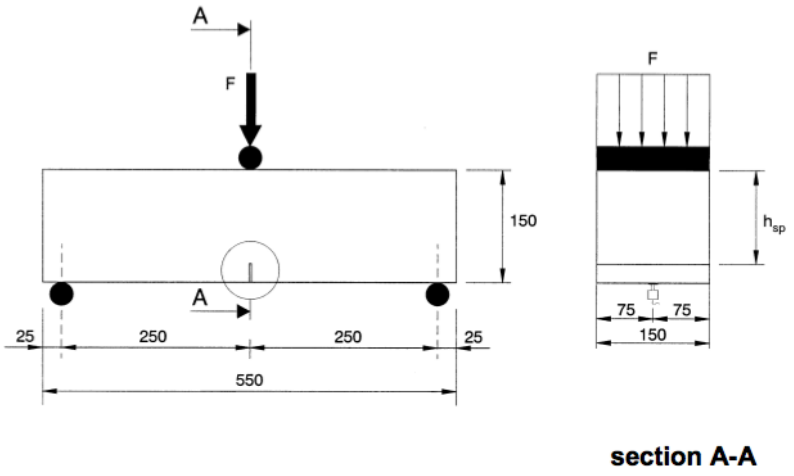

Figure A. 5: Specimen dimensions

A.1.2.4 Expression of the results:

One of the main results provided by EN bending test is the relation between the applied load and the CMOD measured or calculated by experimental data. Two linear displacement transducers are placed across the two external sides of the notch permitting a double measurements of the crack opening. The equation provided by EN guidelines gives the possibility to calculate the crack-opening from the measures of the vertical displacement. Additionally from the load – CMOD diagram, it is possible to calculate the residual flexural tensile strength for different CMOD values – by the equation A.2 – which are fundamental information in the design phase.

$$f_{R,j} = \frac{\left(3 \cdot F_j \cdot l\right)}{\left(2 \cdot b \cdot h_{sp}^2\right)} \tag{A.2}$$

where

$f_{R,j}$ is the residual flexural tensile strength corresponding to CMODj or to δ_j (j = 1,2,3,4), in Newton per square millimetre;

F_j is the load corresponding to CMODj or to δ_j (j = 1,2,3,4), in Newton.

A.1.2.5 Presentation and discussion of the results:

The two diagrams presented herein are the load–displacement and the load–CMOD charts. In this report often charts show the curves concerning the three different concrete mixes together to provide a better comprehension of the effect of the fibre amount on the bending behaviour of SFRC. Figure A. 6 shows the average curve from the 4 curves corresponding to the 4 specimens of a concrete mix. The final relationships describing the post-cracking material correspond to the average curve for every concrete mix, so Figure A. 7 and Figure A. 8 present the average values corresponding to each different concrete mix.

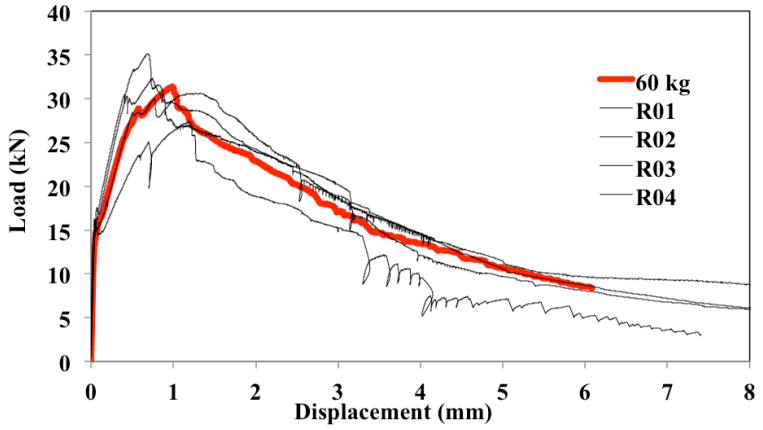

Figure A. 6: Calculation of the average curve (in red) from each single $P - \Delta$ relation

From Figure A. 8, it is clear that the post-cracking tensile strength improve with the fibre content increase, the 100 kg/m^3 mixes presenting the most marked ductility. For all specimens the cracking load corresponds to approximately 15 kN, indicating similar matrix tensile strength of 4.8 MPa. The size of the peak in the three curves is proportional to the quantity of the fibres.

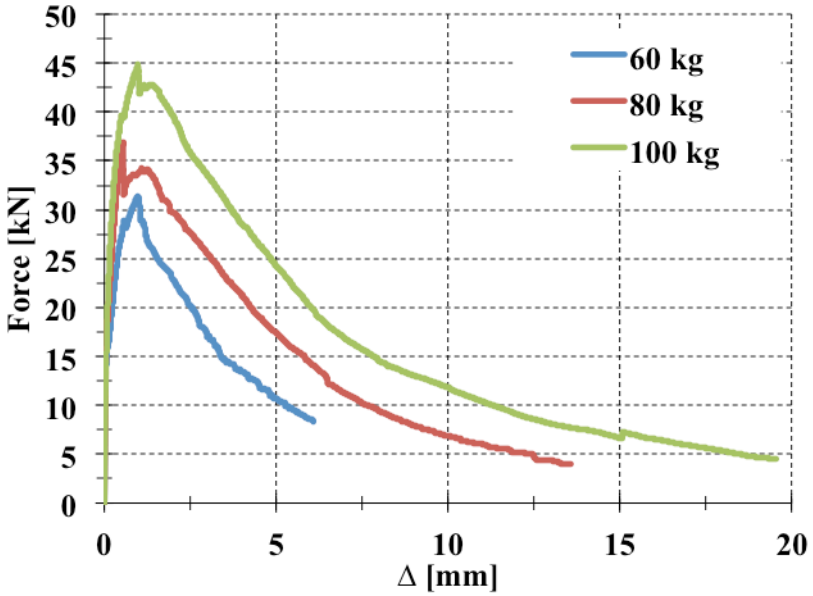

Figure A. 7: Average $P - \Delta$ relations for the three SFRC mixes – notched beam test

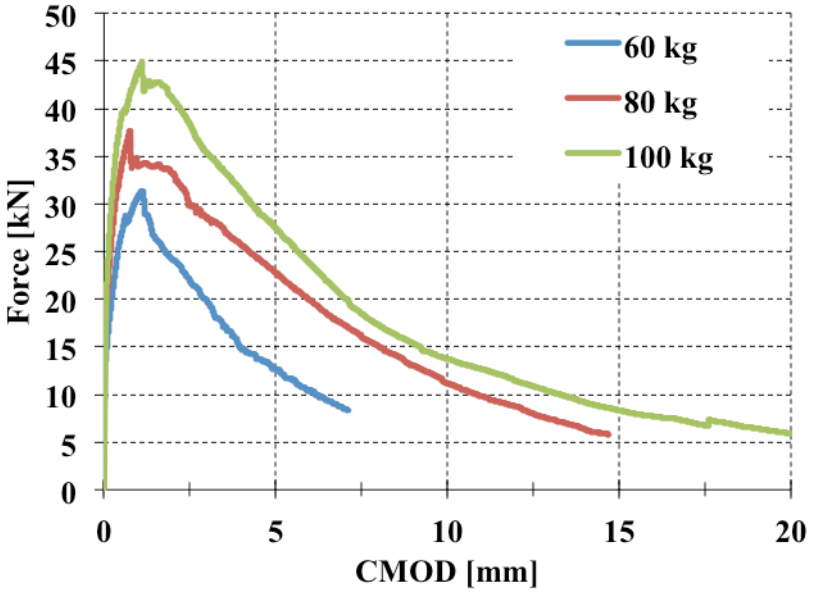

Figure A. 8: Average $P - \mathrm{CMOD}$ relations for the three SFRC mixes – notched beam test

Table A. 2: Peak load and correspondent values of standard deviation

Mix	Peak - load [kN]	DEV. STD.
60 kg/m3	31,36	3,22
80 kg/m3	36,90	3,19
100 kg/m3	44,89	6,09

The load – CMOD response can be determined by the equation (A.1) of the EN or directly from the measurements of the device installed on the notch of the specimen. Only the curve relatives to the direct measure is presented in this report, since the two curves have demonstrated a good accordance for all the tests made.

As indicated EN guidelines, the load – CMOD diagram can be used to deduce the equivalent flexural tensile strengths for CMOD values of: 0.5, 1.5, 2.5 and 3.5 mm. From the crack opening values and the corresponding loads values, the formula (A.2) allows calculating the equivalent flexural tensile strength of the metallic fibre concrete. It is worthwhile indicating that the corresponding direct tensile strength is obtained by dividing the equivalent flexural strength by 3. Table A. 3 to Table A. 5 present the values for the three mixes considered in this experimental program.

Table A. 3 : Residual flexural tensile strength for the 60 kg/m^3 fibre-concrete mix

	60 kg/m3		
j	CMOD	F [kN]	f,R [N/mm2]
1	0,50	26,76	5,95
2	1,50	26,37	5,86
3	2,50	21,91	4,87
4	3,50	17,14	3,81

Table A. 4 : Residual flexural tensile strength for the 80 kg/m^3 fibre-concrete mix

	80 kg/m3		
j	CMOD	F [kN]	f,R [N/mm2]
1	0,50	33,75	7,50
2	1,50	33,96	7,55
3	2,50	29,88	6,64
4	3,50	27,28	6,06

Table A. 5 : Residual flexural tensile strength for the 100 kg/m^3 fibre-concrete mix

	100 kg/m3		
j	CMOD	F [kN]	f,R [N/mm2]
1	0,50	39,02	8,67
2	1,50	42,73	9,50
3	2,50	38,42	8,54
4	3,50	33,45	7,43

A.1.3 ASTM C1550

A.1.3.1 General

This standard bending test aims to determine the flexural toughness of fibre-reinforced concrete by computing the energy absorption in the post-crack behaviour of a round panel on three symmetrical pivots subjected to a central point load (ASTM C1505).

The use of a round concrete specimen eliminates the problems related to sawing the specimen so the panel can crack in the real plane of weakness, and permits certain repeatability in terms of preparation of the specimen. The aim of the standard test is the calculation of the energy absorbed by the circular specimen during the test up to a predefined value of central displacement that is chosen according to the intended application of the material, normally between 5 mm and 40 mm. A smaller value would represent a rigid structure where small deformations are allowed whereas a larger value would represent a structure able to dissipate more energy. The biaxial bending response of the specimen to a centrically load exhibits a mode of failure that can well represents the in situ conditions of slabs or roof sheets. In this current test program it is used to characterise the SFRC post-cracking in girders.

A.3.2 The apparatus

The support fixture of the apparatus shall include three symmetrically pivots on a circle measuring a diameter of 750 mm. The system shall be capable to bear a maximum load of 100 kN. The supports shall be sufficiently rigid with a maximum lateral translation of 0.5 mm. ASTM standard indicates that using grease over the supports to reduce friction with the transfer plate.

The tests at Polytechnique Montréal are carried out using a different type of supports (Figure A. 9) that makes the comparison with results of standard test and the calculation of the total energy inconsistent. Three rollers replacing the rigid pivots compose the apparatus utilised during the test. The rollers allow the radial translation of the specimen. Although de Montaignac (2013) demonstrated the equivalence between the results obtained from a fixed pivots system, allowing free radial displacement eliminates differences between apparatus of different laboratories and allows easier comparison between test series. Moreover, this allows carrying out inverse analyses (de Montaignac 2012; Nour et al. 2012).

Figure A. 9: Apparatus used for the round panel tests at Polytechnique Montréal

A1.3.3 Load – displacement:

The load – displacement diagram represents the average curve between the 4 curves obtained for each type of fibre concrete. The test is considered valid when the specimen cracks along three different lines that clearly arise from the centre of the specimen forming angles of about 120° between the crack lines.

During the test many factors take part in the determination of the cracking pattern and the failure mode; the number and the position of the cracks are not predictable with precision but a three-crack rupture is suitable to be able to take results into consideration. Quality and precision in preparation and positioning phases, the orientation of the fibres in the specimen, the quality of the cure, and the presence of weak plane in the specimen are only some of the factors that can modify the cracking pattern and easily lead to a two-fissure fracture invalidating test results.

In the calculation of the average curves presented in Figure A. 10 only specimens with three-crack pattern were considered.

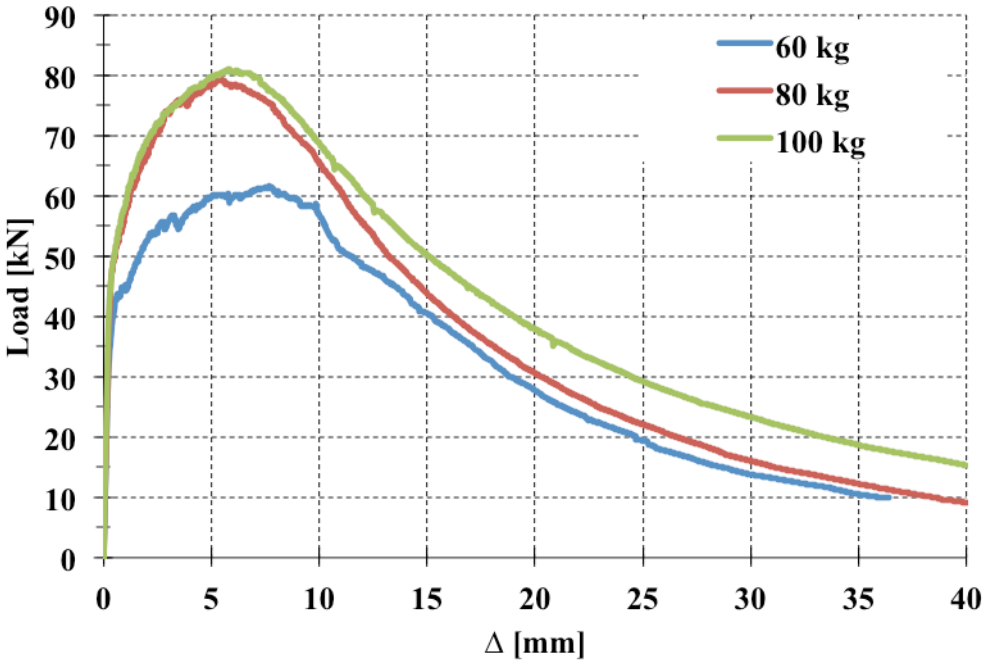

Figure A. 10: Average $P - \Delta$ relations for the three SFRC mixes – round panel test

Looking at the load – displacement diagram, the proximity between the 80 and 100 kg/m^3 curves may lead to consider a certain saturation of the quantity of fibres in the concrete mix. However results for the 80 kg/m^3 are not valid.

For the 80 kg/m^3 concrete mix only one of four specimens broke along three cracks so the curve of 80 kg/m^3 is the only one valid because three of four specimens had two fissures rupture at the end of the test. The variability of the 80 kg/m^3 mix is not taken into account and the saturation of

the mix cannot be stated only considering one specimen result. More tests would have to be carried out to better characterise the 80 kg/m^3 concrete mix. The peak-load between the two concrete mix of 60 and 100 kg/m^3 confirm the same conclusions stated for the EN test. A larger quantity of this kind of fibres increase significantly the ductility of the material and increase the pic-load of about 32% for this kind of test.

Table A. 6: Peak load and its corresponding standard deviation

Mix	Peak - load [kN]	DEV.STD.
60 kg/m3	61,60	3,49
80 kg/m3	79,50	/
100 kg/m3	81,08	8,51

(a) failure with two cracks (b) failure with three cracks

Figure A. 11: Round panels.

A.1.4 Comparison of test results

A.1.4.1 General

This section aims to compare the results obtained with three other SFRC mixes studied for previous research works. The results come from two experimental campaigns carried out respectively by Tordjman (2012) and De Broucker (2013).

The first author studied the behaviour of two different steel fibres: the Dramix 80/60 in three different volume quantities (40, 60 and 80 kg/m^3 for a 50 MPa concrete mix) and the Dramix ZP305 in two different volume quantities (80 and 120 kg/m^3 for a 80 MPa concrete mix). The second author studied the behaviour of the Dramix fibres 65/35 for a 80 MPa concrete mix. The energy dissipation method of all the three types of fibres is concentrated at the extremities. The three fibres used for the comparison present one hook, contrarily to the double hooks presented by the Dramix 5D. Thus the anchorage force is expected to be higher. Characteristics of the fibres are presented in Table A. 7.

Table A. 7 : Different kinds of steel fibres investigated

Fibre type	Length (mm)	L/d	Tensile strength (MPa)
Dramix 80/60	60	80	1050
Dramix ZP_305	30	54.5	1345
Dramix 65/35	35	65	1100
Dramix 5D	60	65	1300

A.1.4.2 Load-displacement

The results are presented in Figure A. 12 and Figure A. 13 in terms of load displacement relationships from round panel and notched beam tests respectively. Only the average curves are shown.

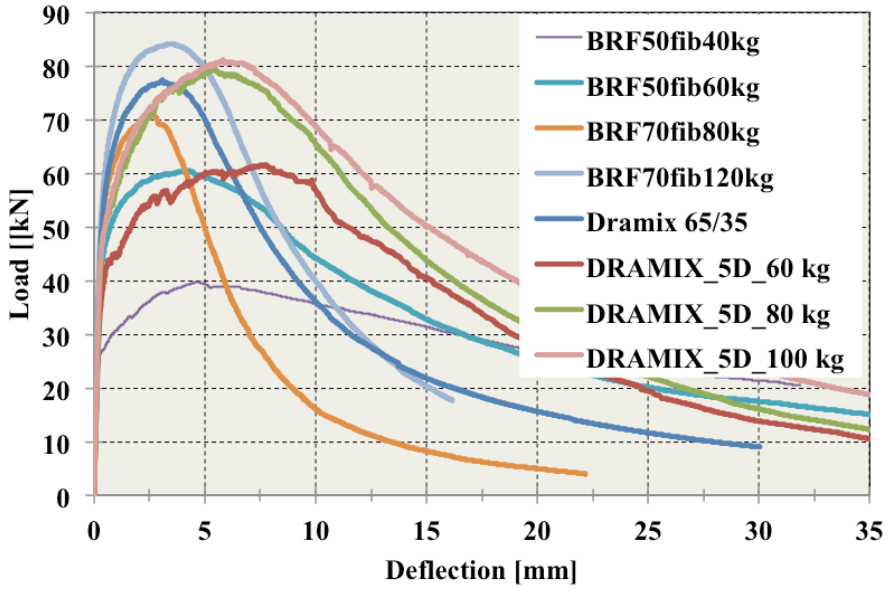

Figure A. 12 : $P - \Delta$ average relations for the eight SFRC mixes tested – round panel test

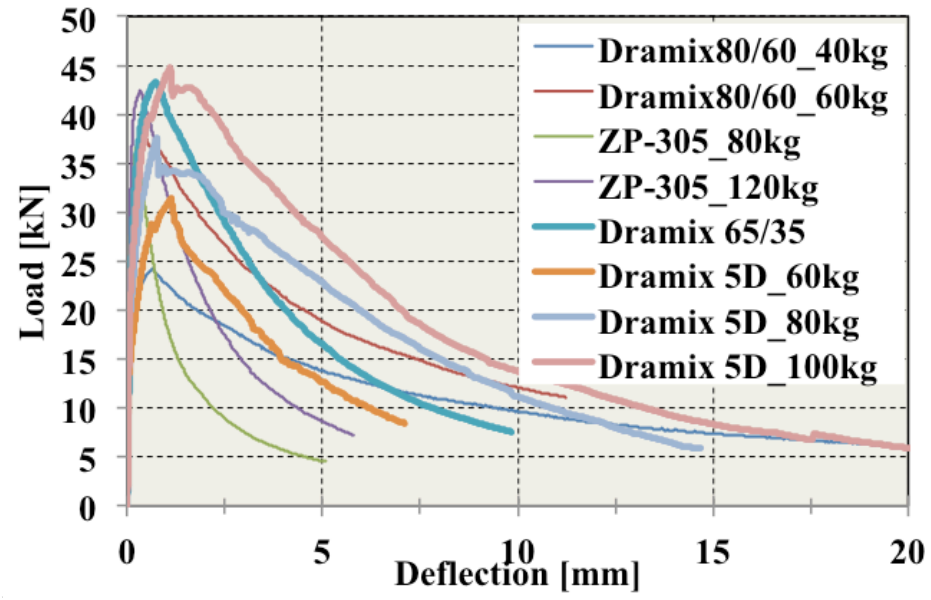

Figure A. 13 : $P - \Delta$ average relations for the eight SFRC mixes tested – notched beam test

As expected the peak-load mainly depends on the fibre content and on the compressive properties of the concrete.

The post-peak softening behaviour is principally related to the fibres characteristics: length, length/diameter ratio and volume content. The double hooked ends of the fibres Dramix 5D demonstrated to provide a better ductility. The peak-loads are reached for higher deflections than for other mixes. Therefore the length of the softening part of the $P - \Delta$ relations seems to be strongly dependent on the volume dosage of steel fibres.

A.1.4.2 Inverse analysis

All the $\sigma - w$ relations presented herein come from the round panel tests. The average $P - \Delta$ curve is been treated with the inverse analyses obtaining the post-cracking relations.

Results are grouped following two characteristics: length of the fibre and volume dosage.

A.1.4.2.1 Comparison of 60 mm long fibres

The volume dosage of fibre seems to be the most important factor affecting the post-cracking behaviour of the SFRC mixes. The peak tensile stress is reached for a crack opening value of about 0.25 mm for all the mixes.

Up to 1 mm of crack opening it is possible to notice a constant stress tensile value for each SFRC mix. The peak stress is related to the fibre content. A crack opening equal to 2 mm seem to equalize the performances of all the fibres tested.

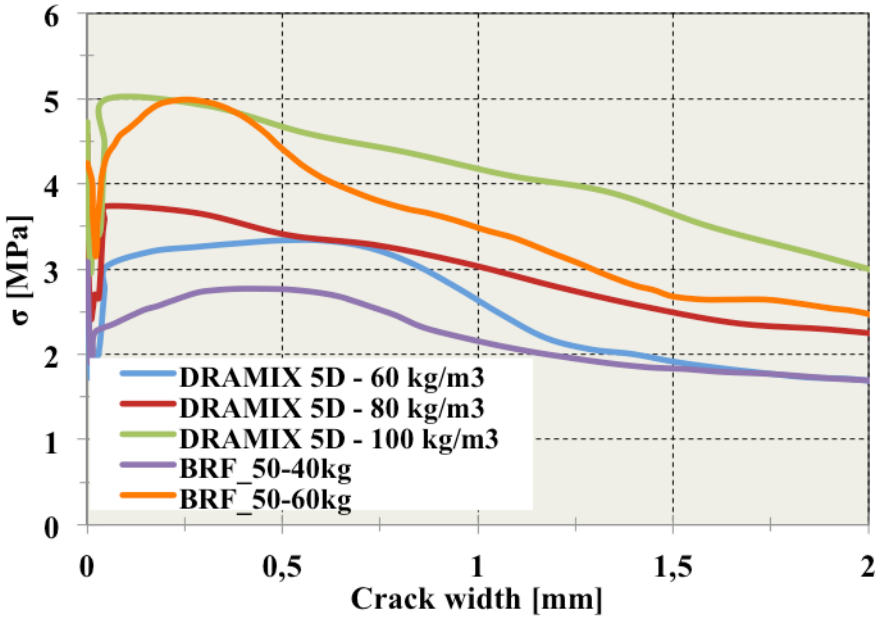

Figure A. 14 : $\sigma - w$ average relations retrieved from round panel tests for 60 mm long fibres

A.1.4.2.2 Comparison of 80kg/m^3 SFRC mixes

Figure A. 15 includes the relationships corresponding to the use of the same dosage equal to 80 kg/m^3. As stated before, the peak tensile stresses seem to be strongly influenced by the volume dosage of fibres. All the relationships presented in the graphic show the same plateau up to an approximate crack opening of 0.5 mm. Starting from 0.5 mm, the relationships seem to be more affected by the length of the fibres used. The Dramix 5D and the Dramix 80/60 – with a length equal to 60 mm – show $\sigma - w$ relations with a little loss in tensile stresses up to a crack opening equal to 2 mm.

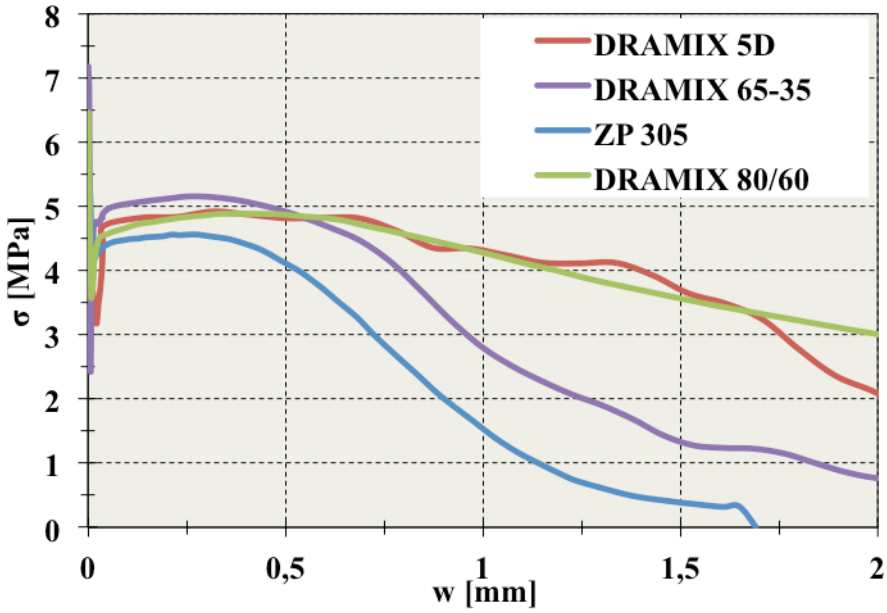

Figure A. 15 : $\sigma - w$ average relations from round panel tests – 80 $^{kg}/_{m^3}$ of fibre dosage

APPENDIX B – SIMPLIFIED METHOD TO COMPUTE THE LIVE LOAD FACTORS

According to the categorisation proposed in the Canadian Code (CSA-S6-06) the bridge considered may be put in the shallow superstructure class as a slab-on-girders bridge deck. The assumed geometry respects all the conditions at the clause 5.7.1.1 of the Code. Thus the simplified method (Clause 5.7.1.2.1.2) for obtaining governing live load moments in the external and internal portions of the bridge may be used.

B.2.1 Longitudinal bending moments for serviceability and ultimate limit states

B.2.1.1 Calculation of M_g

The longitudinal moment per girder is calculated as follows:

$$M_g = F_m \cdot M_{g,avg}$$

F_m = amplification factor to account for the transverse variation in maximum longitudinal moment intensity = $S \cdot N \Big/ F \cdot \left[1 + \frac{\mu \cdot C_f}{100}\right] \geq 1.05$

where

S = Center-to-center girder spacing, [m]

F = width dimension that characterises load distribution for a bridge, [m]

$1 + \mu \cdot C_f \Big/ 100$ = lane width correction factor

where

$\mu = W_e - 3.3 \Big/ 0.6 \leq 1.0$

W_e = the width of design lane, [m] [Clause 3.8.2]

C_f = percentage correction factor obtained from Table 5.3

$M_{g,avg}$ = average moment per girder due to live load determined by sharing equally the total moment on the bridge cross-section among all girders in the cross-section = $n \cdot M_T \cdot R_L / N$

where

n = number of design lanes in accordance with Clause 3.8.2

M_T = maximum moment per design lane at the point of the span under consideration

R_L = modification factor for multi-lane loading in accordance with Clause 3.8.4.2

N = number of girders or longitudinal wood beams in the bridge deck width

B.2.1.2 Calculation of M_T

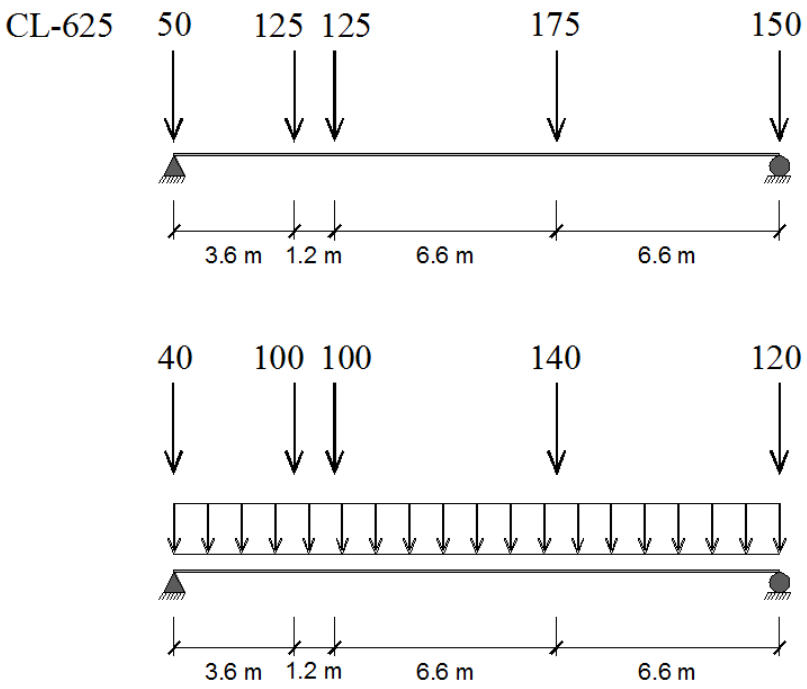

Figure B. 1: Load configurations

For SLS Combination 1 and for ultimate limit states, the traffic load shall be the truck load increased by the dynamic load allowance – Clause 3.8.3.2 – or the lane load – Clause 3.8.3.3 – whichever produces the maximum load effect. This load shall be positioned longitudinally and transversely within each design lane at a location and in the direction that produces maximum load effect.

B.2.2 Longitudinal bending moments for fatigue limit state

B.2.2.1 Calculation of M_g

The longitudinal moment per girder is calculated as follows:

$$M_g = F_m \cdot M_{g,avg}$$

$$F_m = {S \cdot N}/{F \cdot \left[1 + \frac{\mu \cdot C_f}{100} + \frac{C_e}{100}\right]} \geq 1.05$$

where

C_e = percentage correction factor for vehicle edge distance obtained from Table 5.5

C_f = percentage correction factor obtained from Table 5.4

F = width dimension that characterizes load distribution for a bridge, obtained from Table 5.4. For the internal girders of slab-on-girder bridges consisting of two or more lanes, the value of *F* obtained from Table 5.4 shall be modified by the following factor, which accounts for the variation of *F* with girder spacing *S*

$$F = F_{tab} \cdot \left[1.00 + (0.295 - 0.35) \cdot \left[{L - 10}/{40}\right]\right] \text{ For } 10m \leq L \leq 50m$$

$$M_{g,avg} = {M_T}/{N}$$

B.2.2.2 Calculation of M_T

For the FLS, the traffic load shall be one truck only, placed at the centre of one-travelled lane. The lane load shall not be considered.

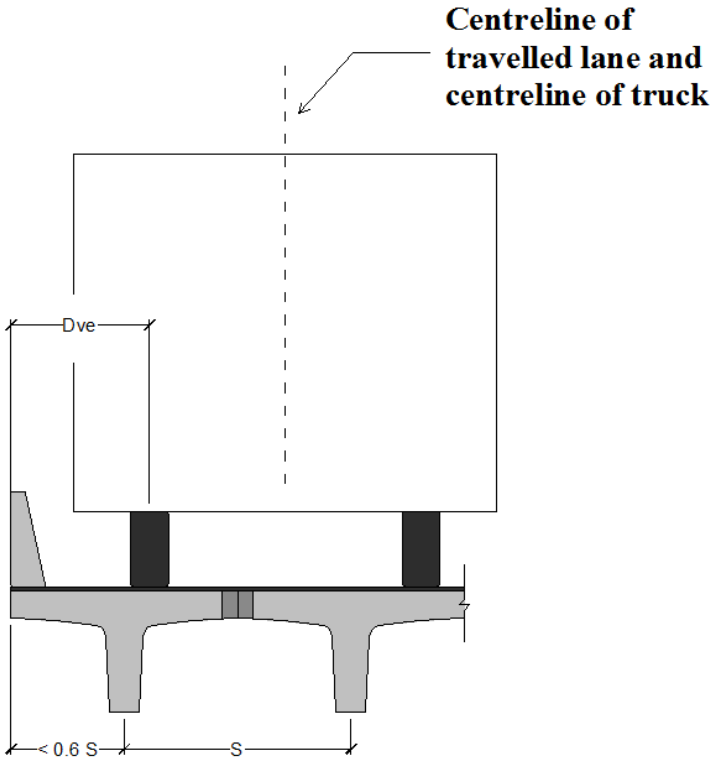

Figure B. 2: Sketch to determine the values of S and D_{VE} following the Code CSA-S06

B.2.3 Longitudinal vertical shear for serviceability and ultimate limit states

As specified for the longitudinal moment the simplified method may be applied to obtain the governing shear forces as follows:

$$V_g = F_v \cdot V_{g,avg}$$

where

F_v = amplification factor to account for the transverse variation in maximum longitudinal vertical shear intensity, as compared to the average longitudinal vertical shear intensity

$= {}^{S \cdot N}/_{F}$

$F =$ width dimension that characterizes load distribution for a bridge. For bridges with up to four design lanes, *F* shall be obtained from Table 5.7. For girder-type bridges, where the spacing, *S*, of longitudinal girders is less than 2.00 m, the value of *F* obtained from Table 5.7 shall be multiplied by $\left({}^{S}/_{2}\right)^{0.25}$.

$V_{g,avg}$ = average shear per girder determined by sharing equally the total shear on the bridge cross-section among all girders in the cross-section $= {}^{n \cdot V_T \cdot R_L}/_{N}$.

B.2.4 Longitudinal vertical shear for fatigue limit state

V_T shall be calculated using a single truck on the bridge, in one lane only, such that n = 1 and R_L = 1.00. the factor F shall be calculated from table 5.8

For serviceability and ultimate limit states the longitudinal vertical shear diagrams shall be obtained by treating the bridge as a beam for two load cases. The truck as described in Clause 3.8.3.2 shall be used, multiplied by the appropriate factor (1 + *DLA*) specified in Clause 3.8.4.5. The second load case shall comprise the lane load specified in Clause 3.8.3.3. For the FLS, the traffic load shall be one truck only, placed at the centre of one-travelled lane. The lane load shall not be considered. The governing shears per design lane thus obtained shall be designated V_T.

APPENDIX C – NUMERICAL σ-W RELATIONSHIPS SED TO VALIDATE EPM3D

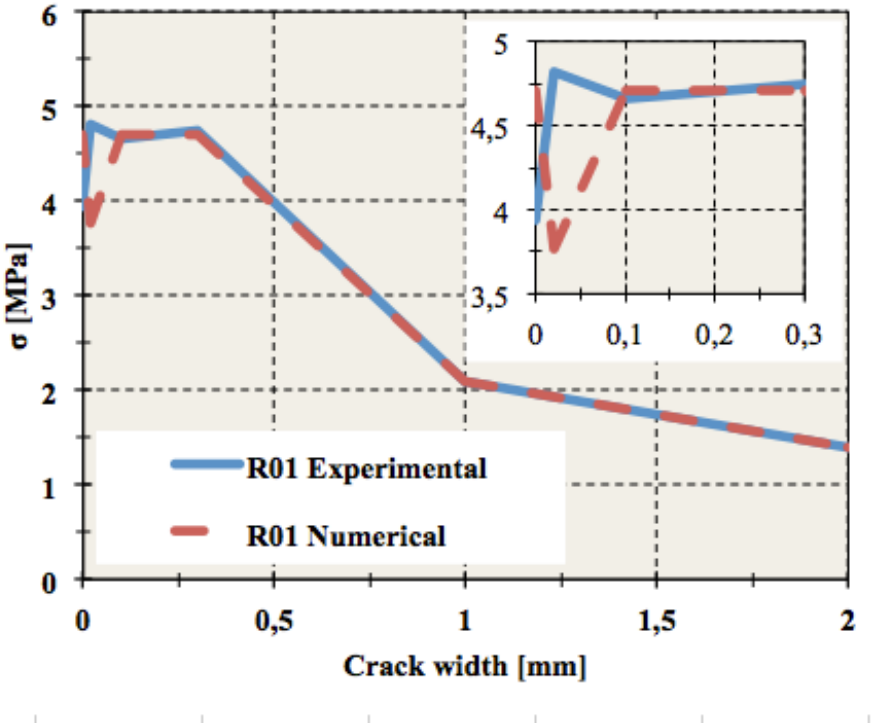

Figure C. 1 : Numerical σ-w relationship used for the beam R01

Table C. 1 : Numerical σ-w relationship values used for the beam R01

R01	Experimental [MPa]	Numerical [MPa]
f't	3.94	4.71
$\sigma_{0.02}$	4.82	3.77
$\sigma_{0.1}$	4.66	4.71
$\sigma_{0.3}$	4.75	4.71
σ_{1}	2.10	2.10
σ_{2}	1.39	1.39
σ_{10}	0	0

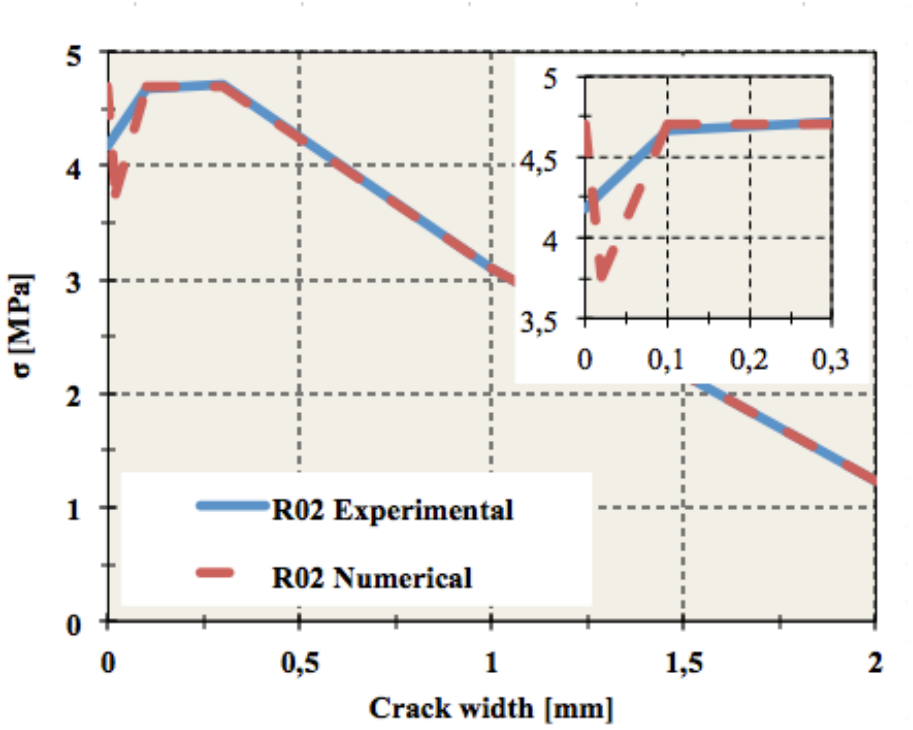

Figure C. 2 : Numerical σ-w relationship used for the beam R02

Table C. 2 : Numerical σ-w relationship values used for the beam R02

R02	Experimental [MPa]	Numerical [MPa]
f't	4.18	4.70
$\sigma_{0.02}$	4.28	3.76
$\sigma_{0.1}$	4.67	4.70
$\sigma_{0.3}$	4.72	4.70
σ_{1}	3.11	3.11
σ_{2}	1.23	1.23
σ_{10}	0	0

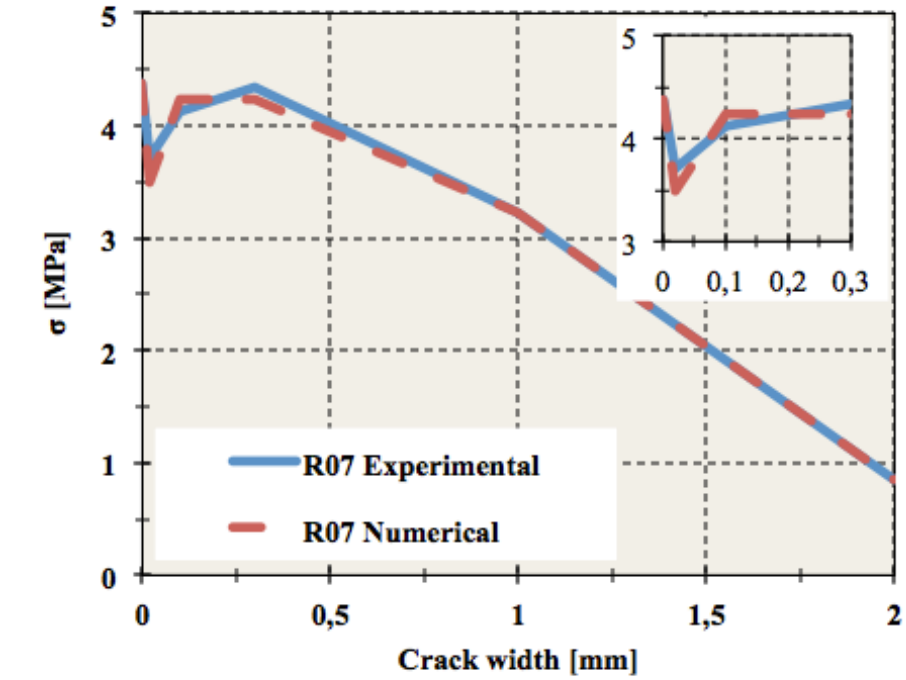

Figure C. 3 : Numerical σ-w relationship used for the beam R07

Table C. 3 : Numerical σ-w relationship values used for the beam R07

R07	Experimental [MPa]	Numerical [MPa]
f't	4.38	4.38
$\sigma_{0.02}$	3.71	3.50
$\sigma_{0.1}$	4.12	4.23
$\sigma_{0.3}$	4.34	4.23
σ_{1}	3.22	3.22
σ_{2}	0.85	0.85
σ_{10}	0	0